OUKA
The University of Osaka
Institutional Knowledge Archive

| | |
|---|---|
| Title | Comprehensive understanding of protein folding and misfolding |
| Author(s) | 野地, 真広 |
| Citation | 大阪大学, 2020, 博士論文 |
| Version Type | VoR |
| URL | https://doi.org/10.18910/76403 |
| rights | © 2019 Noji et al. This is an open access article distributed under the terms of the Creative Commons CC-BY license, which permits unrestricted use, distribution, and reproduction in any medium, provided the original work is properly cited. |
| Note | |

*The University of Osaka Institutional Knowledge Archive : OUKA*

https://ir.library.osaka-u.ac.jp/

The University of Osaka

# Comprehensive understanding of protein folding and misfolding

（蛋白質フォールディングとミスフォールディングの包括的理解）

**A Doctoral Thesis**

**by**

**Masahiro Noji**

**Submitted to the Graduate School of Science,**

**Osaka University**

**February, 2020**

# Comprehensive understanding of protein folding and misfolding

（蛋白質フォールディングとミスフォールディングの包括的理解）

**A Doctoral Thesis**

**by**

**Masahiro Noji**

**Submitted to the Graduate School of Science,**

**Osaka University**

**February, 2020**

# Acknowledgements

This work has been performed under the direction of Professor Yuji Goto (Institute for Protein Research, Osaka University). I would like to express my deepest gratitude to him for guiding my work with detailed discussion and enthusiastic encouragement.

I would like to express sincere gratitude to Associate Professor Maki Onda (Osaka Prefecture University) for the many supports for experiments with OVA and a lot of helpful advice about serpin proteins.

I am deeply indebted to Professor Hironobu Hojo (Osaka University) and Assistant Professor Toshiki Takei (Osaka University) for the attentive guidance and assistance for the peptide synthesis of pOVA.

I would like to acknowledge Professor Genji Kurisu (Osaka University) and Professor Akihito Hashidzume (Osaka University) for their approving this dissertation.

I would like to express my great appreciation to Dr. Yoshihisa Hagihara (National Institute of Advanced Industrial Science and Technology) and Dr. Yoko Akazawa (National Institute of Advanced Industrial Science and Technology) for the supports for cytotoxicity measurements and supply of $C_L$ fragments. I am also deeply grateful to Professor Johannes Buchner (Technische Universität München), Professor Daniel Otzen (Aarhus University), and Professor Eri Chatani (Kobe University). They generously gifted me the purified proteins and we had fruitful discussion for the Chapter 4.

I would like to thank Senior Lecturer József Kardos (Eötvös Loránd University) and Associate Professor Kazumasa Sakurai (Kindai University) for the enthusiastic discussion about thermodynamics.

I gratefully acknowledge the warmhearted cooperation of past and present members of Professor Goto's laboratory (Laboratory of Protein Folding, Osaka University). Assistant Professor Masatomo So always helped me and drug me into the long-distance running. I would not be who I am today without him. Specially Appointed Associate Professor Kenji Sasahara and Specially Appointed Assistant Professor Keiichi Yamaguchi kindly supported my experiments. Dr. Masayuki Adachi taught me to carry out the ThT assay with heating. Ms. Sayaka Kinoshita guided me in the OVA study. Mr.

Tatsushi Samejima provided his data for the Chapter 4. Ms. Yuko Kitamura devoted herself to protein expression and purification.

Finally, I wish to thank my family and friends for their many supports and encouragement. Especially, my fiancée, Yuka, I have to give her my thanks for being so patient.

Dedicated to the memory of my late mother.



Masahiro Noji

February 2020

# Contents

**Chapter 1. General introduction** ..... 1

1.1. Anfinsen's dogma and protein misfolding ..... 2

1.2. Amyloid fibrils ..... 4

1.3. Methods for amyloid detecting ..... 7

**Chapter 2. The relationship between the amyloidogenicity of ovalbumin heated aggregates and the characteristics of serpin proteins** ..... 9

2.1. Introduction ..... 10

2.2. Materials and methods ..... 12

2.3. Results ..... 16

2.4. Discussion ..... 30

2.5. Conclusion ..... 36

**Chapter 3. The comprehension of heating-induced amyloid formation of $\beta_2$-microglobulin by thermodynamics and phase diagrams** ..... 37

3.1. Introduction ..... 38

3.2. Materials and methods ..... 41

3.3. Results ..... 43

3.4. Discussion ..... 53

3.5. Conclusion ..... 61

**Chapter 4. Combining the Anfinsen's intramolecular folding world with the supersaturation-limited intermolecular misfolding world** ..... 62

4.1. Introduction ..... 63

4.2. Materials and methods ..... 67

4.3. Results ..... 69

4.4. Discussion ..... 85

4.5. Conclusion ..... 92

**Chapter 5. Summary and conclusions** ..... 93

**References** ..... 96

**List of publications** ..... 109

# Abbreviations

| | | | |
|---|---|---|---|
| a1AC | $\alpha_1$-antichymotrypsin | LED | light emitting diode |
| a1AT | $\alpha_1$-antitrypsin | LS | light scattering |
| $A\beta_{40}$ | amyloid β 1-40 | MALDI-TOF | matrix assisted laser desorption/ionization-time of flight |
| AcCN | acetonitrile | OVA | ovalbumin |
| AFM | atomic force microscope | PAI-2 | plasminogen activator inhibitor-2 |
| αLA | α-lactalbumin | RCL | reactive center loop |
| ALS | amyotrophic lateral sclerosis | RNaseA | ribonuclease A |
| ANS | 8-anilinonaphthalene-1-sulfonate | s3A | β-strand 3A |
| αSyn | α-synuclein | SCCA | squamous cell carcinoma antigen |
| a.u. | arbitrary units | SDS | sodium dodecyl sulfate |
| β2m | $\beta_2$-microglobulin | serpin | serine protease inhibitor |
| CD | circular dichroism | TDP-43 | TAR DNA-binding protein 43 |
| $C_L$ | constant domain of immunoglobulin light chain | TEM | transmission electron microscope |
| CMC | critical micelle concentration | Tetra-P | tetraphosphate |
| $C_p$ | constant-pressure specific heat capacity | TFA | trifluoroacetic acid |
| DMSO | dimethyl sulfoxide | ThT | thioflavin T |
| DRA | dialysis-related amyloidosis | TIRFM | total internal reflection fluorescence microscope |
| DSC | differential scanning calorimetry | $T_m$ | midpoint temperature |
| FTD | frontotemporal dementia | Tris-HCl | tris(hydroxymethyl)aminomethane-HCl buffer |
| HEWL | hen egg white lysozyme | TTR | transthyretin |
| HPLC | high-performance liquid chromatography | UV | ultraviolet |
| IAPP | islet amyloid polypeptide | $V_L$ | variable domain of immunoglobulin light chain |
| IDP | intrinsically disordered protein | WST | water soluble tetrazolium salts |
| LDH | lactate dehydrogenase | | |

# Chapter 1.

## General introduction

## 1.1. Anfinsen's dogma and protein misfolding

Proteins are biosynthesized as linear polypeptide chains, made of dozens or hundreds of amino acids, following the central dogma. These nascent polypeptide chains, i.e. protein primary structures, fold into individual unique tertiary structures and function under physiological conditions. Protein's native structures are important for their proper biological activities: e.g., enzymes recognize and select substrates by their active site conformations known as the "lock and key" hypothesis. However, several stresses, such as acids, detergents, and heating collapse protein structures, lead to dysfunction. This is protein denaturation and denatured proteins are often refolded when the stresses are removed. Christian B. Anfinsen investigated reversible chemical denaturation of ribonuclease A in 1950's, and then he advocated a thermodynamic hypothesis, also known as "Anfinsen's dogma", which has been widely accepted for a long while; the information determining the native tertiary structure of a protein resides in the chemistry of its primary structure (1-4). This idea can be interpreted to suggest that proteins are spontaneously folded into the thermodynamically most stable native conformations. Thus, protein folding has been construed as a conformational transition from denatured to native states represented by Gibbs free energy change;

$$\Delta G_{Folding} = \Delta H_{Folding} - T\Delta S_{Folding}$$

where $\Delta G_{Folding}$, $\Delta H_{Folding}$, and $\Delta S_{Folding}$ are the Gibbs free energy, enthalpy, and entropy changes of folding at temperature $T$ in Kelvin, respectively (5). The folding enthalpy originates in the intramolecular interactions and the entropy corresponds to the degree of freedom, with the hydrophobic hydration of water molecules modifying these enthalpy and entropy changes. Although various intramolecular forces such as electrostatic interactions and hydrogen-bonding drive folding, hydrophobic interaction has been regarded as the dominant contributor (6,7).

Anfinsen's dogma is indeed one of the most important principles in the protein science, whereas various exceptional phenomena against it have been reported, for example protein misfolding. Although molecular chaperones and protein quality control systems work in our bodies, denatured proteins sometimes fail to regain their native structures and form conformationally distinctive misfolded aggregates under certain conditions (8,9). One of those misfolding phenomena is amorphous aggregation

characterized by the structurally non-ordered protein assembly. Amorphous aggregates can be seen in cataract eyes, in inclusion bodies, or during protein preparation (10-12). Another type of protein misfolding leads to highly-ordered filamentous aggregates, amyloid fibrils. General properties of amyloid fibrils are described in the next section 1.2. The driving forces of misfolding are identical with those of folding, thus protein misfolding can be described by a thermodynamic equation in the same manner as folding;

$$\Delta G_{Misfolding} = \Delta H_{Misfolding} - T\Delta S_{Misfolding}$$

Of course, the intermolecular interactions, not the intramolecular ones, contribute to the misfolding enthalpy. Despite a considerable number of researches, the critical controlling factor, which determines the fate of denatured proteins to undergo folding or misfolding, still remains unclear (**Fig. 1-1**). In this thesis, I tried to unveil this important factor for comprehensive understanding of protein folding and misfolding phenomena.

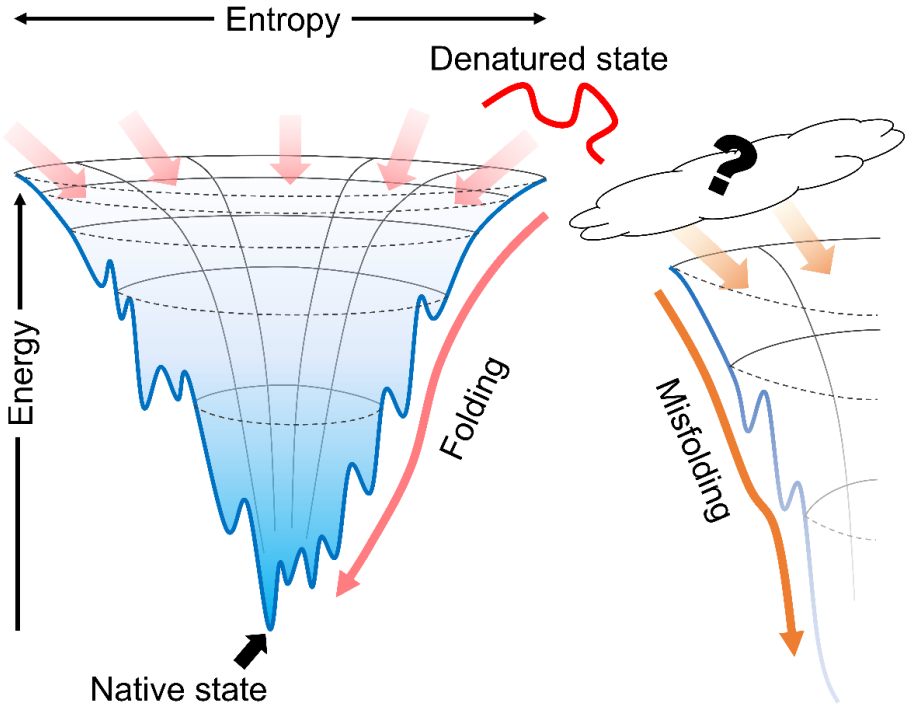



**Figure 1-1. Schematic representation of protein folding energy landscape.** The three-dimensional "folding funnel model" has been accepted rather than the simple 2D specific transition pathway model (13-16). The width and depth of the funnel mean the degree of entropy and energy (or enthalpy), respectively (17). The similar funnel can be drawn for misfolding, but the controlling factor at the crossroads is unknown.

### 1.2. Amyloid fibrils

Amyloid fibrils are highly ordered filamentous aggregates of misfolded proteins and stabilized by intermolecular cross-β structures (18,19). There are a wide range of proteins or peptides that form amyloid fibrils, while the products share several common properties such as the cross-β structure as I mentioned above. According to the X-ray fiber diffraction studies, it consists of β-sheets running parallel to the fibril axis characterized by the 4.8 Å spacing between β-strands and the 10 Å interval between stacked β-sheets (**Fig. 1-2**) (20-22). Hydrophobic residues often form the fibril core region which is stabilized by hydrogen-bonding between backbone amide N-H and C=O groups with neighboring peptide chains (23,24). Amyloid fibrils typically react with several amyloid-specific fluorescent dyes such as Congo Red and thioflavin T, because they bind to the persistent cross-β structure (25-27).

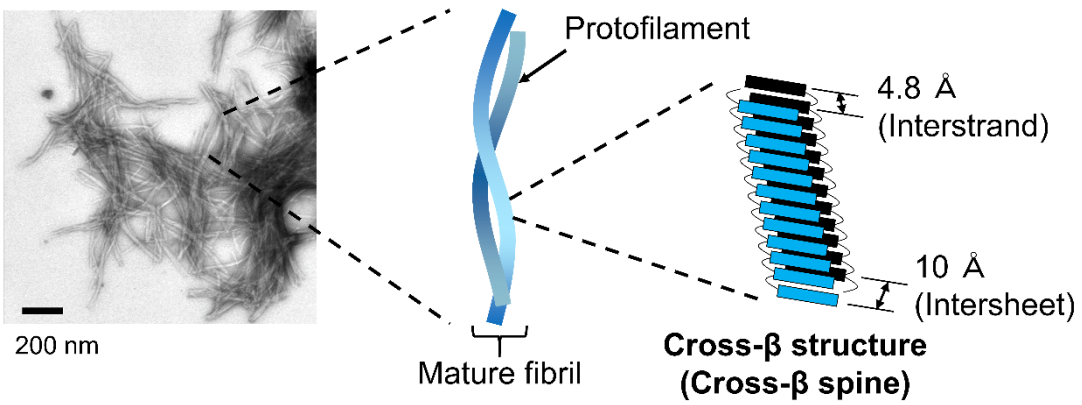



**Figure 1-2. Structural properties of amyloid fibrils.** The left panel shows the morphology of the amyloid fibrils of $\beta_2$-microglobulin by TEM. Scale bar; 200 nm. The middle panel represents a mature fibril which is composed of several thin protofilaments. The right panel illustrates a part of a protofilament "steric zipper" composed of layers of β-sheets. In these β-sheets, β-strands run perpendicular to the fibril axis in a highly-ordered manner and construct a cross-β structure.

Many fatal degenerative diseases are deeply associated with amyloid formation, for example Alzheimer's and Parkinson's diseases, senile systemic amyloidosis, and amyotrophic lateral sclerosis (28-31). The representative human amyloidoses are shown in **Table 1-1**. On the other hand, various functional amyloids have been reported such as biofilms of bacteria, spider silk, and storage of peptide hormones (32-34). These functional amyloids are thought to be essential for normal cell and tissue physiology. Moreover, some proteins or peptides can exhibit amyloid formation under particular conditions, even though they are not disease-causative or functional amyloidogenic strains.

Because of the demands for pathophysiology and nanomaterials engineering as well as that for protein basic science, amyloid formation has been investigated enthusiastically all over the world. Structure-based drug design toward remedy for amyloidoses has been carried out by the atomic resolution structural analysis of many pathogenic amyloids (35,36). Functional materials have been developed using both natural and artificial amyloidogenic peptides (37-39). However, the underlying mechanisms of amyloid formation are yet ambiguous.

Some similarities have been suggested between amyloid formation and crystallization of solutes (40,41). For example, both of their reaction kinetics are divided into three phases; a long static nucleation phase (also known as a "lag phase"), following a rapidly elongation phase, and a final plateau phase (also called an "equilibrium phase") (42). Another common feature is a seeding activity (43,44). Adding short fragmented amyloids or small crystals (i.e. seeds) into unreacting monomer solutions can skip nucleation and accelerate amyloid formation or crystallization. Furthermore, amyloid fibrils resemble crystals in presence of polymorphism (45,46). On the basis of this analogy, one possible key factor controlling amyloidogenesis (moreover misfolding) will arise; the thermodynamic solubility or the critical concentration of the monomer proteins.

One of the most important factors associated with solubility is supersaturation, which is an established concept in solution chemistry and crystallography (47,48). Under supersaturated conditions, solutes remain soluble for an extended period due to a high free energy barrier to nucleation despite the concentration of them exceeds their solubility. Then breakdown of supersaturation metastability causes a drastic phase transition and

precipitation of the solutes in the form of crystals. It has been argued that amyloids are crystal-like aggregates of denatured proteins. In the field of protein misfolding and aggregation, the importance of supersaturation has recently been reported from a pathologic perspective (49,50).

Here, in this thesis, I used various proteins such as $\beta_2$-microglobulin and conducted a series of experiments aiming to reveal a fundamental role of supersaturation in misfolding phenomena. Especially, I focused on heating and combined the Anfinsen's intramolecular folding world with the intermolecular misfolding world.

**Table 1-1. Representative human amyloidoses and associated proteins/peptides.**

| Amyloidoses | Associated proteins or peptides |
|---|---|
| Alzheimer's disease | Amyloid β |
| Parkinson's disease | α-Synuclein |
| Creutzfeldt-Jakob disease | Prion protein |
| Frontotemporal dementia | Tau |
| Huntington's disease | Huntingtin |
| AL amyloidosis | Light chain of immunoglobulin |
| AA amyloidosis | Serum amyloid A |
| Senile systemic amyloidosis | Transthyretin |
| Dialysis-related amyloidosis | $\beta_2$-Microglobulin |
| Type II diabetes | Islet amyloid polypeptide |
| Medullary carcinoma of thyroid | Calcitonin |
| Corneal dystrophy | Lactoferrin |
| Amyotrophic lateral sclerosis | Superoxide dismutase 1 |
| Injection-localized amyloidosis | Insulin |

### 1.3. Methods for amyloid detecting

According to the shared properties of amyloid fibrils, there are several common methods for detecting amyloid formation of various proteins. Thioflavin T (ThT) assay using fluorescence spectrophotometer is one of the most popular methods for following the reaction (51-53). The dye ThT binds to the amyloid cross-β structure followed by change in its fluorescence property and enhances 485 nm emission when excited by 445 nm incident light. Generally, the intensity of ThT fluorescence increases in accordance with the amyloid generation and exhibits sigmoidal profiles with the three phases as I described in the previous section 1.2. Another way of ThT assay is LED direct imaging which was reported recently (54). This method permits us simple visual amyloid detection.

Circular dichroism (CD) spectroscopy is also powerful for amyloid studies. Each type of protein secondary structures shows unique CD spectrum and amyloid formation is indicated by a β-rich spectra representing the cross-β structure (55,56). Typically, a negative peak around 220 nm and a positive peak around 200 nm are observed.

The existence of amyloids can be confirmed by microscopy such as AFM, TEM, and TIRFM (57-59). The typical amyloid fibrils exhibit rigid and straight morphologies, whereas the flexible or curvilinear filaments are also seen for many proteins (60). These morphological differences between rigid and flexible filaments are sometimes represented as “needle-like” and “noodle-like”, respectively.

In this thesis, to measure the amyloid formation, I mainly used ThT assay, CD spectroscopy, and TEM observations. The schematic representations of these methods are illustrated in **Figure 1-3**.

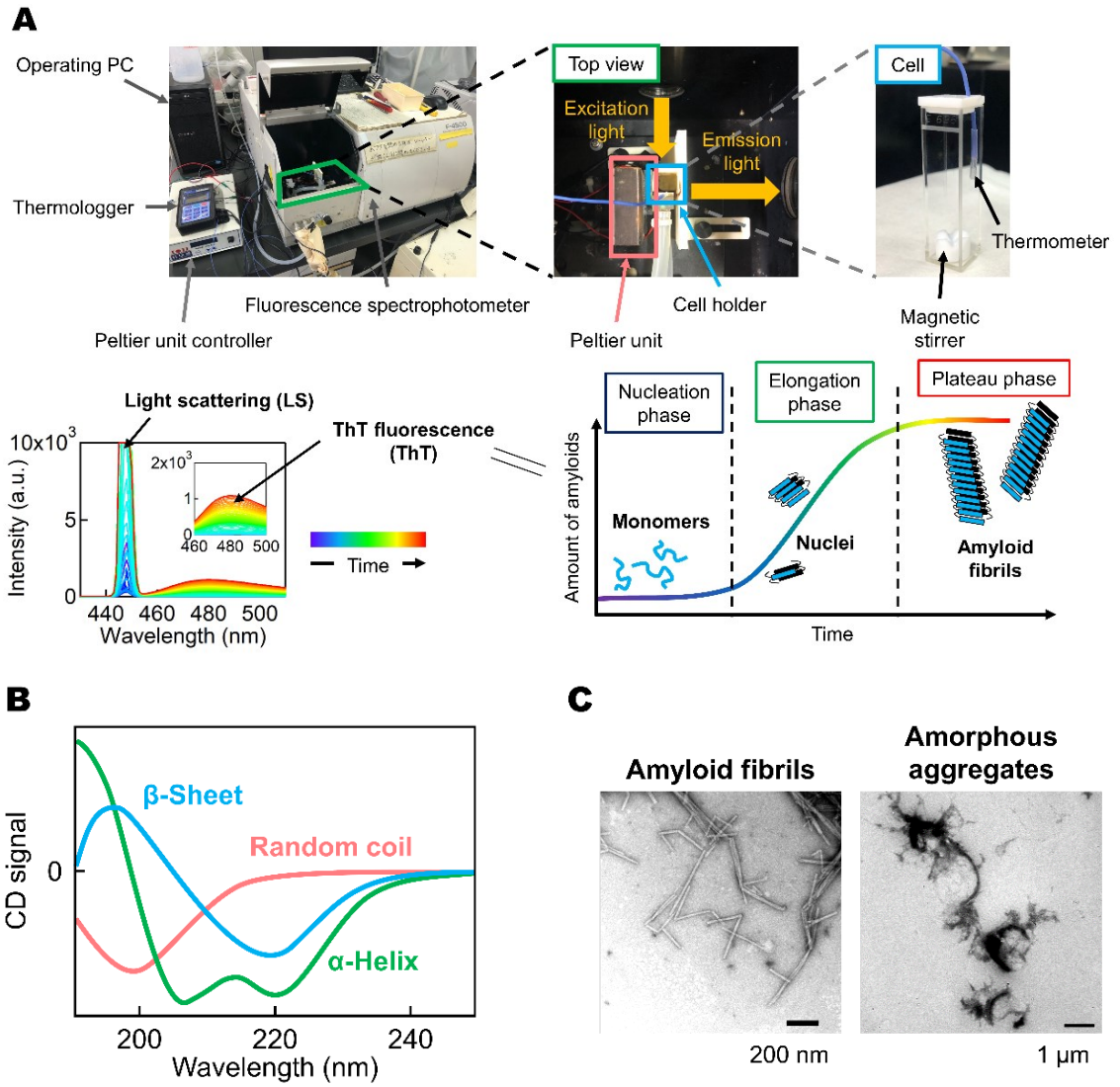



**Figure 1-3. Schematic representation of the methods for amyloid detection used in this thesis. A,** Equipment setup (upper), typical time-lapse spectra (lower left), and a representative kinetic trace (lower right) of ThT assay using fluorescence spectrophotometer. I also used other types of setup in the chapters 2 and 4. Both light scattering (LS) and ThT fluorescence (ThT) are recorded in most experiments. **B,** Typical far-UV CD spectra of random coil (red), α-helix (green), and β-sheet (blue) secondary structures. Amyloid cross-β formation is characterized by β-rich type spectra. **C,** TEM images of $\beta_2$-microglobulin amyloid fibrils (left) and ovalbumin amorphous aggregates (right). These two types of aggregates can be distinguished easily by their distinctive morphologies. Scale bars; 200 nm and 1 μm, respectively.

# Chapter 2.

## The relationship between the amyloidogenicity of ovalbumin heated aggregates and the characteristics of serpin proteins

## 2.1. Introduction

Amyloid fibrils, fibrillar aggregates of denatured proteins and peptides stabilized by intermolecular cross-β-sheets, are associated with more than 30 types of amyloidoses, including Alzheimer's and Parkinson's diseases (18,61). Amyloid fibrils are also formed by various proteins or peptides not associated with diseases (62). Thus, elucidating the mechanisms responsible for amyloid formation is important for improving our understanding of proteins as well as the development of therapeutic strategies against these diseases. Amyloid fibrils form through a nucleation and growth mechanism (43). Although spontaneous nucleation does not easily occur, resulting in a long lag time, the nucleation period is shortened or removed by the addition of preformed seeds. Spontaneous amyloid formation is accelerated by various forms of agitation, such as shaking or stirring. Ohhashi et al. previously reported that ultrasonic irradiation is one of the most effective agitations for promoting fibril formation (63). The ultrasonication-dependent acceleration of fibrillation may be linked to the formation of cavitation bubbles on which proteins are adsorbed and concentrated (64). On the basis of these findings, I revisited the classical view that amyloid formation is similar to the crystallization of solutes: amyloid fibrils form upon breaking the supersaturation of denatured proteins (40,65). Adachi et al. also investigated the role of competition between amyloid fibrils and amorphous aggregates, as observed for the crystallization of solutes, with the aim of obtaining a comprehensive understanding of the aggregation of denatured proteins (66).

Ovalbumin (OVA), a main component of egg white proteins, is a glycoprotein with a molecular weight of 45,000. Hen OVA has 385 amino acid residues, several of which are modified in addition to Asn292 glycosylation, such as the acetylation of the N-terminal Gly and phosphorylation of Ser68 and Ser344 (67,68). Although OVA has been classified as a member of the serine protease inhibitor (serpin) superfamily because of its structural homology, it is a non-inhibitory member. Moreover, serpin latency transition, a dramatic conformational change accompanied by insertion of the reactive center loop (RCL) between β-strands 3A and 5A of a five-stranded β-sheet A to form a six-stranded β-sheet A, does not happen in OVA molecules (69-72). The aggregation of serpin proteins has been extensively studied because of serpinopathies, conformational diseases caused by the polymerization of serpin proteins. In serpin polymerization, the same regions

involved in serpin latency transition (β-strands 4A and 5A) undergo β-hairpin domain-swap polymerization (73,74). The irreversible formation of polymers causes serpin deficiencies, leading to $\alpha_1$-antitrypsin deficiency emphysema, antithrombin deficiency thrombosis, or C1 inhibitor deficiency angioedema (75,76). This serpin polymerization has been recognized as a non-amyloidogenic polymerization, although there are some parallels as described below (72,77). Serpin native structure is thought to be a metastable conformational state, thus both latency transition and polymerization of serpins are the exceptional cases of Anfinsen's dogma.

Some amyloidogenicities of OVA under heating or low-pH conditions have been reported by ThT assays, CD spectroscopy, or TEM; however, the rigid and needle-like morphology typical of amyloid fibrils has not been obtained (78-81). On the basis of current advances in the study of protein aggregation as described above, OVA may provide a unique example in which the regions of amorphous aggregation and amyloid formation coexist in each molecule, illustrating a more complex system of protein aggregation for larger proteins.

To clarify the aggregation mechanism of OVA, I confirm the notable ThT fluorescence of heat-denatured intact OVA, although the apparent morphology is still amorphous. I then isolate the highly amyloidogenic peptide, pOVA corresponding to β-strand 3A, by tryptic digestion, which forms rigid and needle-like fibrils. The high amyloidogenicity of the β-strand 3A region is common to various serpin proteins. The results obtained suggest that the high amyloidogenicity of the β-strand 3A region, which is important for serpin latency transition and responsible for disease-associated serpin polymerization, is retained in OVA, a non-inhibitory serpin, leading to the formation of heat-induced amorphous aggregates with a notable amount of the amyloid component. Taken together, the results provide a new view that the β-strand 3A region in serpin molecules is a key to identifying parallels between amyloid fibrils and serpin domain-swap polymers.

## 2.2. Materials and methods

*Proteins and chemicals*

Ammonium sulfate precipitates of hen egg white OVA were dialyzed three times against 50 mM sodium phosphate buffer (pH 7.0) overnight, then centrifuged at 15,000 rpm, and filtered with a 0.22 μm mesh filter. The highly amyloidogenic peptide pOVA was synthesized as described below or purchased from Peptide Institute, Inc. (Osaka, Japan). ThT was purchased from Wako Pure Chemical Industries, Ltd. (Osaka, Japan). All other reagents, including trypsin from porcine pancreas and sodium tetraphosphate, were obtained from Nacalai Tesque, Inc. (Kyoto, Japan).

*Tryptic digestion-coupled amyloid formation*

The tryptic digestion of OVA (2 mg/mL) was performed in 25 mM Tris-HCl (pH 8.0), 100 mM NaCl, and 5 μM ThT. Trypsin from porcine pancreas was added at various ratios to OVA, and fibril formation was monitored at various temperatures between 30 and 55 ℃. A fluorescence spectrophotometer (model F7000 or F4500, Hitachi High-Technologies Corporation, Tokyo, Japan) was used; to accelerate fibril formation, the sample solution in a cuvette with a 1 cm light path was irradiated with ultrasonic pulses from an ultrasonic generator tightly attached to the sidewall of the cuvette, as reported previously (40). The solution was stirred with a stirring magnet at 600 rpm. Unless otherwise specified, ultrasonic conditions included 4 min ultrasonication and 1 min quiescence cycles. The frequency and power of the ultrasonic pulses were 27.5 kHz and 0.14 W, respectively. Fluorescence emission spectra from 440 to 560 nm were measured repeatedly with excitation at 445 nm, and 90° light scattering at 445 nm and ThT fluorescence at 485 nm were plotted. Sample temperatures were measured using a Compact Thermologger AM-8000K thermocouple (Anritsu Meter Co., Ltd., Tokyo, Japan). Although I used a water bath to maintain the temperature of the sample solution, typically at 40 ℃, the temperature increased by a few degrees during irradiation of the solution (66).

The progression of proteolysis was monitored using reversed-phase high-performance liquid chromatography (HPLC) assays. An aliquot of the reaction mixture was taken, and the reaction was quenched by mixing the sample with an excess amount

of soybean trypsin inhibitor. The decrease observed in the intensity of the intact OVA peak was plotted against the reaction time and compared with the kinetics of fibril formation monitored by the ThT assay.

*HPLC fractionation and fibrillation of OVA digests*

A 5 mg/mL OVA solution was boiled in 100 mM NaCl, 0.5 mM sodium dodecyl sulfate (SDS), and 25 mM Tris-HCl (pH 8.0) for 5 min at 100 ℃, and then trypsin was added at a final concentration of 0.25 mg/mL. The solution was incubated at 37 ℃ for 2 days. Before HPLC fractionation, 1 M HCl was added to the samples to make the final HCl concentration 0.1 M. HPLC fractionation was performed using an ÄKTA explorer 10S (GE Healthcare Life Sciences, Amersham Place, England) pumping systems with a COSMOSIL C4 reverse-phase column (5C4-AR-300, 20 mm × 250 mm, Nacalai Tesque, Inc.). Mobile phase A consisted of 0.05% (v/v) trifluoroacetic acid (TFA) in water, and mobile phase B consisted of 0.05% (v/v) TFA in acetonitrile. Linear gradients were used at a flow rate of 7 mL/min. Column effluents were monitored at 220 and 280 nm.

Lyophilized OVA fractions were dissolved at a concentration of 0.1 mg/mL in 12.5 mM Tris-HCl (pH 7.0) containing 100 mM NaCl, 0.5 mM SDS, and 5 μM ThT. Samples were agitated with 4 min ultrasonic irradiation and 1 min quiescence cycles using an ELESTEIN 07-01 (ELEKON Science Co., Ltd., Chiba, Japan) with high-amplitude ultrasonication introduced into the fluorimeter while the sample was being stirred at 600 rpm. Fibrillation was monitored by the model F4500 fluorescence spectrophotometer with excitation at 445 nm and emission at 485 nm at 37 ℃.

*CD and TEM measurements*

The protein or peptide concentrations were 0.1 or 0.2 mg/mL. Far-UV CD spectra (200–250 nm) were obtained with a model J-720 spectropolarimeter (Jasco Co., Ltd., Tokyo, Japan) at 37 ℃ using a quartz cell with a 1 mm path length. CD data were expressed as mean residue ellipticity.

TEM images were obtained using a transmission electron microscope (H-7650, Hitachi High-Technologies Corporation), as reported previously (54).

*Sequence elucidation of pOVA*

Two microliters of a highly amyloidogenic OVA fraction was mixed with 8 μL of an α-cyano-4-hydroxycinnamic acid matrix solution, and 2 μL of the sample solution was spotted onto a target plate (Bruker Daltonics, Inc., Billerica, USA). After the sample had been dried in air, mass spectra were obtained by a MALDI-TOF mass spectrometer autoflex (Bruker Daltonics, Inc.). Five microliters of the same OVA fraction was injected into the protein sequencer (PPSQ-33A, Shimadzu Co., Kyoto, Japan), and five residues were identified.

*Solid-phase peptide synthesis of pOVA and amyloid formation*

pOVA peptides were synthesized using an automated microwave peptide synthesizer Liberty Blue (CEM Co., Matthews, USA). Synthesis was started with 0.1 mmol of Fmoc-Lys(Boc)-Wang resin LL (Merck KGaA, Darmstadt, Germany). After synthesis, the resin was washed with $CH_2Cl_2$ and methanol three times each, followed by vacuum drying overnight. Synthesized polypeptides were cleaved from the dried resin with a TFA cocktail containing TFA, $H_2O$, and triisopropylsilane [95:2.5:2.5 (v/v)] at room temperature for 2 h. The product was filtered with cotton wool and concentrated with nitrogen gas blowing. Crude pOVA was then precipitated with diethyl ether and moderately centrifuged. The pellet was washed with diethyl ether three times and then subjected to air drying. pOVA was purified from the dried pellet using the ÄKTA explorer 10S with a COSMOSIL C18 reverse-phase column (5C18-AR-II, 20 mm × 250 mm, Nacalai Tesque, Inc.) in the same manner that was used for the fractionation of digested OVA and confirmed by autoflex.

Lyophilized pOVA peptides were dissolved at a concentration of 1.0 mg/mL in dimethyl sulfoxide (DMSO) and diluted to 0.1 mg/mL by an injection with a syringe into the cuvette. Sample solutions contained 40% (v/v) DMSO, 12.5 mM Tris-HCl (pH 8.0), 100 mM NaCl, 0.5 mM SDS, and 5 μM ThT. Amyloid formation was monitored by the F4500 fluorometer with excitation at 445 nm and emission at 485 nm at 37 ℃.

*Aggregation of digested OVA*

Approximately 3 mg/mL OVA solutions were boiled at 100 ℃ for 5 min, and trypsin was then added in an amount that was 1/20 (w/w) of the amount of OVA. Solutions were incubated at 37 ℃ for 2 days for complete digestion. Digested OVA solutions were diluted to 2.0 mg/mL in 20 mM Tris-HCl (pH 8) or 10 mM HCl, including various concentrations of NaCl, SDS, or tetraphosphate. Samples in a cuvette of the model F7000 or F4500 fluorescence spectrophotometer were agitated with 1 min ultrasonic irradiation and 4 min quiescence cycles while being stirred at 600 rpm. The extent of aggregation was monitored by ThT fluorescence at 485 nm with excitation at 445 nm at 37 ℃.

*Visual imaging of aggregates*

Direct photographic images of turbidity and ThT fluorescence were obtained under the illumination of microplate samples using white and blue LED light at 440 nm, respectively, as reported previously (54).

*Cytotoxicity of OVA and pOVA aggregates*

To measure the cytotoxicity, LDH and WST assays were performed using murine colon cancer cells (Colon-26, RIKEN BioResource Center, Tsukuba, Japan), as previously reported (82). The solutions of intact OVA, trypsin-digested samples, or pOVA in amyloidogenic and non-amyloidogenic forms were prepared. Control series did not contain proteins or peptides.

## 2.3. Results

*Heat-induced aggregation of intact OVA*

I examined the effects of heat on intact OVA at 2 mg/mL in 0.1 M NaCl at pH 8.0 (**Fig. 2-1A, B**). When samples were heated at a rate of 1 ℃/min, light scattering increased at approximately 75 ℃, indicating heat denaturation-coupled aggregation. The heat-induced aggregation of OVA was previously reported to be linked to the denaturation of OVA, as monitored by the CD intensity at 222 nm (78). A small increase in ThT fluorescence at 485 nm was observed at 75 ℃, which then decreased at higher temperatures. With a decrease in temperature, the ThT fluorescence markedly increased, demonstrating the temperature dependence of intrinsic ThT fluorescence. Repeated increases and decreases in temperature reproduced the previous curves of ThT fluorescence, showing that heat-induced aggregates with the amyloid component remained stable during subsequent decreases and increases in temperature. The light scattering of heat-induced OVA aggregates remained high, confirming that once aggregates formed, they did not dissolve during cooling and heating cycles.

To further confirm these heat effects, intact OVA was incubated at 100 ℃ for 5 min in the presence of various concentrations of NaCl and fluorescence spectra were measured after samples had cooled to 37 ℃ (**Fig. 2-1C**). Even in the absence of NaCl, heat-treated OVA showed ThT fluorescence with a maximum at approximately 485 nm as well as strong light scattering at 445 nm. With an increase in the NaCl concentration, light scattering at 445 nm increased and ThT fluorescence at 485 nm decreased. The observed decrease in ThT fluorescence with an increase in NaCl concentration might be caused by the strong absorbance and light scattering of aggregates, preventing proper excitation within the observation window of the fluorometer (83). Thus, I examined the ThT fluorescence of heat-induced OVA aggregates by the direct imaging methodology with an LED lamp at 440 nm, which Nitani et al. developed previously (54).

A series of heat-treated OVA samples in the presence of various concentrations of NaCl at pH 8.0 were visualized under LED illumination at 445 nm as well as under white light (**Fig. 2-1C**). I observed notable ThT fluorescence for the aggregates, particularly at high concentrations of NaCl. These aggregates showed turbid images under white light. Similar ThT fluorescence upon heating of intact OVA was observed in the

presence of various concentrations of SDS (**Fig. 2-1D**) or sodium tetraphosphate (**Fig. 2-1E**) when monitored by the fluorometer or direct ThT imaging. The effects of SDS and tetraphosphate will be discussed below (see below).

To validate the notable ThT fluorescence of heat-treated OVA, a series of hen egg white lysozyme (HEWL) samples were prepared at various concentrations of NaCl in 10 mM HCl at 60 ℃ with or without the ultrasonic treatment, with HEWL initially being heat-denatured. Consistent with the previous reports (54), the ultrasonic treatment induced amyloid fibrils and then amorphous aggregates with increases in the concentration of NaCl, as confirmed by the fluorometer and LED imaging (**Fig. 2-1F**). Upon incubation at 60 ℃ without ultrasonication, only amorphous aggregates were induced at high NaCl concentrations (**Fig. 2-1F**).

These results confirmed that marked ThT fluorescence observed for heat-treated OVA was specific to OVA, as reported previously (78); however, the apparent decrease in ThT fluorescence at high concentrations of NaCl monitored by the fluorometer (**Fig. 2-1C**) appeared to be caused by strong absorption (83). Thus, LED imaging showed the ThT fluorescence of heat-aggregated OVA more clearly than the fluorometer did.

However, the maximal ThT fluorescence intensity observed for OVA at 2 mg/mL under the instrumental conditions was 150, approximately 50% of that of HEWL fibrils at 0.2 mg/mL (**Fig. 2-1**). Assuming the same weight concentration for the two proteins, the ThT fluorescence of heat-treated OVA was approximately 1/20 of that of HEWL fibrils, suggesting that although heat-treated OVA contained a ThT-positive amyloid component, their fraction was at most 1/20 of the entire OVA molecule. Only particular region(s) of the OVA molecule appeared to form fibrils upon being subjected to heat treatment.

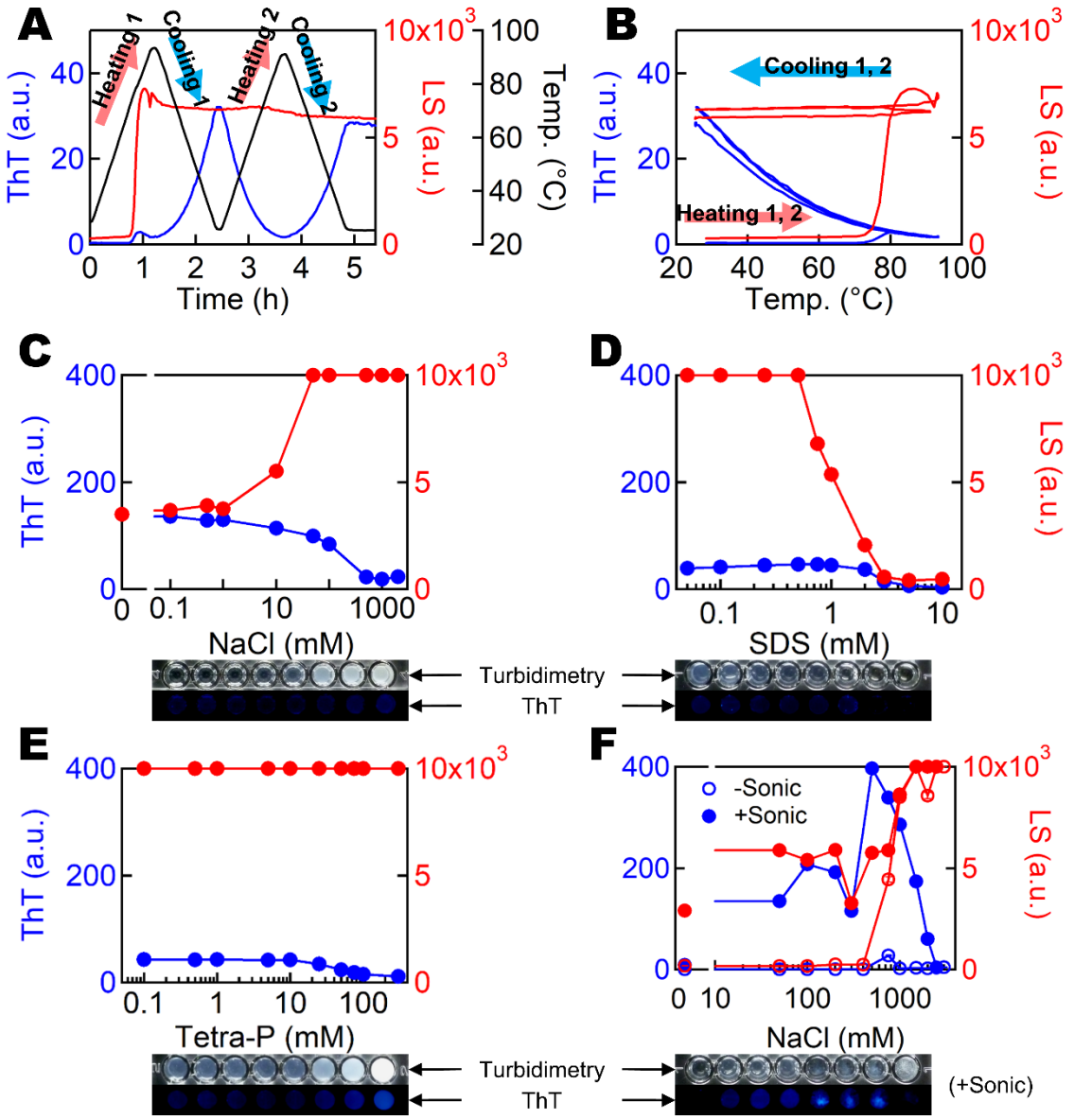



**Figure 2-1. Heat-induced aggregation of intact OVA at pH 8. A, B,** Effects of heat on intact OVA at 2 mg/mL in 0.1 M NaCl at pH 8.0 monitored by LS at 445 nm and ThT at 485 nm. Increases and decreases in temperature were repeated as indicated by the arrows. **C-E,** Dependence of the LS and ThT of heat-treated OVA samples on the NaCl (C), SDS (D), or sodium tetraphosphate (E) concentration. OVA samples (2.0 mg/mL) at pH 8.0 were boiled at 100 ℃ for 5 min, and fluorescence spectra were recorded at 37 ℃. **F,** Dependence of the LS and ThT of HEWL treated at 60 ℃ in the absence or presence of ultrasonic irradiation on the NaCl concentration. Direct turbidimetric and ThT fluorescence photographic images are also shown in panels C-F.

I examined the CD spectra and TEM images of heat-treated OVA after decreasing the temperature (**Fig. 2-2**). The CD spectra at low NaCl concentrations showed a slight change from that of native OVA, and it was not possible to obtain spectra at high salt concentrations correctly because of severe turbidity. TEM showed amorphous aggregates without fibrillar images typical for amyloid fibrils. These results were consistent with the partial formation of amyloid fibrils in heat-treated OVA, suggesting that morphological data are not sufficient to confirm the involvement of a small fraction of the fibrillar component.

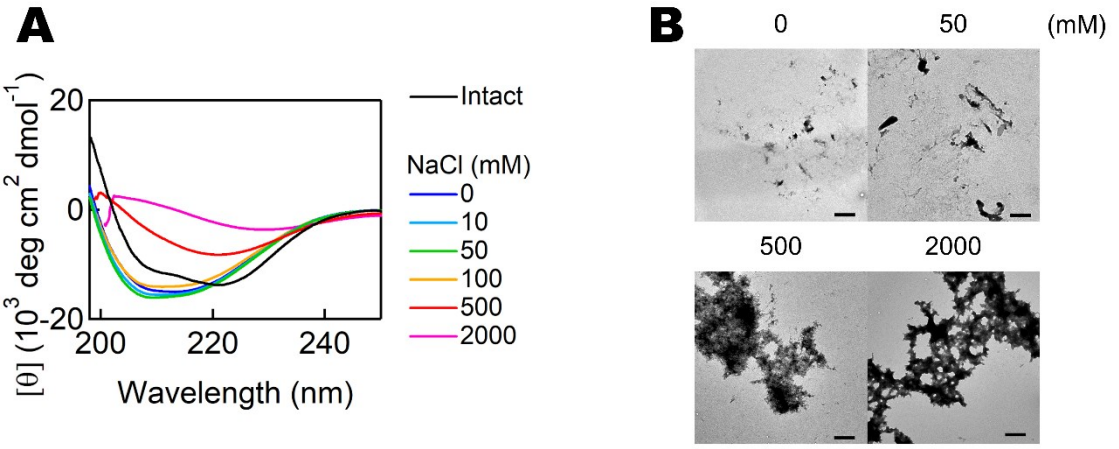



**Figure 2-2. Secondary structures and morphologies of heat-treated OVA. A,** CD spectra of intact OVA samples at various NaCl concentrations. OVA samples at pH 8.0 were heated at 100 ℃ for 5 min and CD spectra were measured at 37 ℃. **B,** TEM images of heat-treated OVA samples at various NaCl concentrations.

*Tryptic digestion-coupled amyloid formation*

I found that the tryptic digestion of intact OVA (2.0 mg/mL) at 30–55 ℃ in the presence of 0.5 mM SDS under ultrasonication markedly increased ThT fluorescence, at which the OVA:trypsin weight ratio was 1:0.05 (**Fig. 2-3**). The 0.5 mM SDS was added because the acceleration of amyloid formation in the presence of SDS at a concentration slightly lower than the critical micelle concentration (CMC) value was reported for several proteins (84,85). Ultrasonication was also employed to further accelerate fibril formation (86). The ThT fluorescence intensity of tryptic digestion-coupled fibrils was approximately 2-fold larger than that of heat-treated intact OVA aggregates. The reaction became faster with an increase in temperature (**Fig. 2-3D**).

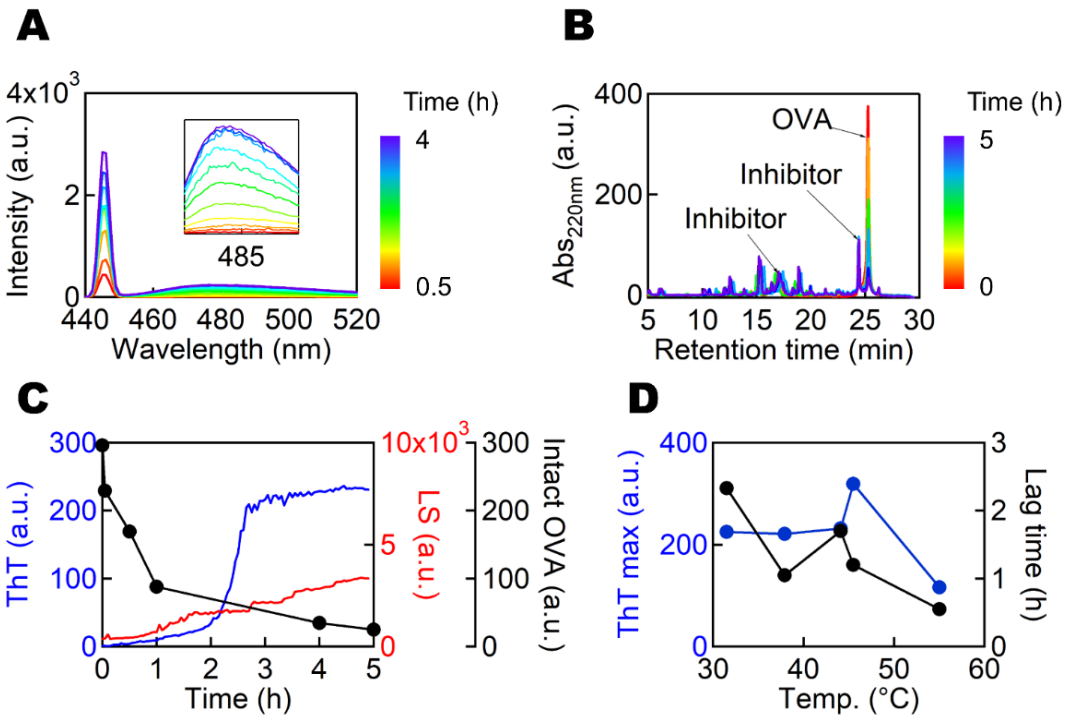



**Figure 2-3. Amyloid fibril formation of OVA coupled with tryptic digestion at various temperatures. A, B,** Tryptic digestion of OVA (2.0 mg/mL) at 45 ℃ and pH 8.0 was monitored using a fluorometer by repeated measurements of fluorescence spectra (A) or an HPLC analysis of digests taken from the fluorometer cell (B). The OVA:trypsin weight ratio was 1:0.05. In panel B, the elution positions of intact OVA and the soy bean trypsin inhibitor are indicated. **C,** Aggregation kinetics monitored by ThT and LS at 45 ℃. **D,** Dependences of the maximal ThT and lag time on temperature.

To elucidate the mechanisms underlying tryptic digestion-coupled fibril formation, I performed the reaction at a constant OVA concentration (2 mg/mL) with varying OVA:trypsin weight ratios from 1:0.00125 to 1:0.5 at 40 ℃. Fibril formation occurred over a wide range of OVA:trypsin ratios (**Fig. 2-4**). Even at the lowest OVA:trypsin ratio of 1:0.00125, the lag time and maximal ThT intensity were similar to those at an OVA:trypsin ratio of 1:0.075 (**Fig. 2-4C**). In contrast, at high concentrations of trypsin, the final ThT intensity decreased, although the lag time remained short (**Fig. 2-4B, C**). LED images were consistent with those obtained with the fluorometer (**Fig. 2-4C**).

The progression of tryptic digestion was monitored by HPLC. At an OVA:trypsin weight ratio of 1:0.05 and 45 ℃, the decrease in the level of intact OVA occurred slightly before fibril formation (**Fig. 2-3C**). This consistency was also observed for the lower trypsin concentration (**Fig. 2-4A**). At an OVA:trypsin weight ratio of 1:0.5, the digestion kinetics was slightly faster than those at lower trypsin concentrations and fibrils were not formed effectively (**Fig. 2-4B**). These results suggest that the tryptic digestion of OVA, which was not dependent on trypsin concentration, occurred prior to fibril formation; however, an excessively high trypsin concentration prevented fibril formation.

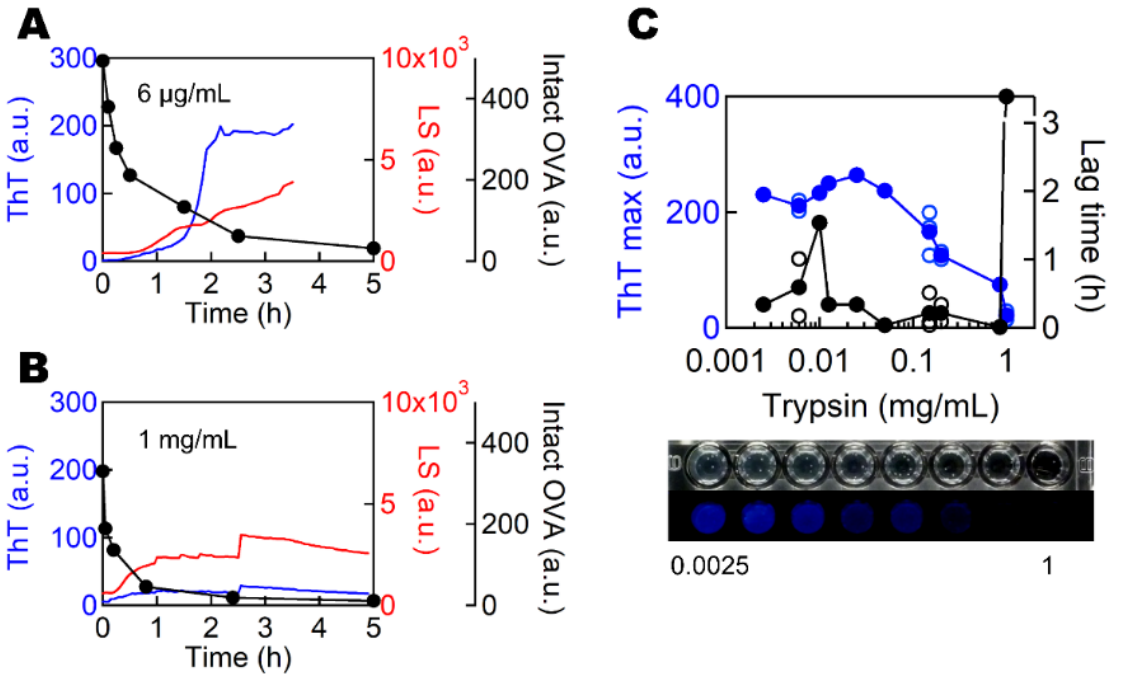



**Figure 2-4. Amyloid fibril formation of OVA (2.0 mg/mL) coupled with tryptic digestion at various trypsin concentrations at pH 8.0 and 40 ℃. A, B,** Fibril formation monitored by ThT and LS are compared with the progression of the tryptic digestion of OVA (filled circles). The OVA:trypsin weight ratio was 1:0.003 (A) and 1:0.5 (B). **C,** Dependence of the ThT maximal intensity and lag time on trypsin concentration (upper). When multiple measurements were performed, filled symbols indicate the average values and empty symbols indicate the observed data. Direct turbidimetric and ThT fluorescence photographic images are also shown (lower).

*Isolation of a highly amyloidogenic peptide*

To identify amyloidogenic region(s), a mixture of tryptic digests of OVA was separated by reverse-phase HPLC into seven fractions (**Fig. 2-5A-C**). The ThT assay of each fraction revealed the high amyloidogenicity of fraction 5. When fraction 5 was divided into two, fraction 5b retained high amyloidogenicity. The CD spectrum typical for the β-structure (**Fig. 2-5E**) and TEM image with the straight fibrillary morphology (**Fig. 2-5F**) revealed the formation of amyloid fibrils. Mass spectrometry indicated a mass of ~2.46 kDa, and peptide sequencer analysis showed that the N-terminal sequence was "NVLQP". Taken together, tryptic digestion produced a 23-residue amyloidogenic peptide, N159-K181, which I call "pOVA" (**Fig. 2-5G**). pOVA corresponds to β-strand 3A (s3A), one of the two β-strands forming a "serpin shutter region" among a five-stranded β-sheet running parallel to the long axis (A-sheet) of the OVA molecule (87).

I synthesized this peptide. HPLC analysis confirmed that the elution time of the synthesized pOVA was the same as that of the amyloidogenic peptide isolated from OVA. When the amyloidogenicity of synthesized pOVA was examined under aqueous conditions, it aggregated rapidly. I then dissolved pOVA in DMSO because DMSO is known to interfere with the protein hydrogen bond network and cause the disassembly of various amyloid fibrils (88,89). DMSO at high concentrations prevented pOVA from forming fibrils. The kinetics of pOVA amyloid formation at 0.1 mg/mL was followed in 40% (v/v) DMSO containing 100 mM NaCl, 0.5 mM SDS, and 5 μM ThT at pH 8.0 and 37 ℃ without agitation and was completed in ~10 min (**Fig. 2-5D**). The formation of amyloid fibrils was confirmed by TEM (**Fig. 2-5F**) and LED imaging (**Fig. 2-5D**). Because of strong absorption, the CD spectrum was not obtained in the presence of DMSO. I then dissolved pOVA at 0.1 mg/mL in 10 mM NaOH. The CD spectrum in 10 mM NaOH indicated the β-sheet structure typical for amyloid fibrils (**Fig. 2-5E**).

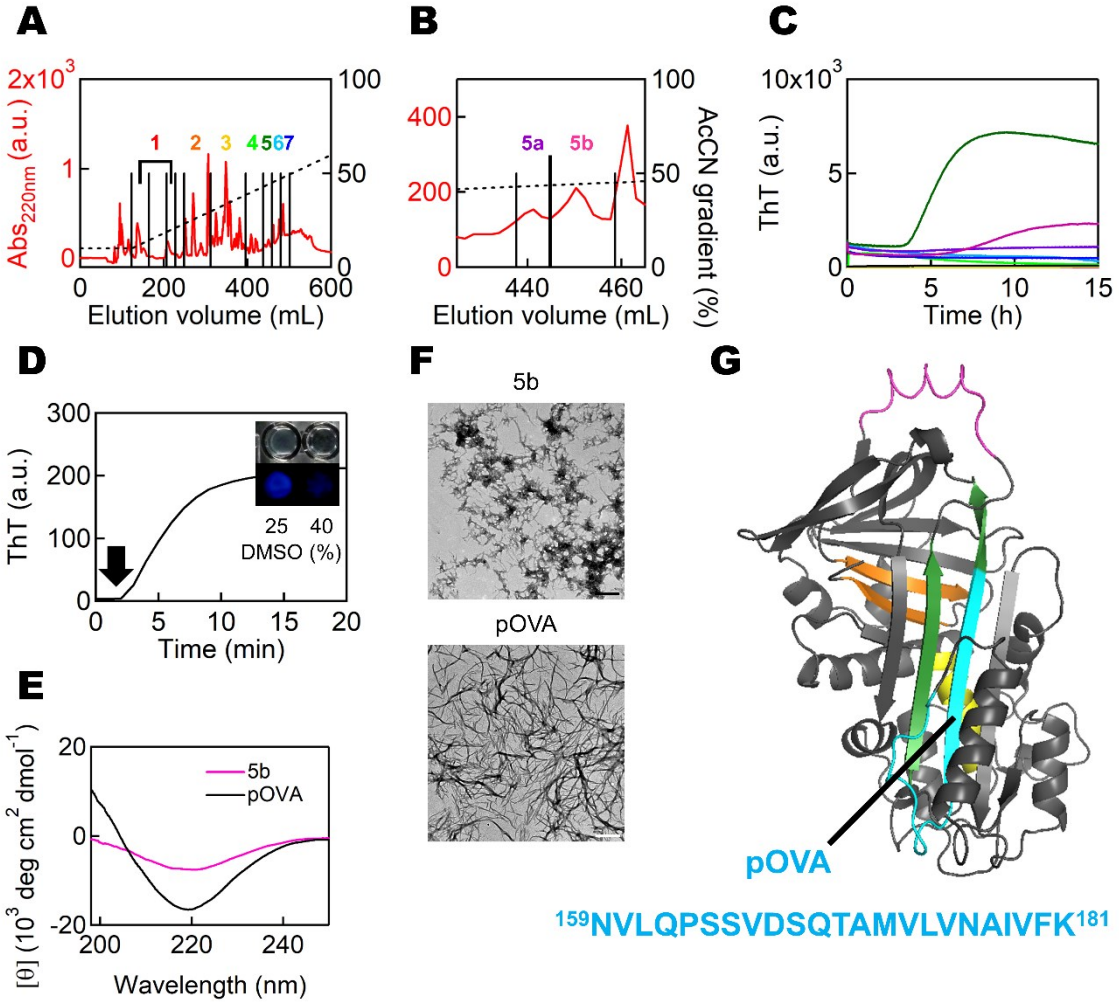



**Figure 2-5. Isolation of a highly amyloidogenic OVA peptide. A,** Reverse-phase HPLC analysis of tryptic digests of OVA in seven fractions. **B,** HPLC separation of fraction 5 into two fractions. **C,** Amyloid assays of HPLC-separated tryptic digests. **D,** Amyloid assay of pOVA in 40% (v/v) DMSO. The arrow indicates the time at which pOVA was added. Direct turbidimetric and ThT fluorescence photographic images of pOVA fibrils in 40 and 25% (v/v) DMSO are shown. **E, F,** CD spectra and TEM images, respectively, of fibrils formed by fraction 5b and synthetic pOVA. **G,** Three-dimensional structure of hen egg OVA with pOVA colored cyan. The sequence of pOVA is shown. Other key regions are also highlighted; helix B (yellow), shutter strands (green), RCL (magenta), s4B (orange), and s5B (orange).

*Effects of additives on the aggregation of OVA tryptic digests at pH 2*

Although the amyloid components of heat-induced OVA aggregates were partly resistant to proteolysis, they were finally digested with trypsin. In the latter experiments with mixtures of tryptic digests, they were prepared by incubating 2 mg/mL OVA with trypsin at a weight ratio of 1:0.05 at 37 ℃ for 2 days. I examined the effects of NaCl, SDS, and sodium tetraphosphate (Tetra-P) because these additives have been reported to promote the formation of amyloid fibrils (84,90,91). The formation of fibrils with a mixture of complete tryptic digests at pH 8 and 37 ℃ was not clear, although fibrils were observed by TEM under certain conditions in the presence of NaCl or SDS (data not shown).

I then studied the aggregation of OVA and its tryptic digests in 10 mM HCl ("pH 2" condition) because amyloid fibril formation was often promoted under acidic conditions, under which peptides have positive charges (92). While pOVA has a 0 net charge at pH 7 (two amino groups and two carboxylic groups), the net charge is +2 at pH 2.

*The effect of NaCl.* A mixture of OVA tryptic digests in 10 mM HCl was incubated under ultrasonication at 37 ℃ in the presence of various concentrations of NaCl. Without NaCl, OVA digests did not exhibit ThT fluorescence, while samples in the presence of NaCl showed time-dependent increases in ThT fluorescence (**Fig. 2-6A, B**). The final ThT fluorescence and light scattering intensities after several hours increased with an increase in NaCl concentration. In contrast, the lag time became shorter with an increase in NaCl concentration. CD spectra showed the formation of β-sheet structures at all NaCl concentrations (**Fig. 2-6C**). TEM images indicated thin fibrils even in the absence of NaCl and a large amount of fibrillar aggregates at 750 mM NaCl (**Fig. 2-6D**). LED images confirmed the formation of fibrils at high NaCl concentrations (**Fig. 2-6A**). Altogether, NaCl promoted the formation of fibrils.

*The effect of SDS.* When the effects of SDS were examined, the intensities of ThT fluorescence markedly increased at approximately 0.5 mM SDS with a shortened lag time (**Fig. 2-6E, F**). On the other hand, 10 mM SDS completely inhibited amyloid formation and stabilized the α-helical structure (**Fig. 2-6G**). TEM images in 0.5 mM SDS showed a large amount of thick fibrils and long thin fibrils remained in 10 mM SDS (**Fig.**

**2-6H**). The LED images confirmed the formation of fibrils most notably between 0.5 and 1.0 mM SDS (**Fig. 2-6E**).

I examined the CMC of SDS under pH 2 conditions because it might differ from the value (i.e., 0.5 mM) at neutral pH. The solution of 50 μM 8-anilinonaphthalene-1-sulfonate (ANS) in 20 mM HCl, 100 mM NaCl, and various concentrations of SDS (0–5 mM) was prepared. ANS fluorescence increased with higher SDS concentrations, and a point of inflection was noted, which indicated that the CMC was 1.13 mM, which was slightly larger than that at neutral pH (data not shown).

*The effect of tetraphosphate.* I examined the effects of sodium tetraphosphate at pH 2 (**Fig. 2-6I, J**). Although low (5 mM) and high (300 mM) concentrations of Tetra-P significantly promoted amyloid formation, intermediate concentrations (25–150 mM) did not induce amyloid fibrils. The CD spectrum of OVA mixtures in 5 mM Tetra-P exhibited a typical β-sheet conformation, while those in 25–150 mM Tetra-P showed a disordered structure (**Fig. 2-6K**). Consistent with CD results, TEM images showed thick fibrils in 5 and 300 mM Tetra-P (**Fig. 2-6L**). The LED images confirmed the formation of fibrils in the presence of low concentrations of Tetra-P (i.e., approximately 5 mM) (**Fig. 2-6I**).

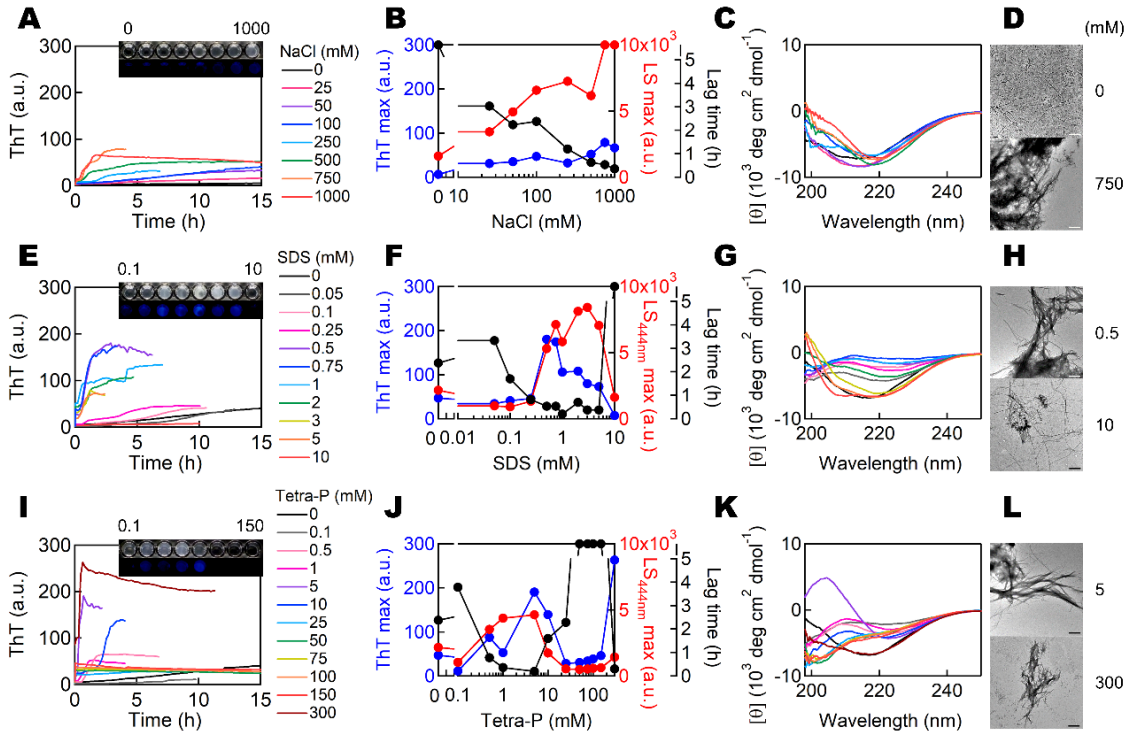



**Figure 2-6. Effects of additives on the aggregation of OVA tryptic digests in 10 mM HCl at 37 °C.** The additives are **A-D,** NaCl, **E-H,** SDS, and **I-L,** Tetra-P. **A, E, and I,** Aggregation kinetics monitored by ThT at 485 nm. Direct turbidimetric and ThT fluorescence photographic images are included. **B, F, and J,** Dependence of ThT, LS, and lag times on additive concentration. **C, G, and K,** CD spectra in the presence of various concentrations of additives. **D, H, and L,** Typical TEM images.

*Cytotoxicity of OVA and pOVA*

I examined the cytotoxicities of various OVA and pOVA samples (**Fig. 2-7A, B**). To measure cytotoxicity, LDH and WST assays were performed using murine colon cancer cells, as described previously (82). Among various samples, only heat- or SDS-induced aggregates of intact OVA exhibited cytotoxicity in both assays. Because the major components of these aggregates are amorphous aggregates and the fibrils of pOVA did not show notable cytotoxicity, the amyloid components of OVA, in either intact OVA or isolated peptides, were not toxic, in contrast to amorphous aggregates. Consistent with this result, the CD spectra of toxic samples (heat-denatured OVA aggregates) did not clearly exhibit the β-sheet component (**Fig. 2-7C, D**).

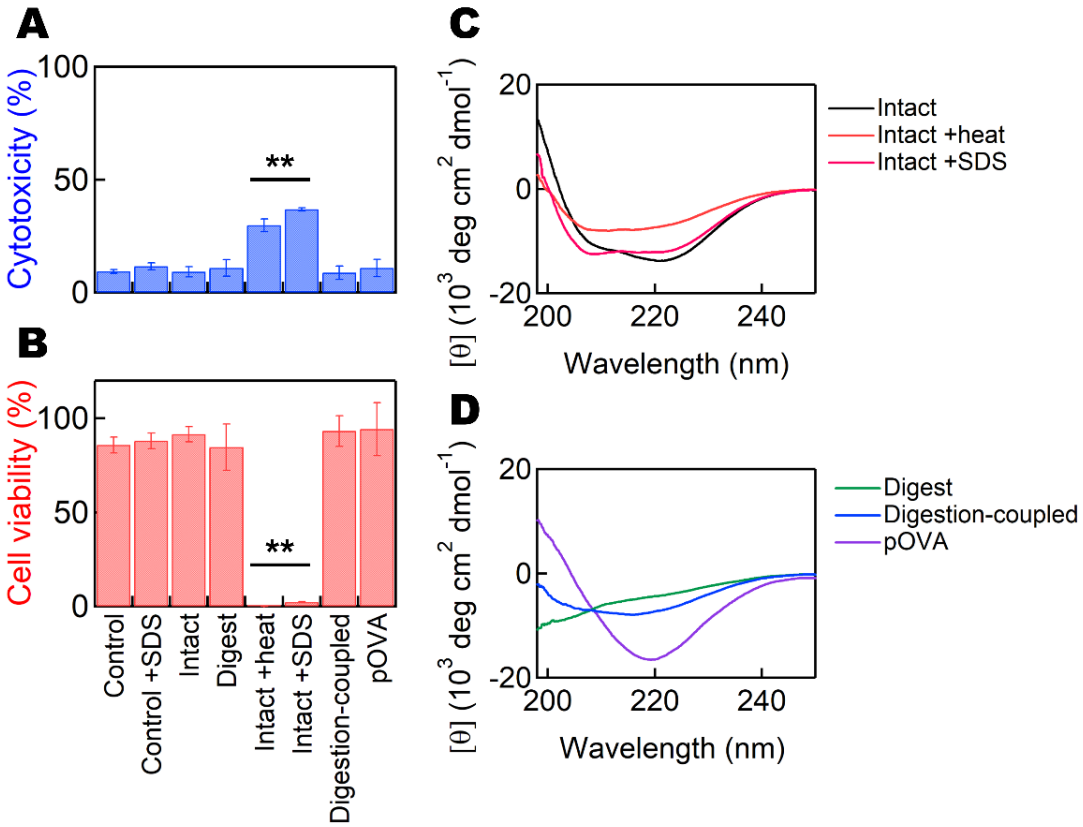



**Figure 2-7. Cytotoxicity of OVA and pOVA aggregates.** Cytotoxicity was examined by **A,** LDH and **B,** WST assays with murine colon cancer cells, as previously reported (82). OVA solutions at 2.0 mg/mL were prepared under the following conditions. Control and Control +SDS: 20 mM Tris-HCl (pH 8) and 100 mM NaCl at 0 or 0.5 mM SDS without OVA. Intact: intact OVA (2.0 mg/mL) in the buffer. Digest: tryptic digests of heat-treated intact OVA. Intact+heat: heattreated intact OVA at 100 ℃ for 5 min. Intact+SDS: heat-treated intact OVA in 0.5 mM SDS at 100 ℃ for 5 min. Digestion-coupled: tryptic digestion-coupled amyloid fibrils. pOVA: pOVA dissolved at a concentration of 1.0 mg/mL in 10 mM NaOH and diluted to 0.1 mg/mL with 20 mM Tris-HCl (pH 8) and 100 mM NaCl. Except for pOVA, samples were incubated for 2 days. pOVA was used without being incubated because of rapid amyloid formation. ** $p < 0.005$. **C, D,** CD spectra of samples used for cytotoxicity assays.

## 2.4. Discussion

*Amyloidogenicity and structural model of heat aggregates of OVA*

Amyloidogenic proteins and peptides are often relatively short in length, up to approximately 200 amino acid residues (e.g., HEWL, 129 amino acids; $\beta_2$-microglobulin, 99 amino acids; insulin, 51 amino acids), or peptides produced from larger precursor proteins (e.g., amyloid β, 40–42 amino acids; islet amyloid polypeptide, 37 amino acids). Thus, although previous studies have suggested amyloid formation of OVA, their validity remains unclear (78,93,94). Kawachi et al. reported that heat-treated OVA showed notable ThT fluorescence in contrast to heat-treated HEWL or ovotransferrin (95). To investigate the amyloidogenicity of OVA, I repeated their experiments and confirmed strong ThT fluorescence upon heat denaturation of intact OVA using the fluorometer and direct imaging with LED (**Fig. 2-1**).

However, the ThT fluorescence intensity was markedly weaker than that of HEWL fibrils. Assuming the same weight concentration, it was 1/20 of that of HEWL fibrils. The overall amorphous-like morphology suggested a structural model in which a particular region made of a relatively small number of amino acid residues forms amyloid cores, while the rest of the molecule is disordered or aggregated amorphously, as suggested by the β-spine amyloid model (**Fig. 2-8**)(96,97). Thus, although heat-treated OVA exhibited marked ThT fluorescence, the overall structure and morphology were amorphous-like.

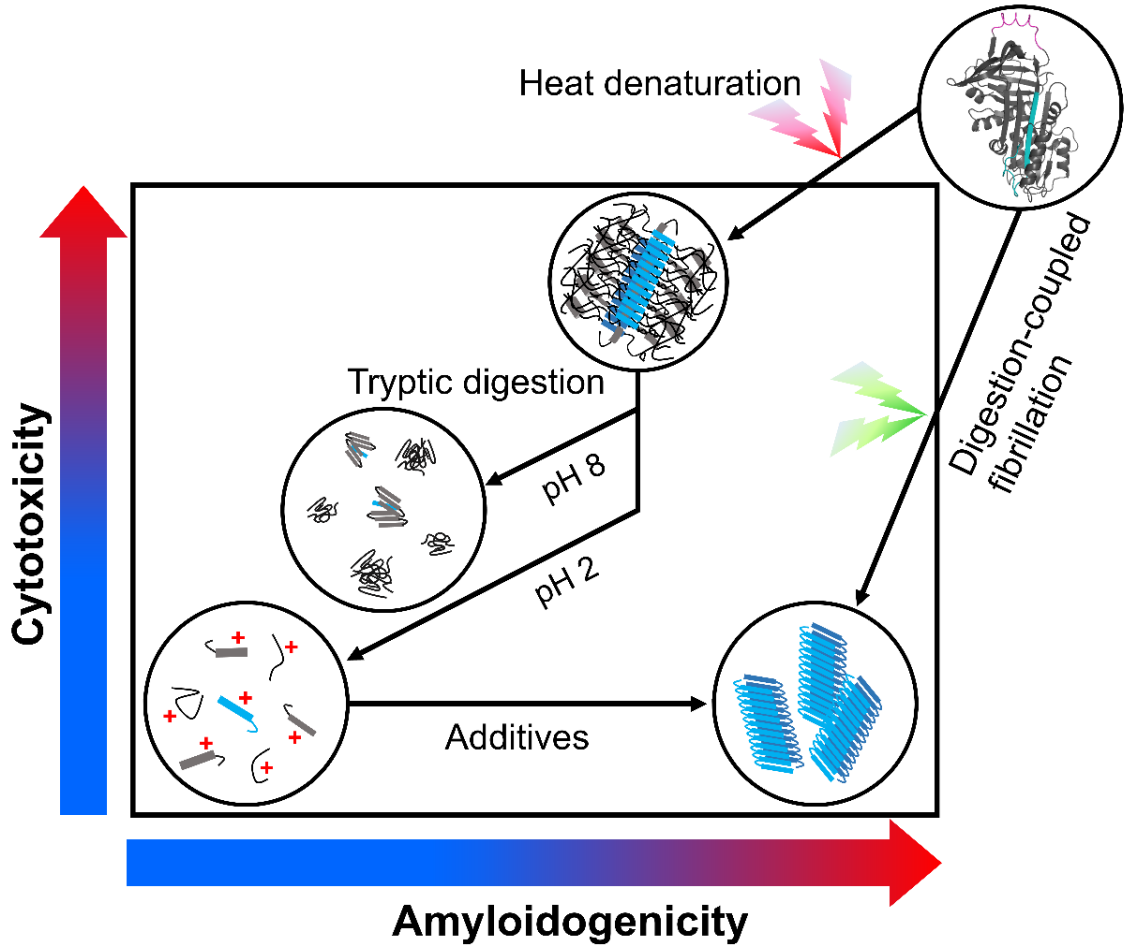



**Figure 2-8. Schematic diagram of aggregation of OVA coupled with heat denaturation or tryptic digestion.** Conformational states are located depending on the degrees of cytotoxicity and amyloidogenicity

*High amyloidogenicity of pOVA*

I then isolated the highly amyloidogenic peptide pOVA from a mixture of tryptic digests. The sequence of pOVA (i.e., N159–K181) corresponds to one (s3A) of two β-strands constituting the serpin shutter region (**Fig. 2-5**). β-Strand 3A and the connecting loop between β-strand 3A and helix F play a key role in both the latency transition and β-hairpin domain-swap polymerization, leading to serpinopathies (73,74,87,98). In the latency transition, an exposed and mobile RCL is inserted between the two β-strands of the shutter region. Although neither the latent form nor the domain-swapped polymer has been reported for a non-inhibitory serpin OVA, a mutation study suggested that OVA has the potential to attain a hyperstable RCL-inserted form (99). This indicates that β-strand 3A of OVA can potentially contribute to stabilizing RCL-inserted forms in domain-swapped polymers.

All aggregation propensities estimated by Aggrescan (100) or Tango (101) and the intrinsic solubility estimated by CamSol (102) predicted the marked amyloidogenicity and insolubility of the pOVA region (s3A) for OVA and other serpin proteins: $\alpha_1$-antitrypsin (a1AT), $\alpha_1$-antichymotrypsin (a1AC), plasminogen activator inhibitor-2 (PAI-2), and squamous cell carcinoma antigen (SCCA) (**Fig. 2-9**). The amyloidogenicity of OVA was higher than those of HEWL and $\beta_2$-microglobulin, typical amyloidogenic proteins. An interesting scenario is that the β-strand 3A, which is important for latency transition and polymerization, constituted β-spine amyloid cores when OVA was heat-aggregated. However, the reaction was hindered more by the dominant non-amyloidogenic regions than the fibril formation of isolated pOVA was (**Fig. 2-8**).

The aggregation propensities (**Fig. 2-9**) also show high amyloidogenicity in the regions of helix B and C-terminal β-strands 4B and 5B, consistent with a previous study with OVA by Tanaka et al. (94) These regions have been considered to have crucial roles in serpin polymerization (74,103,104). My observations suggest that these regions contribute to polymerization through high aggregation propensities as revealed by predictions. Among the five serpin proteins that have had their aggregation propensities analyzed, $\alpha_1$-antichymotrypsin is a rare inhibitory serpin that accelerates amyloid fibril formation of apolipoprotein C-II (105). It is possible that the pOVA (s3A) region of $\alpha_1$-antichymotrypsin plays an important role in the acceleration.

Pathogenic polymers of serpins have been recognized as being non-amyloidogenic, and thus, serpinopathies have been distinguished from amyloid diseases (72,77). However, there are clear parallels between serpinopathies and amyloid diseases (e.g., ordered intermolecular linkage, β-sheet expansion, cell death, dementia, accumulation of insoluble aggregates, and domain swapping). My observations here provide novel and important insights; amyloidogenicity plays a key role in serpin polymerization.

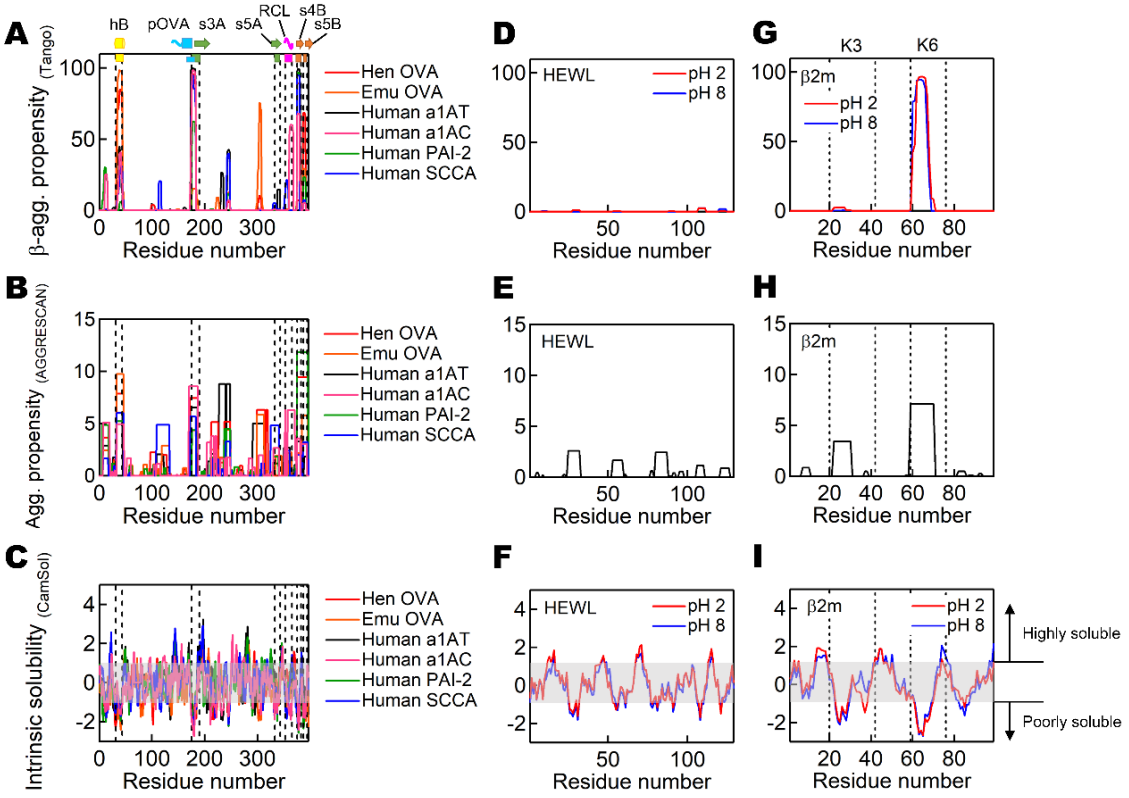



**Figure 2-9. Aggregation propensities of OVA, several serpins and other amyloidogenic proteins. A, D, G,** β-Aggregation propensities by Tango of serpin proteins (A), HEWL (D) and $\beta_2$-microglobulin (β2m) (G). **B, E, H,** Aggregation propensities by AGGRESCAN of serpin proteins (B), HEWL (E) and β2m (H). **C, F, I,** Intrinsic solubility predicted by CamSol of serpin proteins (C), HEWL (F) and β2m (I). Serpin proteins are hen OVA, emu OVA, human $\alpha_1$-antitrypsin (a1AT), human $\alpha_1$-antichymotrypsin (a1AC), human plasminogen activator inhibitor (PAI-2), and squamous cell carcinoma antigen (SCCA). The key regions of serpin are indicated in panel A. The highly-amyloidogenic regions of β2m are indicated in panel G.

*Coupled amyloid formation and tryptic digestion*

The amyloidogenicity of a mixture of tryptic digests at pH 8.0 was lower than that of intact OVA. On the basis of the scenario of the combined structure of dominantly amorphous and a small amount of amyloidogenic regions described above, this may be explained by the efficient inhibitory effects of other non-amyloidogenic peptides under crowding conditions after proteolysis. Consistent with this idea, I unexpectedly found that the trypsin digestion of intact OVA under ultrasonic irradiation most effectively induced the formation of fibrils (**Figs. 2-3 and 4**). These results suggest the importance of coupled proteolysis and fibril formation for the efficient formation of fibrils. Coupled proteolysis and fibril formation may have prevented transient and excessively high concentrations of amyloidogenic peptides and, thus, suppressed nonproductive amorphous aggregation. This gradual release of amyloidogenic peptides may be one of the key factors of amyloid formation in vivo. The importance of the coupling of proteolysis and fibril formation has been reported for insulin and transthyretin, for which the intermediates of proteolysis trigger amyloid formation (106-108).

*Mechanism of tryptic digestion-coupled fibril formation*

To elucidate the mechanisms underlying tryptic digestion-coupled amyloid formation, I varied trypsin concentrations at a constant OVA concentration (**Fig. 2-4**). The kinetics of fibril formation monitored by ThT fluorescence did not significantly depend on the trypsin concentration. Moreover, the kinetics of tryptic digestion monitored by HPLC did not depend on the trypsin concentration. Therefore, tryptic digestion and the formation of fibrils were not limited by trypsin concentrations but were determined by conformational changes in OVA exposing tryptic digestion sites. Similar conformational change-limited protease digestion has been proposed for several systems, including HEWL (109,110), and is similar to the EX1 mechanism of the hydrogen/deuterium exchange of the amide protons of proteins (111,112). Although fibril formation was suppressed at very high trypsin concentrations, the exact mechanism underlying this suppression is unclear because the direct effects of high concentrations of trypsin need to be considered.

*Effects of additives on the aggregation of tryptic digests*

Even if the amyloidogenicity of a mixture of tryptic digests was suppressed at pH 8, I revealed hidden amyloidgenicity by adding several additives at pH 2. Amyloid formation of $\beta_2$-microglobulin at pH 2 was enhanced by several salts, including NaCl (113). SDS at concentrations slightly below the CMC is known to enhance fibril formation by various proteins, including $\beta_2$-microglobulin, under low- and neutral-pH conditions (85). Tetraphosphate has recently been shown to enhance amyloidogenicity, possibly by combined electrostatic and salting-out effects (91,114,115). pOVA at pH 8 has two positive charges (N-terminal amino and 23 lysine amino residues) and two negative charges (9 aspartic acid and C-terminal carboxylic residues), with the net charge being zero. At pH 2, the net charge becomes +2 because of the protonation of carboxylic groups. This may be the major reason for enhanced amyloidogenicity at pH 2.

*Cytotoxicity of various aggregates*

Although amyloid fibrils are associated with various types of amyloidoses, the exact role of amyloid fibrils in cytotoxicity and, thus, in the development of neurodegenerative diseases remains unclear. The causative role of oligomeric aggregates in cytotoxicity has been actively argued (116,117). Among various types of aggregates, only heat-treated intact OVA revealed significant cytotoxicity during LDH and WST assays using murine colon cancer cells. Although heat-treated OVA evidently contained the amyloid component, their fraction was low at mostly 5% of all regions, and the dominant conformation was amorphous. Because of the absence of clear cytotoxicity for more typical amyloid samples, I concluded that the cytotoxicity of the OVA amyloid component was lower than that of amorphous aggregates.

## 2.5. Conclusion

The aggregation of serpin proteins has been extensively studied because of serpinopathies, conformational diseases caused by the domain-swap polymerization of serpin proteins. Although OVA has been classified as a member of the serpin superfamily, neither the latent form nor the domain-swapped polymer has been reported for a non-inhibitory serpin OVA. On the other hand, some amyloidogenicity of OVA has been reported.

In this chapter, I isolated the highly amyloidogenic peptide, corresponding to the β-strand 3A region. The high amyloidogenicity of the β-strand 3A region is common to various serpin proteins, suggesting that the high amyloidogenicity, important for serpin latency transition and serpin polymerization, is retained in OVA. I also examined the effects of various external factors (pH, NaCl, SDS, and Tetra-P) on aggregation of OVA, its tryptic digests, and amyloidogenic pOVA. The results provide a new view for determining parallels between amyloid fibrils and serpin domain-swap polymers.

# Chapter 3.

## The comprehension of heating-induced amyloid formation of $\beta_2$-microglobulin by thermodynamics and phase diagrams

## 3.1. Introduction

Amyloid fibrils, fibrillar aggregates of denatured proteins or peptides stabilized by intermolecular cross-β structures, are associated with many amyloidoses, including neurodegenerative disorders, such as Alzheimer's and Parkinson's diseases, and dialysis-related amyloidosis (DRA) (29). The kinetics of amyloid formation are common to amyloidogenic proteins and are typically separated into nucleation, elongation, and equilibrium phases. The nucleation phase, the duration of which is considered a lag time, is often long because of its high free energy barrier. Once amyloid nuclei form, the elongation of fibrils occurs rapidly. The equilibrium phase is a thermodynamic state where the monomer concentration has reached its solubility. Seed-dependent elongation is a common property of amyloid formation, in which the nucleation phase is shortened or escaped. Another type of protein misfolding leads to amorphous aggregates. Amorphous aggregates with no ordered structure are seen in cataracts, in inclusion bodies, or during protein preparation (11). Rapid amorphous aggregation without a lag time competes with the slow nucleation-dependent amyloid formation, producing kinetic complexity of amyloid formation (118).

$\beta_2$-Microglobulin (β2m), a typical amyloidogenic protein with a folded native structure, is a component of the major histocompatibility complex 1. It is filtered by the glomerulus and catabolized by proximal tubular cells in the kidneys in healthy persons. However, β2m remains in the blood and sometimes forms amyloid fibrils in patients receiving long-term hemodialysis. Accumulation and deposition of these amyloids in tissues cause DRA (119,120). It has been established that amyloid formation of acid-unfolded β2m readily occurs (63,113). The atomic structure of β2m fibrils under acidic conditions has been reported (**Fig. 3-1**)(121). In contrast, amyloid formation under neutral pH conditions, under which patients develop diseases, does not occur easily because of the amyloid-resistant native structure (122,123). Based on previous studies performed with N-terminal truncated or mutant β2m (124) or those in the presence of additives, such as collagen, heparin (125), SDS, or glycosaminoglycans (120), the denaturation or local enrichment of β2m on biological membranes or extracellular matrix molecules has been suggested to induce amyloid formation in vivo. Recently, Cremers et al. (91) reported that polyphosphates with linearly linked phosphate units are markedly effective in inducing

amyloid fibrils of various proteins. Zhang et al. found that polyphosphates effectively induced amyloid formation of β2m at neutral pH (114). However, the exact mechanism of DRA, in particular the factors inducing amyloid nucleation in patients, remains unclear.

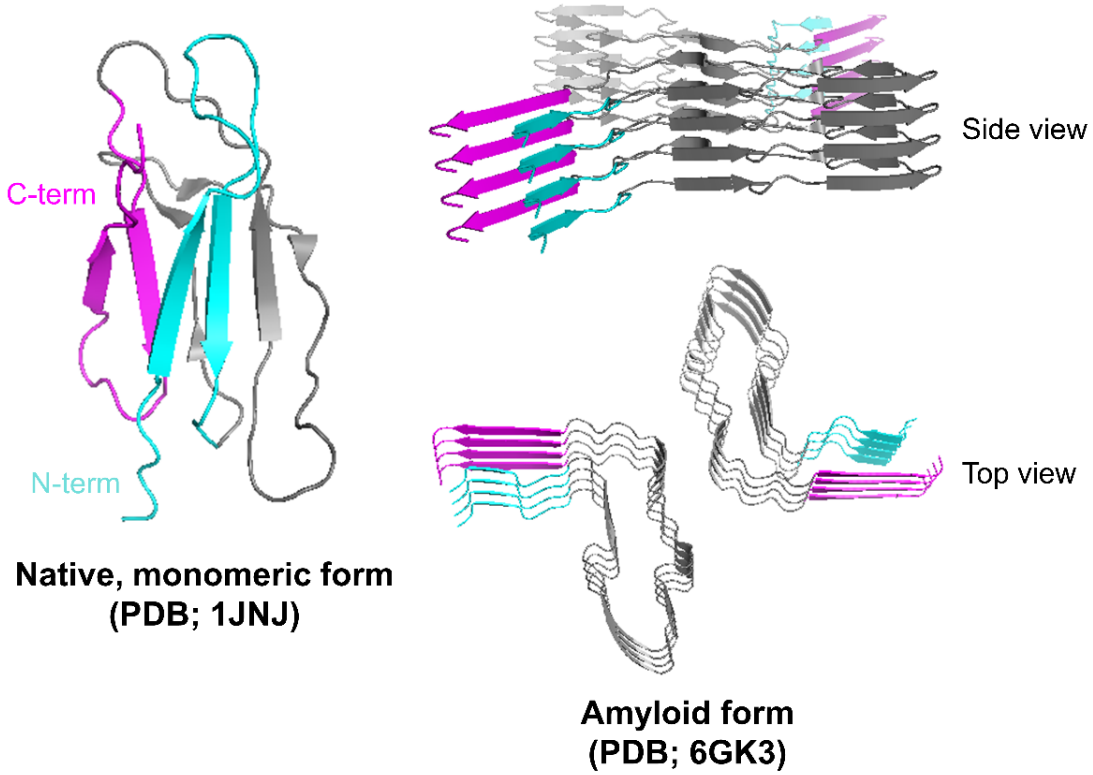



**Figure 3-1. Structures of native and amyloid states of β2m drawn with PyMOL.**

Studies on protein aggregation have been also performed from the thermodynamic perspective. Otzen and colleagues reported the relationship between thermodynamic parameters and polymorphism of glucagon amyloid fibrils (126,127). Dzwolak and colleagues reported the thermal stability and degradation of insulin fibrils (128). The effects of heat on the amyloid formation of β2m and other proteins have also been investigated using calorimetry and thermodynamic parameters were compared with those of protein folding (129-131). Recently, Adachi and I examined the effects of heating on β2m at low pH (118). Acid-unfolded β2m formed amyloid fibrils and amorphous aggregates competitively in a temperature- and NaCl concentration-dependent manner. A unified phase diagram of conformational states suggested that amyloid fibrils depolymerize at both low and high temperatures, reminiscent of cold and heat

denaturation of globular proteins (132,133). The phase diagram also accommodated a region of amorphous aggregates, which were formed under the strong forces of precipitation. Taken together, amyloid fibrils and amorphous aggregates may correspond to crystals and glasses of solutes, respectively, and the breakdown of supersaturation may lead to the formation of crystal-like amyloid fibrils (65,118). However, such a diagram has not been constructed at neutral pH where DRA develops, and the relationship between protein folding/unfolding and amyloid formation is not clear. Recently, Wang et al. reported the thermodynamic phase diagram of β-amyloid peptide based on a coarse-grained molecular dynamic simulation (134), in which amyloid fibrils depolymerized with an increase in temperature similar to the heat-induced depolymerization of β2m fibrils (118).

In this chapter, I demonstrate that amyloid formation of β2m occurs even under neutral pH conditions at high temperatures. Of note, although heating causes unfolding (i.e. denaturation) of β2m, a necessary condition of amyloid formation, it is not sufficient for amyloid formation. Amyloid formation occurs only when heat unfolding is performed under agitation, which forces the breakdown of supersaturated unfolded monomers. In other words, both unfolding and breakdown of supersaturation are required. The temperature- and NaCl concentration-dependent conformational phase diagrams reveal that the unfolding temperature of the native state decreases once amyloids form, which is exactly reproduced by the linked function of protein folding/unfolding and amyloid misfolding.

## 3.2. Materials and methods

*Protein and chemicals*

Recombinant human β2m protein with an additional methionine residue at the N terminus was expressed in *Escherichia coli* and purified as previously reported (135,136). ThT was obtained from Wako Pure Chemical Industries, Ltd. (Osaka, Japan). All other reagents were purchased from Nacalai Tesque, Inc. (Kyoto, Japan).

*ThT assays with heating*

Lyophilized β2m was dissolved in deionized water. β2m concentrations were measured spectrophotometrically using a molar extinction coefficient of 19,300 $M^{-1}$ $cm^{-1}$ at 280 nm based on its amino acid composition. The sample solution of 2.5 mL in a cuvette with a 1-cm light path contained 8.5 μM β2m, 5 μM ThT, 20 mM phosphate buffer (pH 7.0), and variable NaCl concentrations. Amyloid formation was detected by ThT fluorescence with an excitation wavelength of 445 nm and an emission wavelength of 485 nm using an F4500 fluorescence spectrophotometer (Hitachi High-Technologies Corporation, Tokyo, Japan). Light scattering at 450 nm was also measured to detect whole protein aggregation. All fluorescence measurements were performed under stirring using a magnetic stirring bar at a stirring speed of 600 rpm, except for the experiments under quiescence. The sample temperature was controlled using a Peltier element (Nippon Tecmo Co., Ltd., Fukuoka, Japan) and measured by a thermocouple Compact Thermologger AM-8000K (Anritsu Meter Co., Ltd., Tokyo, Japan). The equipment setup and the assay scheme were described in Chapter 1.

*CD and TEM measurements*

Far-UV CD spectra (212–250 nm) were obtained with a model J-720 spectropolarimeter (Jasco Co., Ltd., Tokyo, Japan) using a quartz cell with a 1-mm or 1-cm path length. CD data were expressed as mean residue ellipticity.

TEM images were obtained using a transmission electron microscope (H-7650, Hitachi High-Technologies Corporation) with 5 μL of 0.5% (w/v) hafnium chloride as the staining agent.

*Seeding reactions*

Seeds were obtained from the preformed fibrils of heat-induced spontaneous amyloid formation under stirring and sonicated moderately before seeding experiments. The conditions for the sample preparation and measurements were the same as for standard ThT assays, except for the addition of 5% (v/v) seeds.

Calorimetric measurements were carried out using a MicroCal VP-DSC calorimeter (Malvern Panalytical, Ltd., Worcestershire, UK), as described previously (137). The sample solution contained 42.5 μM β2m, 20 mM phosphate buffer (pH 7.0), and 1.0 M NaCl with or without 1% (v/v) seeds.

*Fibril depolymerization*

Heat-induced amyloid fibrils of β2m were formed under the same conditions used for the ThT assays with 500 mM NaCl at 70 ℃. These fibrils were centrifuged at 15,000 rpm and 25 ℃ for 20 min and then suspended at 5 μM ThT in 20 mM phosphate buffer (pH 7.0). The CD measurement and ThT assay were carried out at 25 ℃, and the solution was then incubated at 90 ℃ under stirring at 600 rpm. Intermittent ThT assays were performed every 10 min during the incubation. After the incubation, the CD measurement and ThT assay were performed at 25 ℃.

## 3.3. Results

*Amyloid formation of β2m upon heat unfolding under agitation*

I monitored the conformational change of β2m upon heating at neutral pH by far-UV CD measurements. β2m samples in 20 mM sodium phosphate buffer (pH 7.0) and 1.0 M NaCl were heated from 25 to 90 ℃ with a heating rate of 0.5 ℃/min. Without stirring, the CD spectrum demonstrated reversible heat unfolding, with β2m refolded to the native state after cooling to 25 ℃ (**Fig. 3-2A, B**). In contrast, under stirring, structural conversion to the pronounced β-sheet conformation occurred at 60 ℃, and β2m did not refold to the native conformation (**Fig. 3-2C, D**).

To confirm that the conformational change under stirring led to amyloid formation, I carried out ThT assays (**Fig. 3-2E, F**). I added 5 μM ThT to the same samples as above and measured the ThT fluorescence at 485 nm at a heating rate of 1 ℃/min. I simultaneously measured the LS at 450 nm to monitor the total amount of aggregates. In the absence of stirring, neither ThT fluorescence nor LS changed up to 90 ℃. Under stirring, both ThT fluorescence and LS increased markedly beginning at 66 ℃, which was near the midpoint temperature ($T_m$) for heat unfolding of β2m under these conditions (**Fig. 3-2E, F**).

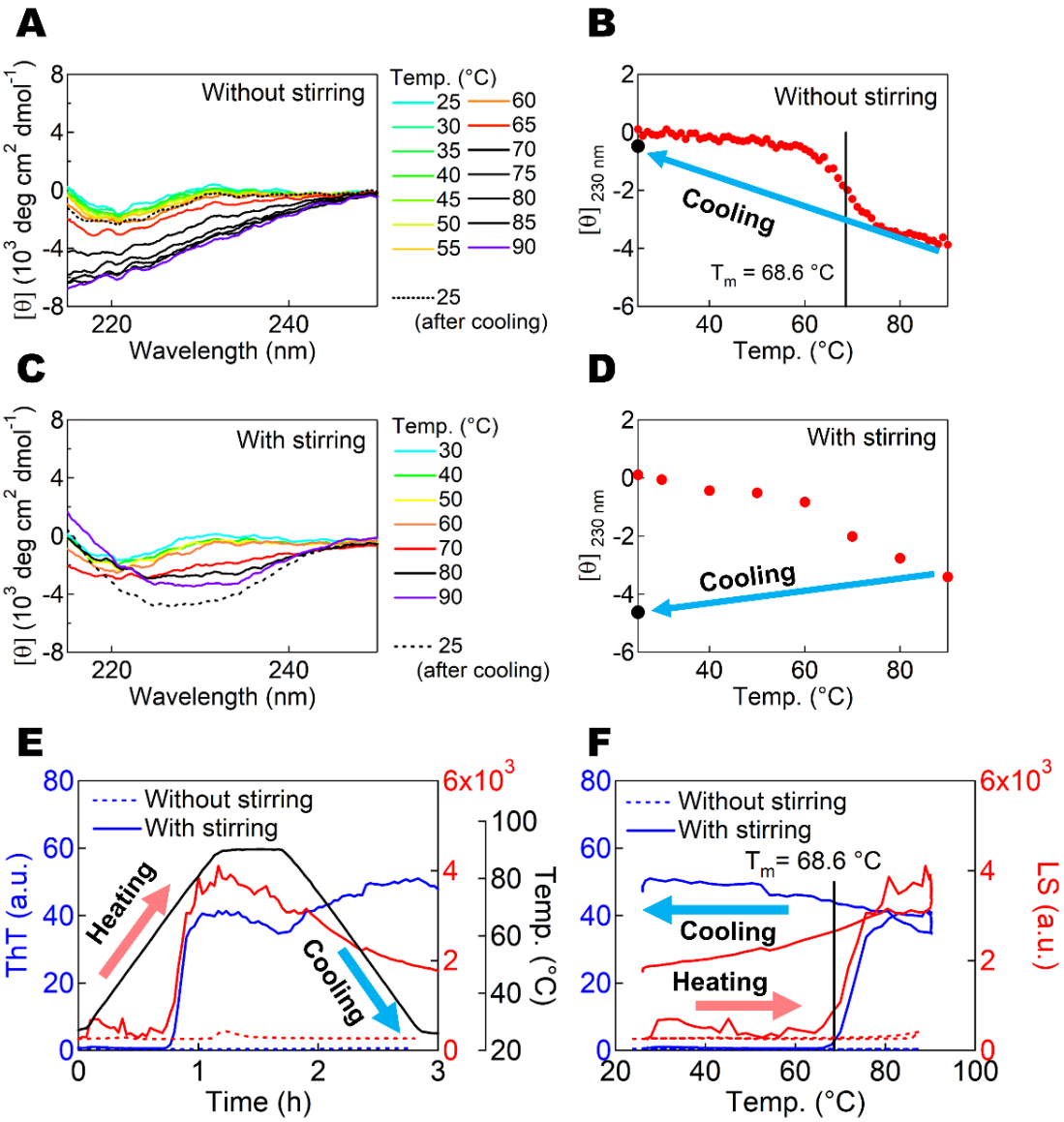



**Figure 3-2. Amyloid formation of β2m at neutral pH requires both heat unfolding and agitation. A-D,** CD spectra of 8.5 μM β2m at pH 7.0 with 1.0 M NaCl upon heating in the absence (A) or presence of stirring (C). The values of [θ] at 230 nm in the absence (B) or presence (D) of stirring were plotted against temperature. The arrows indicate the values after cooling to 25 °C. **E, F,** ThT assays of β2m under the same conditions as A-D. The intensities of ThT fluorescence and LS are indicated by blue and red, respectively. Dashed lines, absence of stirring; solid lines, presence of stirring. In E, the time course of temperature change is shown by the black line. In F, the $T_m$ value estimated from B is shown. The measurements shown in E and F were repeated three times, and the representative data are shown.

*Temperature dependence of heat-induced amyloid formation*

ThT assays with 0.1 mg/mL β2m were performed in 20 mM sodium phosphate buffer (pH 7.0), 1.0 M NaCl, and 5 μM ThT at varying temperatures under stirring. Amyloid formation occurred at all temperatures between 40 and 90 ℃, although the reaction accelerated markedly with an increase in temperature (**Fig. 3-3A, B**). After these assays, I measured the final ThT intensity at 25 ℃ to remove complexity caused by thermal effects on ThT fluorescence. ThT fluorescence at 25 ℃ did not depend on the reaction temperature, although the final LS value slightly increased with an increase in temperature. In contrast, the lag time became significantly shorter at higher temperatures (**Fig. 3-3C**). I also carried out CD measurements at the reaction temperatures. All CD spectra after heat-induced transition exhibited β-structures typical for amyloid fibrils (**Fig. 3-3D**). Additionally, I confirmed amyloid formation by TEM images (**Fig. 3-3E-J**).

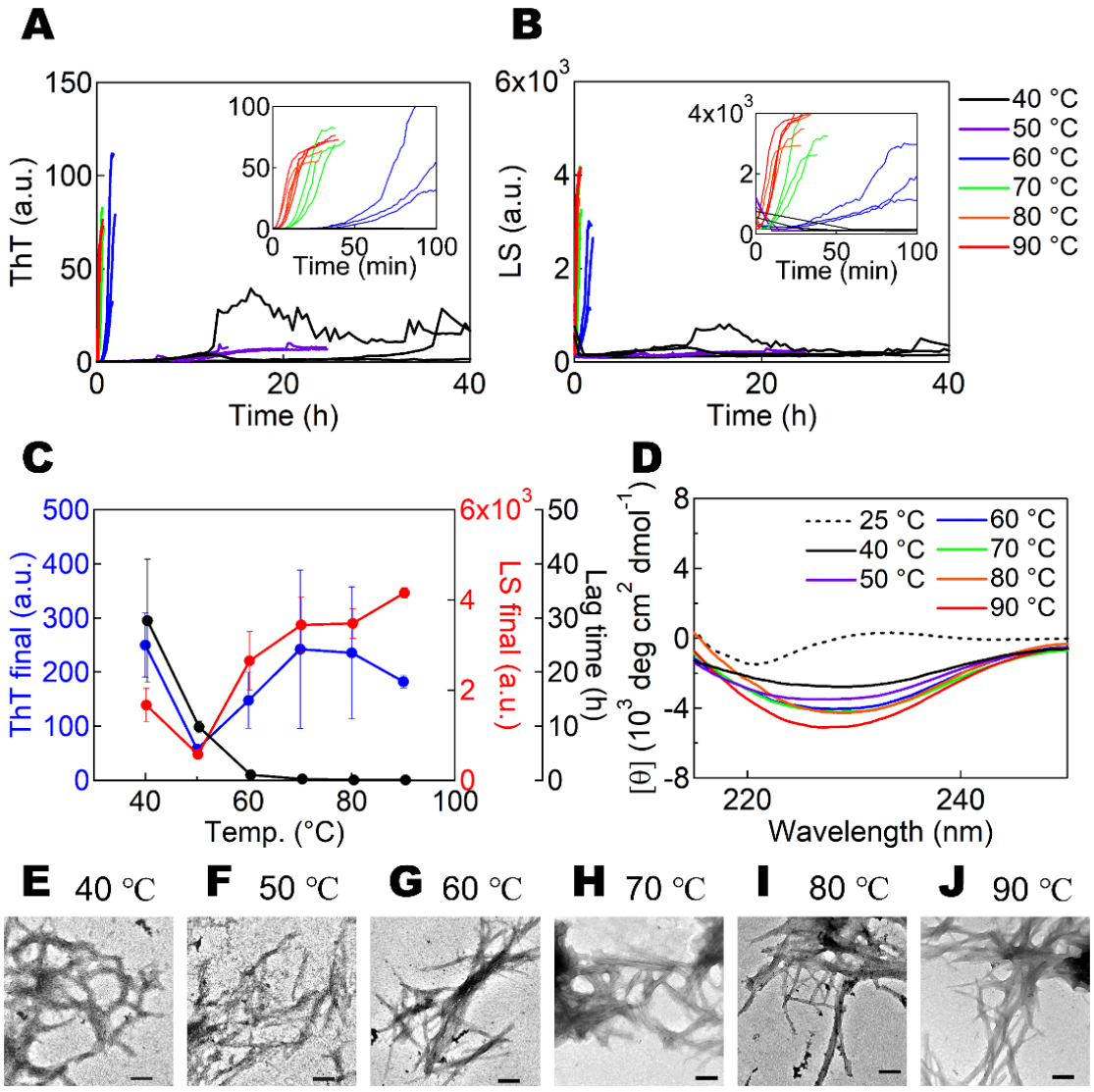



**Figure 3-3. Effects of temperature on heat-induced β2m amyloid formation. A, B,** Amyloid formation of 8.5 μM β2m at pH 7.0 with 1.0 M NaCl under stirring was monitored by ThT fluorescence (A) and LS (B) at varying temperatures with $n$ = 3. **C,** Dependences of final ThT intensity (blue), final LS intensity (red), and lag time monitored by ThT (black) on temperature. The final ThT and LS intensities were measured at 25 ℃. **D,** CD spectra of the samples after the assays of amyloid formation. Each measurement was carried out at the reaction temperature indicated by the spectral color. The dashed black line indicates the spectrum of the native state at 25 ℃. **E-J,** TEM images of the β2m samples after the conformational transition. Scale bars; 200 nm.

*Effects of NaCl on amyloid formation*

To investigate the effects of NaCl on the amyloid formation, I carried out the same ThT assays as those shown in **Fig. 3-3 (A, B)** at varying NaCl concentrations (0–3.0 M) and temperatures (50–90 °C). With 0.5–3.0 M NaCl, amyloid formation monitored by ThT fluorescence occurred at varying temperatures and NaCl concentrations. However, with 0–0.25 M NaCl, no reaction occurred at 90 °C, although amyloid fibrils formed at lower temperatures (**Fig. 3-4**).

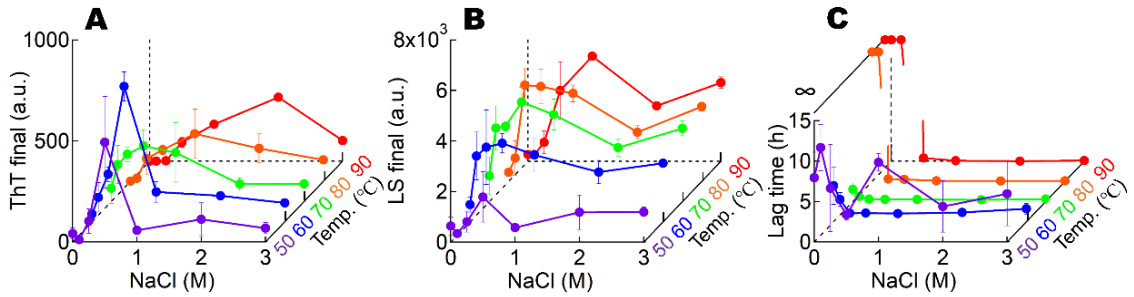



**Figure 3-4. Effects of NaCl concentration on heat-induced β2m amyloid formation.** Comparisons of the final ThT intensities (A), final LS intensities (B), and ThT-monitored lag times (C) at varying NaCl concentrations and temperatures. $n = 3$.

I assessed the secondary structures and morphologies after ThT assays. Samples without an increase in ThT fluorescence or LS remained unfolded when monitored by CD and exhibited no fibrous aggregates when examined by TEM (**Fig. 3-5**). In contrast, the samples with increases in ThT fluorescence and LS had amyloid fibrils even at lower NaCl concentrations (**Fig. 3-5**).

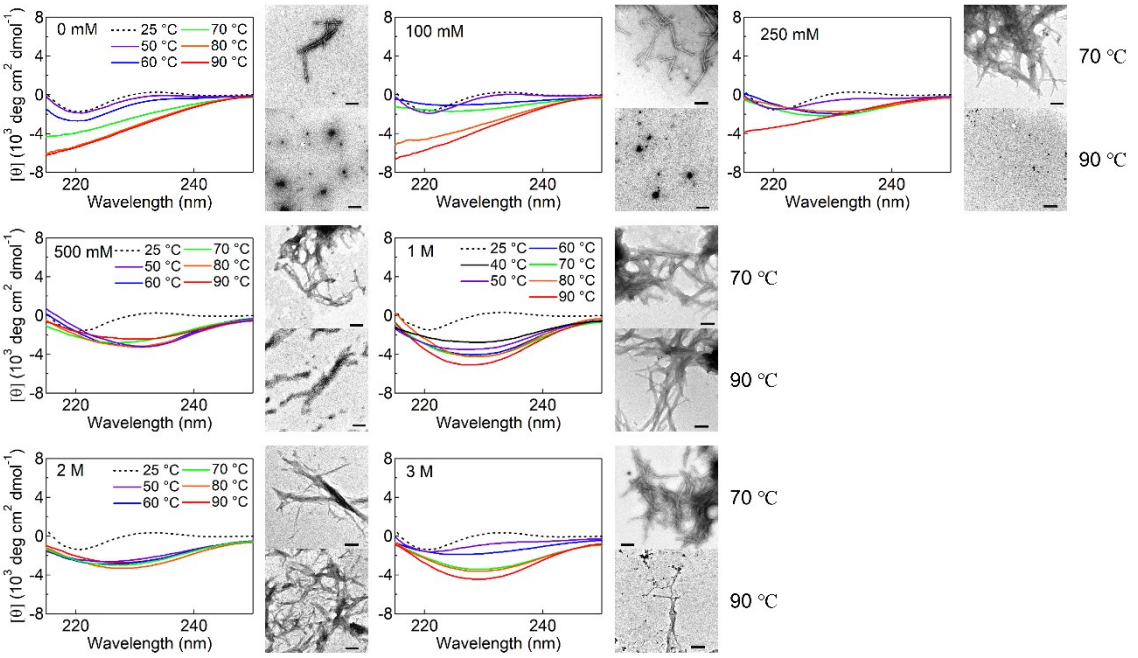



**Figure 3-5. CD spectra and TEM images of β2m after heating experiments with varying NaCl concentrations.** The CD measurements were performed at the indicated temperatures. The spectra of dotted lines indicate those of the native state at 25 ℃ without heat treatment. Scale bars; 200 nm.

I previously described that visualization using white and blue LED lamps is a useful method for detecting amyloid fibrils (Chapter 2). The heat-treated β2m samples at pH 7.0 without agitation exhibited neither turbidity nor ThT fluorescence, consistent with the reversible heat unfolding under these conditions. Under stirring, samples with lower concentrations of NaCl at higher temperatures exhibited neither turbidity nor ThT fluorescence, confirming that they remained soluble below the solubility limit. The remaining samples at pH 7.0 under agitation exhibited slight turbidity and strong ThT fluorescence, suggesting that agitation broke supersaturation and led to amyloid formation. For comparison, I prepared amorphous aggregates of β2m with 1.0 M NaCl at pH 2.0 (40,118). These amorphous aggregates exhibited strong turbidity without ThT fluorescence (**Fig. 3-6**).

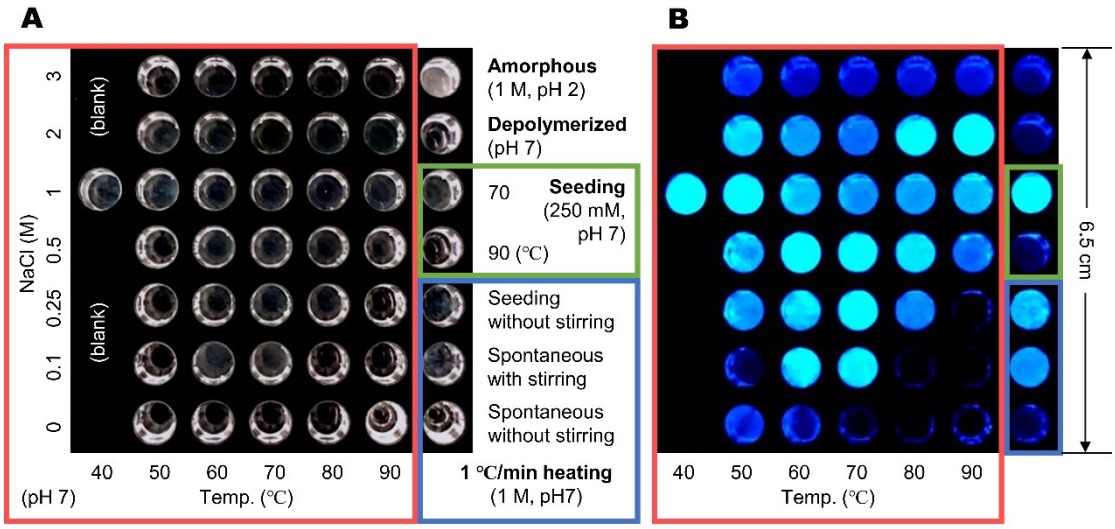



**Figure 3-6. Direct LED visualization images of β2m samples.** Turbidimetry (A) and ThT fluorescence (B) images were obtained using white and blue LED lamps, respectively. The real size of images is 6.5 cm × 6.5 cm.

*Seeding activity of heat-induced amyloid fibrils*

I investigated the seeding activity of heat-induced β2m amyloid fibrils prepared with 1.0 M NaCl. Although no amyloid formation occurred without stirring when monitored by ThT fluorescence or LS at a heating rate of 1 ℃/min, it occurred in the presence of seeds even under quiescent conditions (**Fig. 3-7A**). After these experiments, I carried out CD measurements at 25 ℃. The seeded sample after heat-induced transition exhibited β-structure typical of amyloid fibrils, whereas the non-seeded sample demonstrated refolding to native β2m (**Fig. 3-7C**). Under stirring, I detected no difference between heating-dependent spontaneous amyloid formation and seed-dependent reactions (**Fig. 3-7B**). Additionally, I performed differential scanning calorimetry (DSC) measurements in the presence or absence of seeds, confirming that seeds broke supersaturation when combined with unfolding of the native state (**Fig. 3-7D**). These results were confirmed by the LED visualization images (**Fig. 3-6**).

With 250 mM NaCl at 70 ℃, the seeds shortened the lag time (**Fig. 3-7E**). In contrast, with 250 mM NaCl at 90 ℃, no reaction occurred even in the presence of seeds (**Fig. 3-7F**). TEM images confirmed amyloid fibrils and no fibrous aggregates at 70 and 90 ℃, respectively (**Fig. 3-7E, F**). The LED visualization images were consistent with these temperature-dependent seeding reactions (**Fig. 3-6**). The results suggested that because the solubility of β2m with 250 mM NaCl at 90 ℃ was higher than the protein concentration (8.5 μM), no fibrils formed, even with seeds.

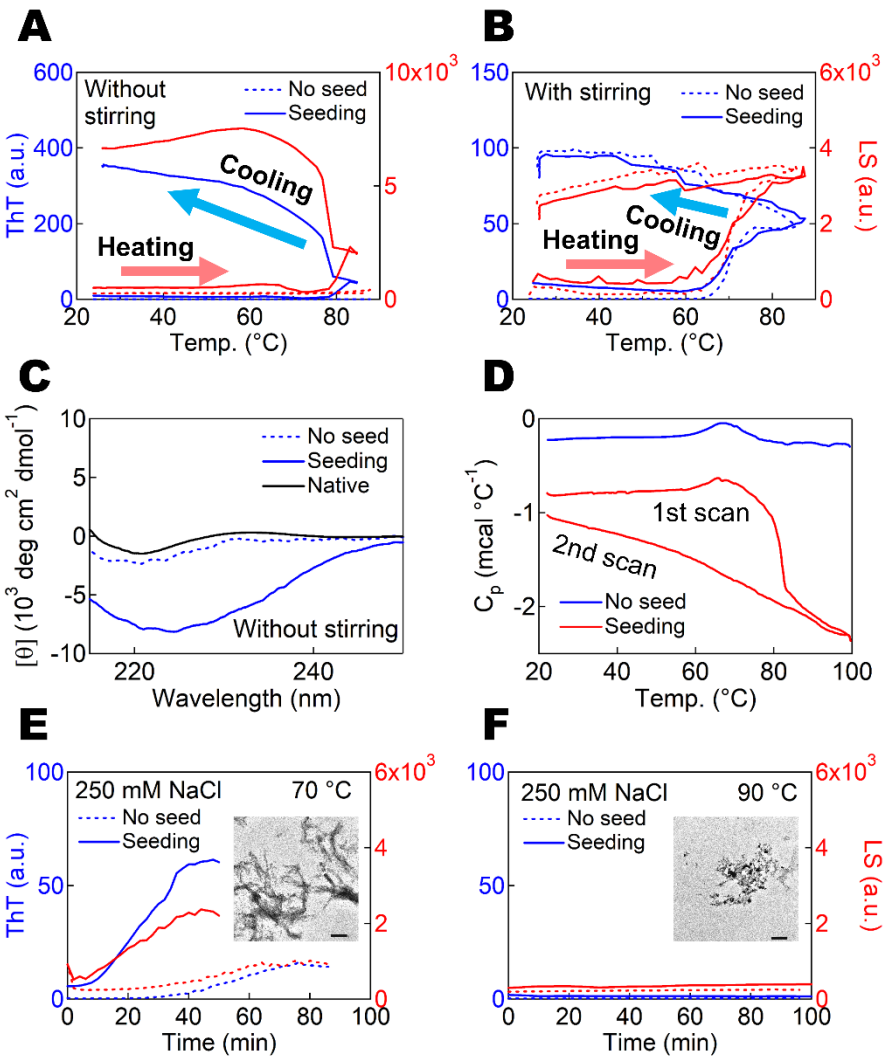



**Figure 3-7. Seeding activities of the heat-induced β2m amyloid fibrils. A, B,** ThT assays with or without 5% preformed seed fibrils under the same conditions as (Fig. 3-2C) with (B) or without (A) stirring. Time courses of ThT and LS are represented by the blue and red lines, respectively. Spontaneous and seed-dependent reactions are represented by the dashed and solid lines, respectively. **C,** CD spectra of the samples after assays shown in A and the native β2m. The measurements were performed at 25 °C. **D,** DSC measurements of 42.5 μM β2m with 1.0 M NaCl at pH 7.0 in the absence or presence of 1% seeds. The lines represent the $C_p$ values for the nonseeded (blue) and seeded (red) reactions. **E, F,** Seeding experiments under the conditions of spontaneous amyloid formation (i.e. 250 mM NaCl and 70 °C) (E) and of no amyloid formation (i.e. 250 mM NaCl and 90 °C) (F). Insets show the TEM images of seeded samples. Scale bars; 200 nm.

*Depolymerization of heat-induced amyloid fibrils*

First, β2m amyloid fibrils were prepared in 0.5 M NaCl at pH 7.0 and 70 ℃. The fibrils were recovered by centrifugation and then suspended in 0 M NaCl at pH 7.0. When these fibrils were incubated at 90 ℃, significant decreases in both LS and ThT intensities were observed (**Fig. 3-8A**). However, the LS intensity remained relatively high, and the CD spectrum did not represent the refolded β2m structure (**Fig. 3-8B, C**), suggesting that fibril depolymerization occurred partially. According to the TEM images, long amyloid fibrils were observed with 0.5 M NaCl at 70 ℃, whereas no significant fibrils remained after the incubation with 0 M NaCl at 90 ℃ (**Fig. 3-8D, E**). I also examined fibril depolymerization by the LED images, which demonstrated weakened ThT fluorescence (**Fig. 3-6**).

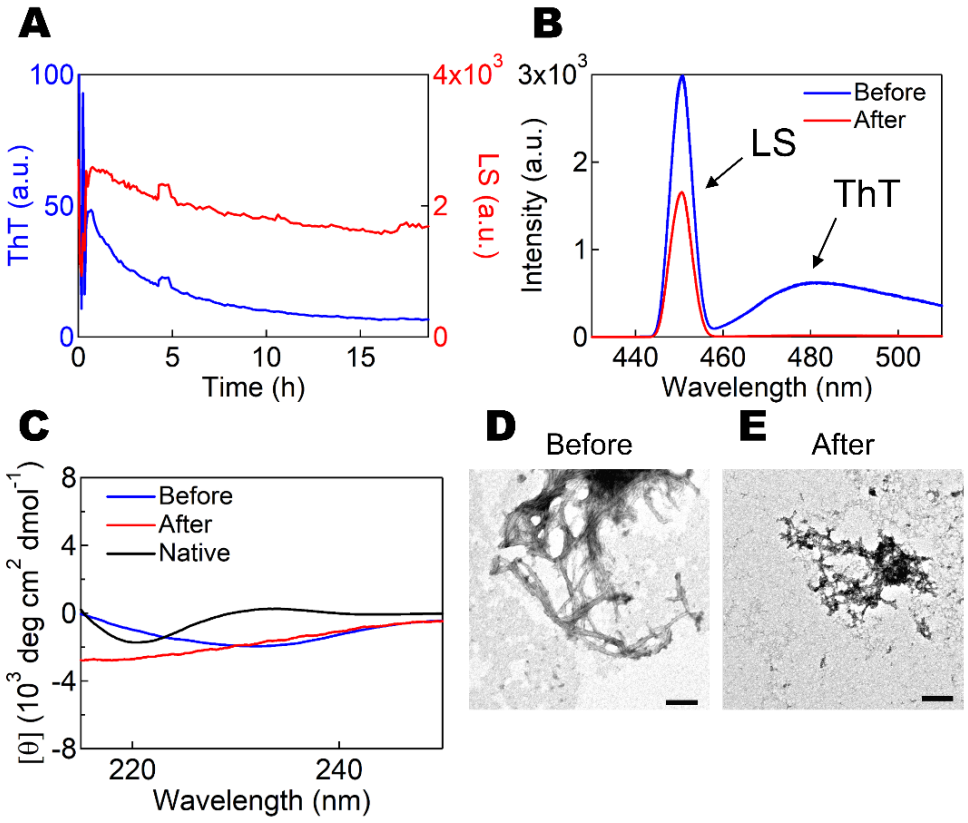



**Figure 3-8. Heat-induced depolymerization of β2m amyloid fibrils. A, B,** Kinetics (A) and spectra (B) monitored by ThT assay. **C,** CD spectra of the samples after ThT assays and the native β2m. The measurements were performed at 25 ℃. **D, E,** TEM images of the samples before (D) and after (E) ThT assays. Scale bars; 200 nm.

### 3.4. Discussion

*Comparison of monomer folding and amyloid misfolding*

To address the mechanism underlying the temperature-dependent amyloid formation/depolymerization, I recalled the thermodynamics of monomer folding/unfolding (Chapter 1)(132,133). The stability of the native state of globular proteins depends on temperature, exhibiting "heat denaturation" and occasionally "cold denaturation." I assumed folding transition from the denatured (D) to native (N) states (D ⇌ N) with the equilibrium constant of folding ($K_N$) to compare with amyloid "misfolding":

$$\mathrm{D} \rightleftharpoons \mathrm{N}$$

Mechanism 1

$$K_\mathrm{N} = [\mathrm{N}]/[\mathrm{D}] \qquad \text{(Eq. 1)}$$

Gibbs free energy change of folding to the native state ($\Delta G_N(T) = -RT \ln K_N$) at temperature $T$ in Kelvin is determined by the enthalpy ($\Delta H_N(T)$) and entropy changes ($\Delta S_N(T)$),

$$\Delta G_\mathrm{N}(T) = -RT\ln K_\mathrm{N} = \Delta H_\mathrm{N}(T) - T\Delta S_\mathrm{N}(T) - a[\mathrm{NaCl}] \qquad \text{(Eq. 2)}$$

$$\Delta H_\mathrm{N}(T) = \Delta H_\mathrm{N}(T_0) + \Delta C_{\mathrm{p,N}}(T - T_0) \qquad \text{(Eq. 3)}$$

$$\Delta S_\mathrm{N}(T) = \Delta S_\mathrm{N}(T_0) + \Delta C_{\mathrm{p,N}} \ln(T/T_0) \qquad \text{(Eq. 4)}$$

where $\Delta H_N(T_0)$, $\Delta S_N(T_0)$, $\Delta C_{p,N}$, and $a$[NaCl] are the enthalpy and entropy changes at a reference temperature $T_0$, heat capacity change of folding, and a contribution of NaCl at [NaCl] with a coefficient $a$, respectively. The temperature dependencies of $\Delta G_N(T)$, $\Delta H_N(T)$, and $T\Delta S_N(T)$, assuming $T_0$ = 310 K, $\Delta H_N(T_0) = -174.7$ kJ mol$^{-1}$, $\Delta S_N(T_0) = -0.5$ kJ mol$^{-1}$ K$^{-1}$, $\Delta C_{p,N} = -5.6$ kJ mol$^{-1}$ K$^{-1}$, which were taken from Kardos et al. (138), and $a$ = 2.5 kJ mol$^{-1}$ $M_{NaCl}^{-1}$, which was estimated from the $T_m$ measurements (**Fig. 3-9B, panel i**), are shown in **panel i of Fig. 3-9A**.

The fraction of the N state ($F_N$) was defined by the following.

$$F_\mathrm{N} = \frac{[\mathrm{N}]}{[\mathrm{N}] + [\mathrm{D}]} = \frac{K_\mathrm{N}}{K_\mathrm{N} + 1} = \frac{\exp(-\Delta G_\mathrm{N}(T)/RT)}{\exp(-\Delta G_\mathrm{N}(T)/RT) + 1} \qquad \text{(Eq. 5)}$$

The temperature dependences of $F_N$ and $F_D$ (= 1 − $F_N$) at 1.0 M NaCl are shown in **panel iii of Fig. 3-9A**. I constructed the temperature- and NaCl concentration-dependent folding phase diagram drawn using the following,

$$[\mathrm{NaCl}]_{\mathrm{N},0.5}(T) = \frac{\Delta H_{\mathrm{N}}(T) - T\Delta S_{\mathrm{N}}(T)}{a} \qquad \text{(Eq. 6)}$$

where $[\mathrm{NaCl}]_{\mathrm{N},0.5}(T)$ is the midpoint NaCl concentration of folding ($\Delta G_{\mathrm{N}}(T) = 0$, $F_{\mathrm{N}} = 0.5$) at $T$ (**Fig. 3-9B, panel i**).

The $\Delta H_{\mathrm{N}}(T)$ value, which is "negative" above 20 °C, decreases with an increase in temperature because of a negative heat capacity change of folding ($\Delta C_{\mathrm{p,N}}$). The $\Delta C_{\mathrm{p,N}}$ value, and thus temperature dependence of $\Delta H_{\mathrm{N}}(T)$, largely result from hydrophobic interactions that stabilize the native state. On the other hand, $-T\Delta S_{\mathrm{N}}(T)$ term, which includes the decrease in conformational entropy upon folding, increases in magnitude with an increase in temperature more than does that of the enthalpy term. The combined effects of destabilizing entropy and stabilizing enthalpy terms are the "negative" $\Delta G_{\mathrm{N}}(T)$ (folding) around room temperature and "positive" $\Delta G_{\mathrm{N}}(T)$ (unfolding) at high temperatures, leading to heat denaturation. Regarding cold denaturation, which was not evident for β2m, the decrease in $\Delta H_{\mathrm{N}}(T)$ in magnitude directly explains the conversion of negative $\Delta G_{\mathrm{N}}(T)$ (folding) to positive $\Delta G_{\mathrm{N}}(T)$ (unfolding) upon cooling (132,133).

*Thermodynamics of amyloid formation*

Although the detailed mechanisms of amyloid formation remain elusive, a simplified model (Mechanism 2) is valid for describing the equilibrium between monomers (M) and polymeric fibrils (P) (43,139).

$$\mathrm{P} + \mathrm{M} \rightleftharpoons \mathrm{P}$$

Mechanism 2

The elongation of fibrils is defined by the equilibrium association constant ($K_{\mathrm{Pol}}$) as follows.

$$K_{\mathrm{Pol}} = \frac{[\mathrm{P}]}{[\mathrm{P}][\mathrm{M}]} \qquad \text{(Eq. 7)}$$

The equilibrium is independent of the molar concentration of amyloid fibrils, [P]. Hence, I obtained the equilibrium monomer concentration $[\mathrm{M}]_{\mathrm{C}}$ as follows.

$$[\mathrm{M}]_{\mathrm{C}} = \frac{1}{K_{\mathrm{Pol}}} \qquad \text{(Eq. 8)}$$

$[M]_C$ is referred to as the "critical concentration" (43,130,131,139) because amyloid fibrils form when the concentration of monomers exceeds $[M]_C$. By determining $[M]_C$, the apparent free energy change of amyloid formation ($\Delta G_{Pol}(T)$) is calculated by the following.

$$\Delta G_{\mathrm{Pol}}(T) = -RT \ln K_{\mathrm{Pol}} = RT \ln[M]_C \quad \text{(Eq. 9)}$$

As I described in Chapter 1, I assumed that Gibbs free energy equations (i.e. $\Delta H_{Pol}(T)$ and $\Delta S_{Pol}(T)$) also hold true for polymeric amyloid fibrils (**Fig. 3-9A, panel ii**),

$$\Delta G_{\mathrm{Pol}}(T) = \Delta H_{\mathrm{Pol}}(T) - T\Delta S_{\mathrm{Pol}}(T) - b[\mathrm{NaCl}] \quad \text{(Eq. 10)}$$

$$\Delta H_{\mathrm{Pol}}(T) = \Delta H_{\mathrm{Pol}}(T_0) + \Delta C_{\mathrm{p,Pol}}(T - T_0) \quad \text{(Eq. 11)}$$

$$\Delta S_{\mathrm{Pol}}(T) = \Delta S_{\mathrm{Pol}}(T_0) + \Delta C_{\mathrm{p,Pol}} \ln(T/T_0) \quad \text{(Eq. 12)}$$

where $b$[NaCl] represents the contribution of NaCl at [NaCl] with a coefficient $b$. Ikenoue et al. previously reported that the $\Delta H_{Pol}(T)$ value for β2m at pH 2 was linearly dependent on temperature, giving a $\Delta C_{p,Pol}$ value of ~5.0 kJ mol$^{-1}$ K$^{-1}$ (130), a slightly smaller value than that of the native state: ~5.6 kJ mol$^{-1}$ K$^{-1}$ (131). I assumed the same $\Delta C_{p,Pol}$ value for the amyloid fibrils at pH 7.

If the total protein concentration, $[Prot]_T$, is higher than $[M]_C$, the fraction of the polymeric P state is defined by the following.

$$F_{\mathrm{Pol}} = \frac{[\mathrm{Prot}]_\mathrm{T} - [\mathrm{M}]_\mathrm{C}}{[\mathrm{Prot}]_\mathrm{T}} = \frac{[\mathrm{Prot}]_\mathrm{T} - \exp(\Delta G_{\mathrm{Pol}}(T)/RT)}{[\mathrm{Prot}]_\mathrm{T}} \quad \text{(Eq. 13)}$$

Temperature dependences of fractions of D and P states for amyloid formation are shown in **panel iv of Fig. 3-9A**. If $[Prot]_T$ is smaller than $[M]_C$, $F_{Pol} = 0$. The NaCl concentration, $[NaCl]_{Pol,0}(T)$, where $[Prot]_T = [M]_C$, is obtained by the following equation.

$$[\mathrm{NaCl}]_{\mathrm{Pol},0}(T) = \frac{-RT \ln[Prot]_\mathrm{T} + \Delta H_{\mathrm{Pol}}(T) - T\Delta S_{\mathrm{Pol}}(T)}{b} \quad \text{(Eq. 14)}$$

Based on these considerations, I constructed the temperature- and NaCl concentration-dependent phase diagram of amyloid formation at $[Prot]_T$ = 0.1 mg/mL drawn by the following,

$$[\mathrm{NaCl}]_{\mathrm{Pol},0.5}(T) = \frac{\Delta H_{\mathrm{Pol}}(T) - T\Delta S_{\mathrm{Pol}}(T) - RTln([\mathrm{Prot}]_\mathrm{T}/2)}{b} \quad \text{(Eq. 15)}$$

where $[NaCl]_{Pol,0.5}(T)$ is the midpoint NaCl concentration of amyloid formation ($F_{Pol}$ = 0.5), assuming $b$ = 25.0 kJ mol$^{-1}$ $M_{NaCl}^{-1}$ (**Fig. 3-9B, panel ii**).

The previous reports (43,130,139) and current considerations argue that the solubility of monomers ($[M]_C$) and thus the stability of amyloid fibrils are determined by a mechanism similar to that of protein folding. This is not surprising considering that intramolecular protein folding and intermolecular amyloid misfolding are driven by similar forces, including hydrophobic interactions, hydrogen bonds, and van der Waals interactions (Chapter 1). It is well-known that the solubility in water of hydrophobic substances against temperature exhibits a U-shaped dependence, representing the large positive $\Delta C_p$ value for "dissolution" (140). Thus, the simplified mechanism of amyloid dissolution resembles the dissolution equilibrium of a hydrophobic solute in which the equilibrium solute concentration (i.e. solubility) represents the free energy change of dissolution.

Assuming the similarity of protein folding and amyloid misfolding, heat-induced depolymerization of amyloid fibrils is expected because of the increased conformational entropy. On the other hand, the low temperature-induced depolymerization (141) or decreased amyloid formation at low temperatures is expected to occur because of the decreased hydrophobic interactions. Although the rigid tight packing of side chains producing steric zippers and more extensive cross-β network (Chapter 1) may provide distinct properties, including supersaturation-limited amyloid formation, the overall calorimetric properties of amyloid formation resemble those of protein folding.

*Linkage between reversible unfolding and supersaturation-limited misfolding*

Three conformational states are linked after the breakdown of supersaturation (N ⇌ D ⇌ P) and are under a thermodynamic equilibrium (Mechanism 3):

$$\mathrm{N} \rightleftharpoons \mathrm{D} \rightleftharpoons \mathrm{P}$$

Mechanism 3

Although equations for the processes of N ⇌ D and D ⇌ P did not change, the fractions of N ($F_N$), D ($F_D$), and P ($F_{Pol}$) are newly defined as follows,

$$F_{\mathrm{N}} = \frac{[\mathrm{N}]}{[\mathrm{N}]+[\mathrm{D}]+[\mathrm{P}]} = \frac{K_{\mathrm{N}}[\mathrm{D}]}{[\mathrm{Prot}]_{\mathrm{T}}} = \frac{\exp((-\Delta G_{\mathrm{N}}(T)+\Delta G_{\mathrm{Pol}}(T))/RT)}{[\mathrm{Prot}]_{\mathrm{T}}} \quad \text{(Eq. 16)}$$

$$F_{\mathrm{D}} = \frac{[\mathrm{D}]}{[\mathrm{N}]+[\mathrm{D}]+[\mathrm{P}]} = \frac{\exp(\Delta G_{\mathrm{Pol}}(T)/RT)}{[\mathrm{Prot}]_{\mathrm{T}}} \quad \text{(Eq. 17)}$$

and $F_{\mathrm{Pol}} = 1 - F_{\mathrm{N}} - F_{\mathrm{D}}$. These equations are valid when $[\mathrm{Prot}]_{\mathrm{T}} > (1 + K_{\mathrm{N}})[\mathrm{M}]_{\mathrm{C}}$, where the right side indicates the maximal equilibrium monomer concentration. When $[\mathrm{Prot}]_{\mathrm{T}} < (1 + K_{\mathrm{N}})[\mathrm{M}]_{\mathrm{C}}$, the fractions of respective species are the same as those described under supersaturation (i.e. without amyloid fibrils).

The temperature dependences of the three conformational states with 1.0 M NaCl shown in **Fig. 3-9 (A, panel v, and B, panel iii)** were distinct from those under supersaturation. Most notably, the unfolding transition started at significantly lower temperatures than that under supersaturation, indicating a significant decrease in $T_{\mathrm{m}}$ for thermal denaturation. This can be simply explained by the law of mass action: the N ⇌ D equilibrium shifts to D because the newly participating amyloid fibrils (P) drive the overall equilibrium to P. Indeed, with 1.0 M NaCl, amyloid fibrils formed at 40 °C, even though the lag time was as long as 30 h (**Fig. 3-3C**), consistent with the consideration addressed here. Although the law of mass action has not been addressed previously in the formation of amyloid fibrils starting from the native state, it may have an important role in explaining the propagation of amyloid fibrils even under conditions where the precursor amyloidogenic states are negligibly small.

I constructed the temperature- and NaCl concentration-dependent "three states" phase diagram defined by the midpoint NaCl concentrations for the native state ($[\mathrm{NaCl}]_{\mathrm{N},0.5}(T)$) and polymeric amyloid ($[\mathrm{NaCl}]_{\mathrm{Pol},0.5}(T)$).

$$[\mathrm{NaCl}]_{\mathrm{N},0.5}(T) = \frac{\Delta H_{\mathrm{Pol}}(T) - \Delta H_{\mathrm{N}}(T) - T\Delta S_{\mathrm{Pol}}(T) + T\Delta S_{\mathrm{N}}(T) - RT\ln([\mathrm{Prot}]_{\mathrm{T}}/2)}{b - a} \quad \text{(Eq. 18)}$$

$$[\mathrm{NaCl}]_{\mathrm{Pol},0.5}(T) \frac{RT\ln([\mathrm{Prot}]_{\mathrm{T}}/2) - 2\Delta H_{\mathrm{Pol}}(T) + \Delta H_{\mathrm{N}}(T) + 2T\Delta S_{\mathrm{Pol}}(T) - T\Delta S_{\mathrm{N}}(T)}{a - 2b} \quad \text{(Eq. 19)}$$

The calculated and experimental phase diagrams are shown in **Fig. 3-9B (panel iii)**. It is noted that at NaCl concentrations below 0.1 M, where the three states coexisted, I calculated the boundaries by estimating the points where the concentrations of two species are equal. This type of linkage between protein unfolding and aggregation will occur for any type of aggregate, and the consideration presented here provides a quantitative explanation as to how the linkage affects the stability of the native state.

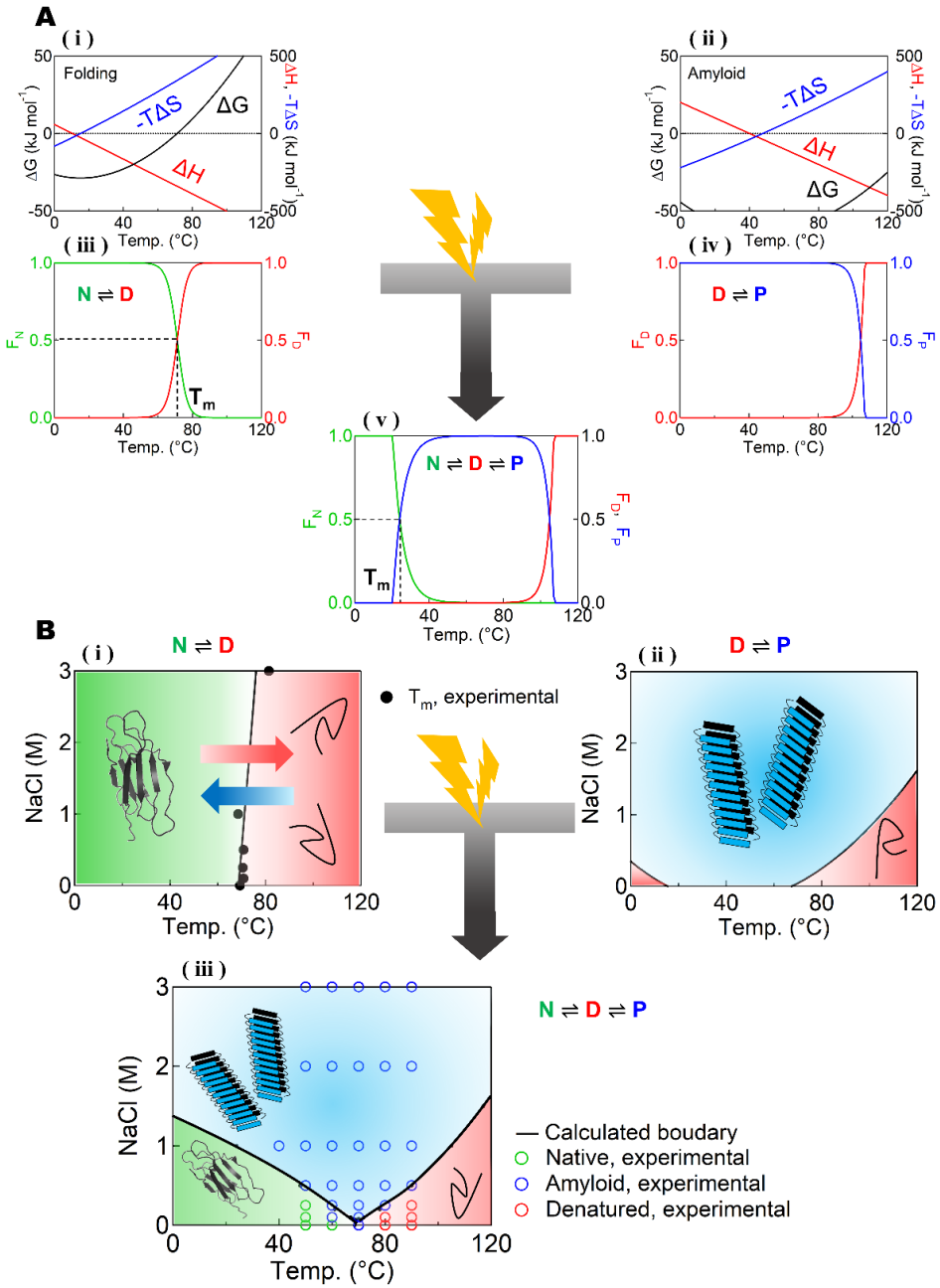



**Figure 3-9. Temperature- and NaCl concentration-dependent conformational phase diagrams of β2m. A,** Temperature dependences of thermodynamic parameters for folding (Mechanism 1, panel i) and amyloid formation (Mechanism 2, panel ii). Fractions of N, D, and P states for folding (panel iii), amyloid formation (panel iv), and their linked conditions (Mechanism 3, panel v) are also shown. The plots were made using 0.1 mg/mL β2m, 1.0 M NaCl, pH 7.0. **B,** Phase diagrams for folding/unfolding (Mechanism 1, panel i), amyloid misfolding (Mechanism 2, panel ii), and their linked conditions (Mechanism 3, panel iii). Lines show the simulated phase boundaries and dots show the experimental data at 0.1 mg/mL β2m and pH 7.0.

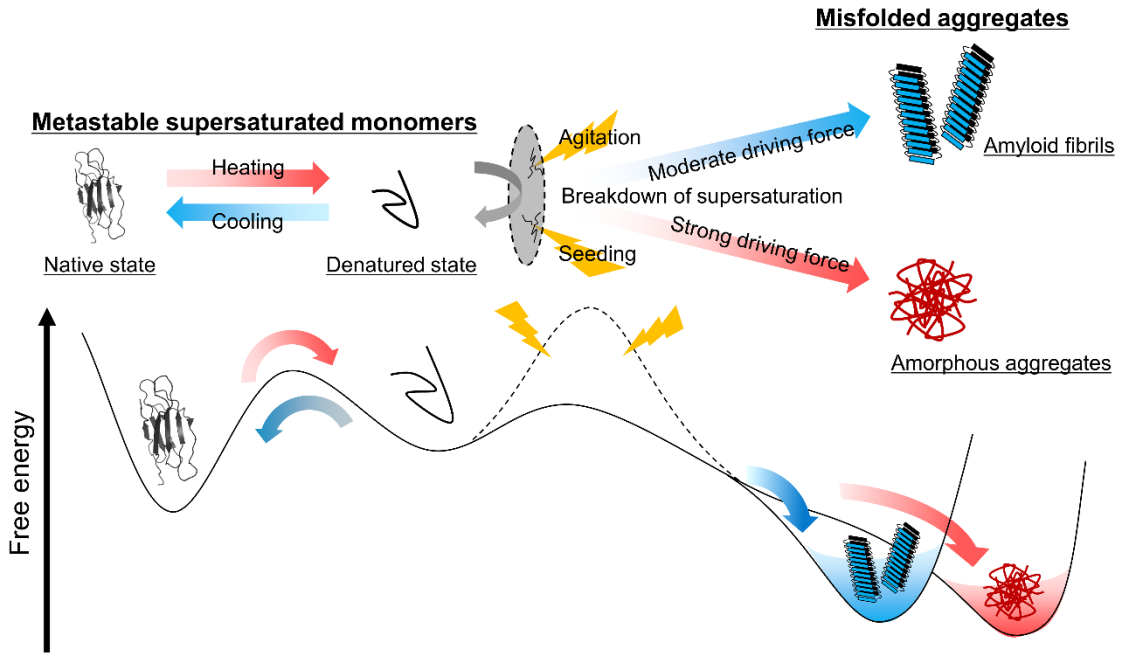



**Figure 3-10. Schematic representations of β2m before and after the linkage of folding and misfolding transitions.** Schematic (upper) and free-energy (lower) representations of the linkage of β2m unfolding with two types of aggregates, in which amyloid misfolding occurs after agitation-dependent breakdown of supersaturation or by seeding.

*Implications for amyloid formation under physiological conditions*

Although I demonstrated amyloid formation of β2m at pH 7.0 and temperatures higher than 40 ℃, similar amyloid formation likely effectively occurs even at physiological temperatures once helped by additional amyloid-promoting factors. These include various biological factors (heparins, lysophosphatidic acids, and polyphosphates) and mechanical agitation, which will cause the onset of DRA (91,114,115,120,125,142,143). Localized unfolding and/or enhanced aggregation at air-liquid interface are likely to be additional important factors breaking supersaturation. I further argue that because of the linkage of protein unfolding with amyloid misfolding, local high temperatures, even if moderate (e.g. 40 ℃), are an important risk factor.

Another important parameter determining the phase diagram is the protein concentration. As protein aggregates form above the solubility of their monomers, high protein concentrations enhance protein aggregation (65,66). I carried out heat-induced amyloid formation at 25.5 μM (0.3 mg/mL) β2m under neutral pH conditions (data not shown). β2m at 25.5 μM formed amyloid fibrils under several conditions, whereas β2m at 8.5 μM did not form fibrils with lower NaCl concentrations at higher temperatures. Of note, 25.5 μM β2m with 1.0 M $Na_2SO_4$ formed a mixture of amyloid fibrils and amorphous aggregates, although 8.5 μM β2m formed only amyloid fibrils under the same conditions (data not shown).

### 3.5. Conclusion

In this chapter, I demonstrated that heat unfolding under agitation effectively caused amyloid formation of intact β2m even at neutral pH and temperatures slightly higher than physiological. Importantly, heat-induced amyloid formation of β2m occurred only under agitation or seeding, which suggested that the breakdown of supersaturation is necessary for amyloid formation, in addition to protein unfolding. I formulated a relationship between the reversible protein unfolding and supersaturation-limited amyloid misfolding. Upon the breakdown of supersaturation, the law of mass action shifts the monomer equilibrium to the direction of the unfolded state, destabilizing the native state and thereby enabling amyloid formation even under physiological conditions with a negligible amount of the unfolded precursor. It is possible that the linked function under seeding conditions plays a role in the pathology of various amyloidoses, including the marked infectious behavior observed for prion seeds.

Moreover, I compared heat-dependent protein unfolding and amyloid formation to obtain a unified mechanism of protein folding and misfolding. In the past decades, studies on protein folding/unfolding often employed heat denaturation at non-physiological high temperatures (132,133). The thermodynamic parameters elucidated under those extreme conditions have been valuable for clarifying the mechanism of protein folding under physiological conditions, because they can be extrapolated back to the physiological conditions. The same was true for amyloid misfolding. The properties elucidated under non-physiological high temperatures could be extrapolated to the physiological conditions. Most importantly, I elucidate that the linkage of protein unfolding and misfolding promotes amyloid formation even at physiological temperatures. Taken together, the heating and agitation used in this chapter, although they were non-physiological, will be powerful for further addressing the mechanism of amyloid formation under physiological conditions.

# Chapter 4.

## Combining the Anfinsen's intramolecular folding world with the supersaturation-limited intermolecular misfolding world

## 4.1. Introduction

In 1950's, Christian B. Anfinsen and his colleagues showed reversible protein denaturation/renaturation phenomena by unfolding/refolding of ribonuclease A (RNaseA), where reduction and reformation of four disulfide bonds are coupled (Chapter 1). Based on their finding, Anfinsen proposed a thermodynamic hypothesis for protein folding; the information determining the native structure of a protein resides in the chemistry of its primary structure (4). His idea has been widely known as "Anfinsen's dogma", proposing that the native structure is a state of free energy minimum under physiological conditions. Anfinsen's dogma has been accepted for a long while, supporting the structural predictions of the native structures on the basis of amino acid sequences (144).

On the other hand, various exceptional phenomena have been found. For example, serpin proteins transform their semi-stable native structure into the most stable loop-inserted form during enzymatic reactions (Chapter 2) Intrinsically disordered proteins (IDPs) have no ordered structures under the native conditions (145,146). Another example is protein misfolding. Although many small globular proteins refold to their native conformations even after unfolding, as Anfinsen's dogma predicted, they sometimes misfold forming substantially different non-ordered amorphous aggregates or highly-ordered amyloid fibrils, as I described above (Chapter 1). Especially, amyloid formation has been investigated extensively because it is deeply associated with various amyloidoses (Chapter 1). Although numerous studies have been carried out, the mechanisms of amyloid formation still remain unclear. We often see illustrations with folding and misfolding funnels set aside, arguing that folding and misfolding are competitive events for unfolded proteins. However, exact relationship between folding and misfolding funnels has not been established. One of the most important questions toward comprehensive understanding of folding and misfolding is what the critical factor is for leading an unfolded protein to the amyloid pathway rather than the refolding pathway.

In the previous chapter, I focused on the breakdown of supersaturation as a critical factor required for a pathway to amyloid fibrils in addition to the unfolding of proteins. I performed heating-induced amyloid formation of β2m, which is a causative protein of DRA, at pH 7, and found that it occurred only in the presence of agitation at

high temperature, where unfolding of β2m is at least partly induced. Thus, I proposed that the breakdown of supersaturation above solubility is necessary for opening a misfolding pathway, in addition to protein unfolding, and that the linkage with misfolded state itself destabilizes the native state by the law of mass action.

In this chapter, to extend my consideration, I examine amyloid formation of various proteins by "heating and agitation" methodology. The list of target proteins includes not only typical amyloidogenic proteins such as α-synuclein (αSyn) and transthyretin (TTR), but also several textbook proteins of folding/unfolding study such as RNaseA, hen egg white lysozyme (HEWL), and α-lactalbumin (αLA) (**Table 4-1**). The representative tertiary structures of them are illustrated in **Fig. 4-1**. In agreement with the Anfinsen's dogma, most small globular proteins simply show reversible unfolding/refolding in the absence of agitation, in agreement with the calorimetric studies extensively performed previously (132,133). On the other hand, as I anticipated, they form amyloid fibrils in the presence of agitation at high temperatures, where linkage of unfolding and amyloid formation destabilizes the native state. Of note, I succeed in spontaneous amyloid formation of wild-type TTR and wild-type RNaseA, which have never been achieved previously. My results reveal the power of "heating and agitation" methodology and argue that the breakdown of supersaturation links the Anfinsen's intramolecular folding/unfolding world to the intermolecular misfolding world, establishing the comprehensive understanding of protein folding and misfolding.

**Table 4-1. List of the target proteins/peptides in this thesis.**

| General properties | | | | | | Experimental conditions | | Types of transition |
|---|---|---|---|---|---|---|---|---|
| **Classification** | **Name** | **Length** | **Mw** | **pI** | **Related amyloidoses** | **pH** | **NaCl conc.** | |
| Short peptides | pOVA | 23 | 2.5 kDa | 5.84 | - | 8 | 0.1 M | A |
| | Glucagon | 29 | 3.5 kDa | 6.75 | - | 7 | 0.1 M | |
| | IAPP | 37 | 3.9 kDa | 8.90 | Type II diabetes | 7 | 0.1 M | |
| | $A\beta_{40}$ | 40 | 4.3 kDa | 5.31 | Alzheimer's disease | 7 | 0.1 M | |
| | Insulin | 51 | 5.8 kDa | 5.39 | - | 7 | 0.1 M | |
| Immunoglobulin folds | β2m | 99 | 12 kDa | 6.07 | DRA | 7 | 0-3 M | S |
| | $C_L$ | 100 | 11 kDa | 5.55 | AL amyloidosis | 7 | 0.5 M | |
| | $V_L$ | 112 | 12 kDa | 4.99 | | | 0.2 M | |
| Globular proteins | Ubiquitin | 76 | 8.6 kDa | 6.56 | - | 2 | 0.5 M | |
| | αLA | 123 | 14 kDa | 4.80 | - | 2 | 0.5 M | |
| | RNaseA | 124 | 14 kDa | 8.64 | - | 5 | 0.2 M | |
| | TTR | 127 | 14 kDa | 5.31 | SSA, FAP, FAC | 2 | 0.1 M | |
| | HEWL | 129 | 14 kDa | 9.32 | - | 2 | 0.5 M | |
| | OVA | 386 | 43 kDa | 5.19 | - | 8 | 0.1 M | B |
| IDPs | αSyn | 140 | 14 kDa | 4.67 | Parkinson's disease | 7 | 1 M | S |
| | TDP-43 | 414 | 45 kDa | 5.85 | ALS, FTD | 7 | 1 M | B |
| | Tau | 441 | 46 kDa | 8.24 | Alzheimer's disease | 7 | 0.15 M | |

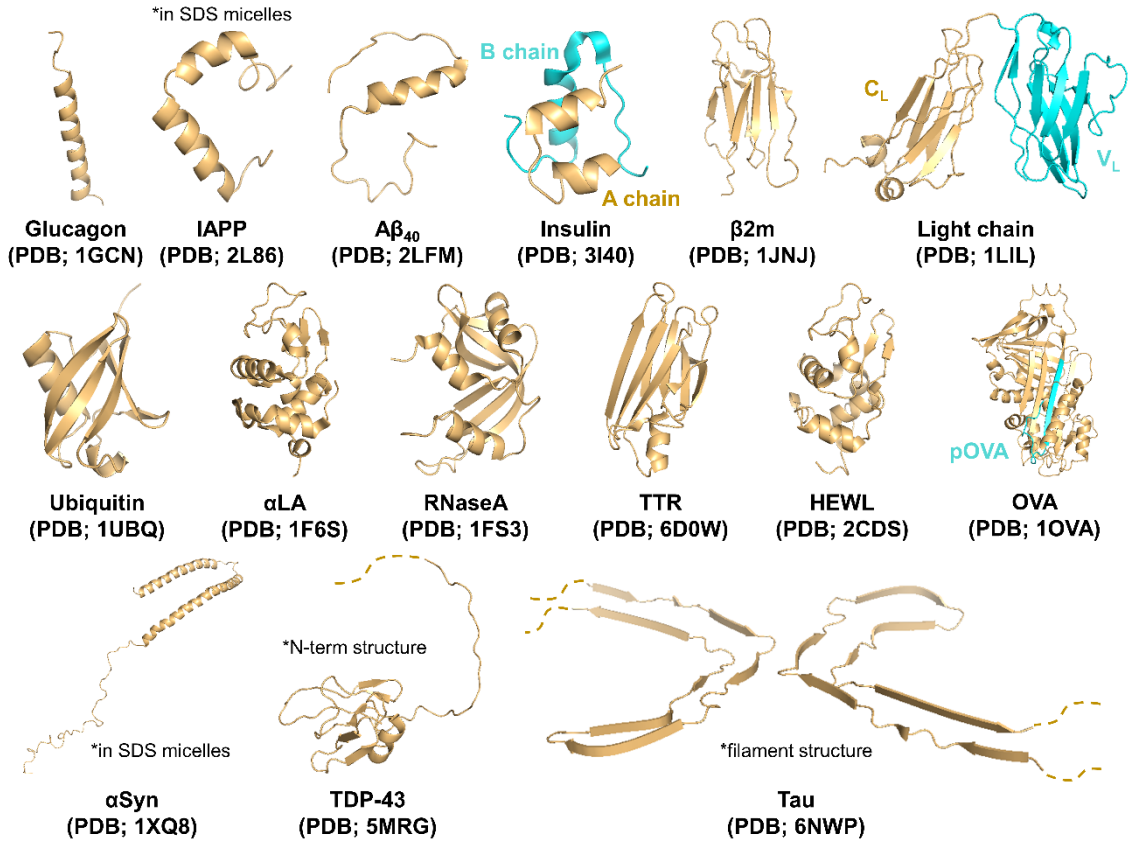



**Figure 4-1. Representative structures of the target proteins/peptides drawn with PyMOL.**

## 4.2. Materials and methods

*Proteins and chemicals*

Recombinant human αSyn protein was expressed in *Escherichia coli* and purified as previously reported (147). $V_L$ fragment was gifted by Prof. Buchner (Technische Universität München, München, Germany). $C_L$ fragment was gifted by Dr. Akazawa (National Institute of Advanced Industrial Science and Technology, Osaka, Japan). TTR protein was gifted by Prof. Chatani (Kobe University, Kobe, Japan). Glucagon peptide was gifted by Prof. Otzen (Aarhus University, Aarhus, Denmark). TDP-43 protein was gifted by Assist. Prof. Yamaguchi (Osaka University, Osaka, Japan). Tau protein was gifted by Assist. Prof. So (Osaka University, Osaka, Japan). αLA, RNaseA, and insulin proteins were purchased from Sigma-Aldrich Co., LLC. (St. Louis, USA). Ubiquitin protein was purchased from Funakoshi Co., Ltd. (Tokyo, Japan). $A\beta_{40}$ and IAPP peptides were purchased from Peptide Institute, Inc. (Osaka, Japan). All other reagents, including HEWL protein, were obtained from Nacalai Tesque, Inc. (Kyoto, Japan).

*ThT assays with heating*

Each protein was dissolved in deionized water except for $C_L$, $A\beta_{40}$, TDP-43, and glucagon; they were dissolved in 10 mM acetate buffer (pH 4.7), 0.05% (w/w) ammonia solution, 10 mM Tris-HCl buffer (pH 8) containing 4 M urea, and 20 mM HCl, respectively. Protein concentrations were measured spectrophotometrically using individual theoretical molar extinction coefficients. The sample solution of 2.0 mL in a cuvette with a 1-cm light path contained each protein under the conditions described in the main text. Amyloid formation was detected by ThT fluorescence with an excitation wavelength of 445 nm and an emission wavelength of 485 nm using F4500 or F7100 fluorescence spectrophotometer (Hitachi High-Technologies Corporation, Tokyo, Japan). Light scattering at 450 nm was also measured to detect whole protein aggregation. In the presence of stirring, all fluorescence measurements were performed using a magnetic stirring bar at a stirring speed of 600 rpm. The sample temperature was controlled using a Peltier element (Nippon Tecmo Co., Ltd., Fukuoka, Japan) and measured by a thermocouple Compact Thermologger AM-8000K (Anritsu Meter Co., Ltd., Tokyo, Japan). The equipment setup and the assay scheme were described in Chapter 1.

*CD and TEM measurements*

Far-UV CD spectra (approximately 200–250 nm) were obtained with a model J-720 spectropolarimeter (Jasco Co., Ltd., Tokyo, Japan) using a quartz cell with a 1-mm path length. CD data were expressed as mean residue ellipticity.

TEM images were obtained using a transmission electron microscope (H-7650, Hitachi High-Technologies Corporation) with 5 μL of 0.5% (w/v) hafnium chloride as the staining agent.

*TTR seeding reactions*

TTR seeds were obtained from the preformed fibrils of heat-induced spontaneous amyloid formation under stirring and sonicated moderately before seeding experiments. The conditions for the sample preparation and measurements were the same as for standard ThT assays, except for the addition of 5% (v/v) seeds.

## 4.3. Results

*Amyloidogenic proteins with an immunoglobulin fold*

In the previous chapter, I showed heating-induced amyloid formation of β2m, which is a component of the major histocompatibility complex 1 and has an immunoglobulin fold. To monitor the reactions, I carried out ThT assays with a fluorescence spectrophotometer equipped with a Peltier element for temperature control (represented in Chapter 1). In this chapter, I applied the same methods to monitor the heating-induced amyloid formation of various proteins. First, I chose small globular proteins with an immunoglobulin fold like β2m; the variable ($V_L$) and constant ($C_L$) domains of immunoglobulin light chain. An excess amount of the monoclonal light chains or $V_L$ fragments secreted into the blood stream sometimes forms amyloids and causes AL amyloidosis, whereas $C_L$ domain is assumed to modulate their amyloidogenicity (148-151).

As I expected, at pH 7.0, 200 mM NaCl and a heating rate of 1 °C/min in the presence of stirring, 0.1 mg/mL $V_L$ fragment showed increases in ThT fluorescence at approximately 65 °C, while no reactions were observed in the absence of stirring (**Fig. 4-2A**). The unfolding midpoint temperature of another $V_L$ strain under similar conditions was reported to be 52 °C (152). The amyloid formation was verified by CD spectroscopy and TEM observation (**Fig. 4-2B**). These results were consistent with those observed for β2m.

$C_L$ fragment also showed heating-induced amyloid formation as observed for $V_L$, although $C_L$ amyloid formation occurred at a higher temperature (**Fig. 4-2C**). The unfolding midpoint temperature of another $C_L$ strain under similar conditions was reported to be 53 °C (152). Moreover, even fibrous aggregates were observed by TEM, its conformational change monitored by CD was not so significant compared with that of $V_L$ (**Fig. 4-2D**). These results were consistent with the previously reported high and low amyloidogenicities of $V_L$ and $C_L$, respectively (149).

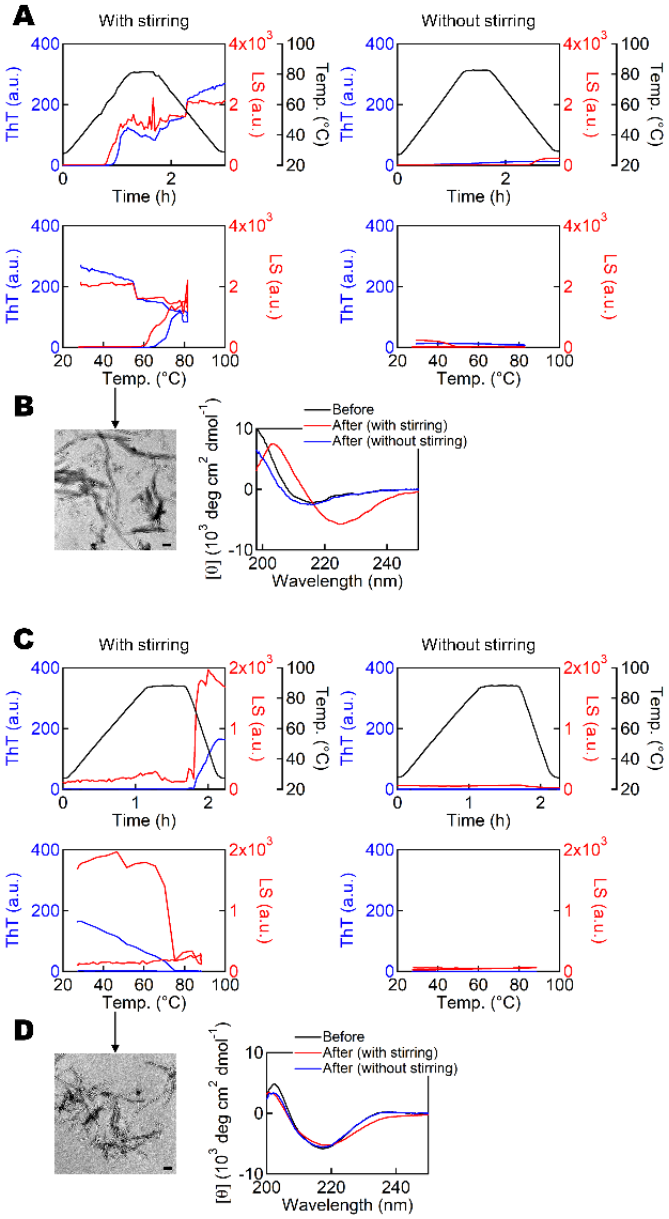



**Figure 4-2. Heating-induced amyloid formation of immunoglobulin fold proteins. A, C,** ThT assays of 0.1 mg/mL $V_L$ (A) and 0.2 mg/mL $C_L$ (C) at pH 7.0 with 200 and 500 mM NaCl, respectively, upon heating in the presence (each left panel) or absence (each right panel) of stirring. The intensities of ThT fluorescence and LS are indicated by blue and red, respectively. In upper panels, the time courses of temperature change are shown by the black lines. **B, D,** CD spectra and TEM images of the $V_L$ (B) and $C_L$ (D) samples after ThT assays. The CD measurements were performed at 25 ℃ and the line representations for the spectra are described in the panels. Scale bars of the TEM images; 200 nm.

*Stably-structured small globular proteins*

Second, I performed heating-induced amyloid formation of several small globular proteins with a tightly folded native structure. HEWL is one of the most extensively studied proteins in terms of protein unfolding/folding and its homologue human lysozyme is associated with lysozyme amyloidosis, a rare autosomal dominant hereditary systemic amyloidosis (153,154). Because it is well-known that HEWL easily forms amyloid fibrils at high temperatures under acidic conditions (129,155,156), I used this protein as a model to examine the role of agitation for the heating-induced amyloid formation. My methodology indeed showed that agitation is required for amyloid formation of 0.2 mg/mL HEWL at pH 2.0 and 500 mM NaCl (**Fig. 4-3A, B**). HEWL showed increases in ThT fluorescence at approximately 60 ℃ and the midpoint temperature of HEWL unfolding under similar conditions was reported to be 57 ℃ (54). In contrast, although small increases in ThT fluorescence and LS were observed under quiescent conditions, neither conformational change nor aggregate was detected (**Fig. 4-3A, B**).

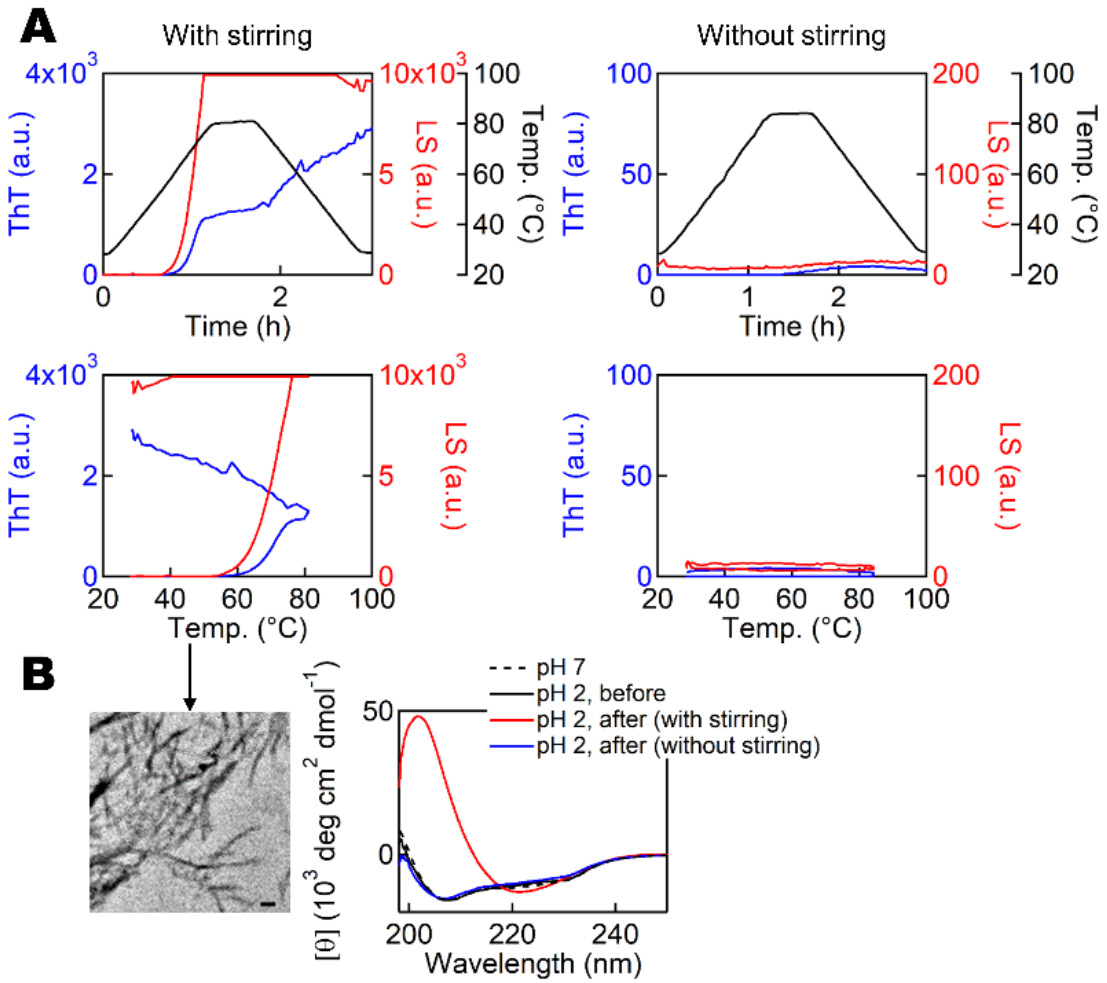



**Figure 4-3. Heating-induced amyloid formation of HEWL at low pH. A,** ThT assays of 0.2 mg/mL HEWL with 20 mM HCl and 500 mM NaCl, upon heating in the presence (left panels) or absence (right panels) of stirring. The intensities of ThT fluorescence and LS are indicated by blue and red, respectively. In upper panels, the time courses of temperature change are shown by the black lines. **B,** CD spectra and TEM image of the HEWL samples after ThT assays. The CD measurements were performed at 25 ℃ and the line representation for the spectra is described in the panel. Scale bar of the TEM image; 200 nm.

A tetrameric transporter plasma protein TTR has been studied actively because of its association with several fatal amyloidoses such as senile systemic amyloidosis, familial amyloid polyneuropathy, and familial amyloid cardiomyopathy (157). Although not only a large number of pathogenic familial mutants but also wild-type TTR can form amyloid fibrils in patients, in vitro spontaneous amyloid formation of wild-type TTR has never been reported unless fragmentation was induced by proteolysis (108). I found that wild-type full length TTR exhibited amyloid formation upon incubation under stirring at pH 2 and 50 ℃ in 100 mM NaCl with a lag time of approximately 2 h, where TTR kept a native-like conformation before heating (**Fig. 4-4A, B**). Although I monitored the fibril formation upon increasing temperature as used for HEWL (**Fig. 4-3A**), no significant increase in ThT fluorescence was observed suggesting a long lag time even at high temperatures under agitation.

Mr. Samejima (Osaka University) examined the dependence of TTR amyloid formation on the NaCl concentration at pH 2 and 50 ℃, showing that the amyloid formation occurred only at a limited NaCl concentration range of 50−150 mM (**Fig. 4-4C**). Moreover, he examined the various conditions of pH between 5 and 7 at various concentrations of NaCl or sodium sulfate. However, when TTR aggregated, only amorphous aggregates without ThT fluorescence were formed. These results indicated that TTR had a less propensity than do other small globular proteins to form amyloid fibrils, although it did form amyloid fibrils with my methodology of "heating under agitation" at pH 2, 100 mM NaCl, and 50 ℃, where amyloid formation was preferred to amorphous aggregation.

It has been reported that TTR easily forms ThT-negative and seeding-inactive filamentous aggregates (158), which seems to correspond to amorphous aggregates observed by Samejima under various conditions or curvilinear fibrils reported by others. In contrast, the amyloid fibrils I prepared at pH 2, 100 mM NaCl, and 50 ℃ showed a seeding activity under the same solvent conditions (**Fig. 4-4D**). It is noted that a seeding activity is one of the typical properties, defining crystal-like mechanism of amyloid formation. Notably, I used TTR for these experiments at a concentration of 0.2 mg/mL, which corresponds to the concentration in human plasma (159).

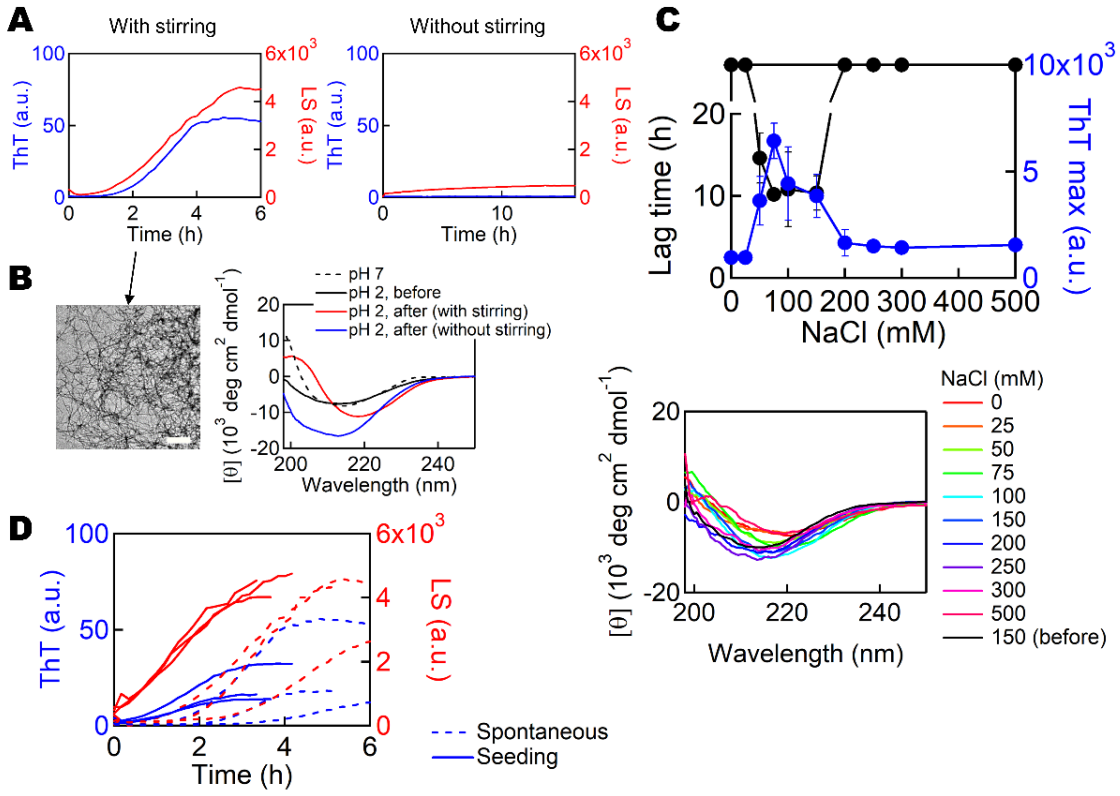



**Figure 4-4. Amyloid formation of wild-type TTR at low pH. A,** ThT assays of spontaneous reactions of 0.2 mg/mL TTR with 20 mM HCl and 100 mM NaCl upon incubation at 50 ℃ in the presence (left) or absence (right) of stirring. The intensities of ThT fluorescence and LS are indicated by blue and red, respectively. **B,** CD spectra and TEM image of the TTR samples after ThT assays. The CD measurements were performed at 25 ℃ and the line representation for the spectra is described in the panel. Scale bar of the TEM image; 500 nm. **C,** Dependence of 0.3 mg/mL TTR amyloid formation on various NaCl concentrations (0–500 mM) at pH 2 and 50 ℃ monitored by ThT assays (upper) and CD measurements (lower). In upper panel, reaction lag times and ThT maximal intensities are indicated by black and blue lines, respectively. The original data were provided by Mr. Samejima (Osaka University). **D,** ThT assays with (solid lines) or without (dashed lines) 5% preformed seed fibrils under the same conditions as the above (A). $n = 3$.

I also challenged amyloid formation of RNaseA and αLA, which are textbook proteins for folding studies. It has been reported that the hinge loop-expanded mutant of RNaseA generated amyloid-like fibrils via 3D domain swapping, whereas the wild-type RNaseA did not (160,161). It has been reported that αLA formed amyloid fibrils at low pH or under reduction conditions (162).

The most importantly, I succeeded in amyloid formation of wild-type RNaseA at 200 mM NaCl and pH 5, starting at approximately 80 ℃, where stirring was essential (**Fig. 4-5A, B**). In the case of αLA, my methodology of heating under agitation produced amyloid fibrils, consistent with the previous reports, although stirring was essential for the amyloid formation (**Fig. 4-5C, D**). The amyloid formation of αLA seemed to start at approximately 65 ℃.

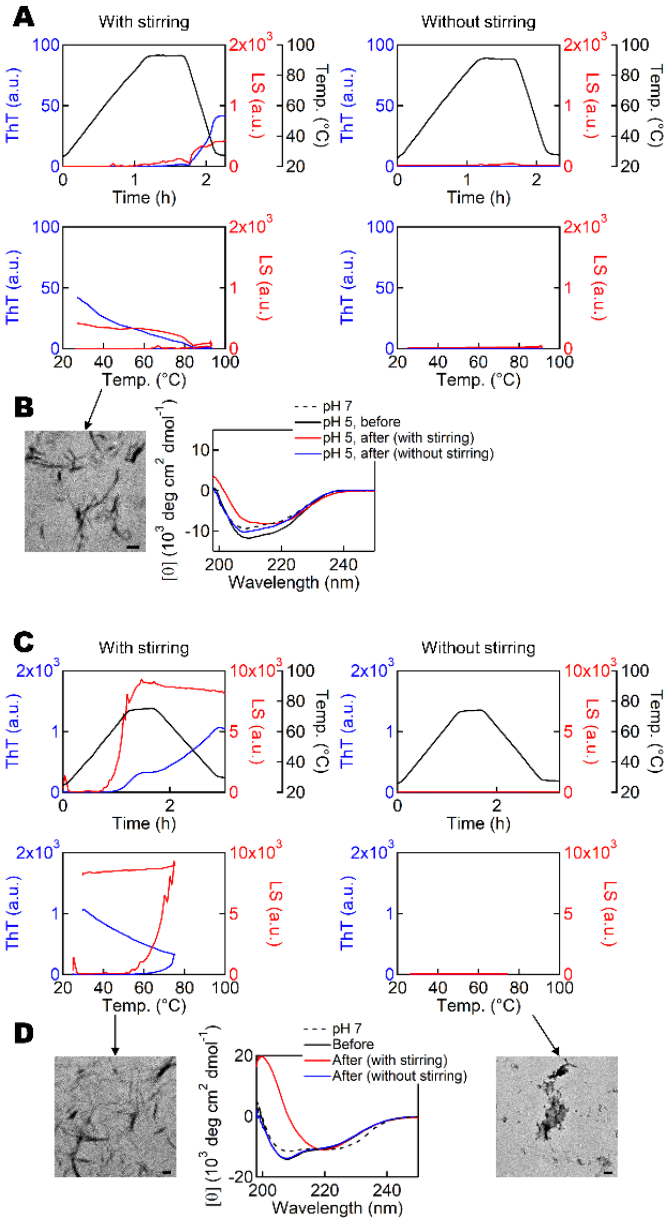



**Figure 4-5. Heating-induced amyloid formation of small globular proteins often used for protein folding studies. A, C,** ThT assays of RNaseA (A) and αLA (C), upon heating in the presence (each left panel) or absence (each right panel) of stirring. Solution conditions; 0.2 mg/mL RNaseA in 20 mM acetate buffer (pH 5.0) and 200 mM NaCl; 0.2 mg/mL αLA in 20 mM HCl and 500mM NaCl. The intensities of ThT fluorescence and LS are indicated by blue and red, respectively. In upper panels, the time courses of temperature change are shown by the black lines. **B, D,** CD spectra and TEM images of the RNaseA (B) and αLA (D) samples after ThT assays. The CD measurements were performed at 25 ℃ and the line representations for the spectra are described in the panels. Scale bars of the TEM images; 200 nm.

A 8.6 kDa small protein ubiquitin, which is a protein modifier, appears ubiquitously in various biological phenomena as its name suggests and the sequence is highly conserved among all eukaryotes (163), is also used as a model protein following the Anfinsen's dogma (164). Recently, amyloid-like fibril formation of heat-treated polyubiquitin chains has been reported (165). Thus, I examined whether monoubiquitin could form amyloid fibrils by heating under agitation. As I expected, increases in ThT fluorescence occurred upon incubation at 90 ℃ and pH 2, where stirring was essential (**Fig. 4-6A**). Of note, the ThT intensities were very weak despite the strong LS even after cooling to 25 ℃ (**Fig. 4-6B**). Nevertheless, the CD spectra indicated a β-rich type conformational change and fibrous aggregates were observed in the TEM image (**Fig. 4-6C**).

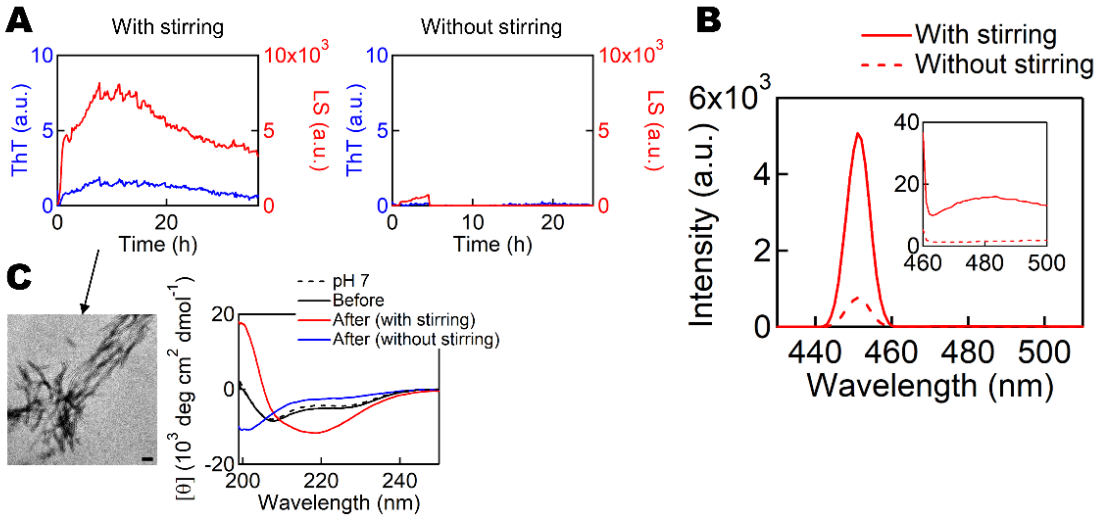



**Figure 4-6. Heating-induced amyloid formation of monoubiquitin upon incubation at 90 ℃. A,** ThT assays of 0.2 mg/mL ubiquitin with 20 mM HCl and 500 mM NaCl upon incubation at 90 ℃ in the presence (left) or absence (right) of stirring. The intensities of ThT fluorescence and LS are indicated by blue and red, respectively. **B,** Fluorescence spectra of the ubiquitin samples after ThT assays in the presence (solid line) and absence (dashed line) of stirring. The inset spectra highlight the wavelength range of ThT fluorescence. **C,** CD spectra and TEM image of the ubiquitin samples after ThT assays. The CD measurements were performed at 25 ℃ and the line representation for the spectra is described in the panel. Scale bar of the TEM image; 200 nm.

*Highly-amyloidogenic short peptides*

Many short peptides without ordered structures form amyloid fibrils. Amyloid β peptides 1-40 ($A\beta_{40}$) or 1-42 ($A\beta_{42}$) are two of the most famous amyloidogenic peptides. Amyloid formations of $A\beta_{40}$ and $A\beta_{42}$ have been suggested to play key roles in Alzheimer's disease, where senile plaques (amyloid plaques) in the grey matter of the brain contain a large amount of $A\beta_{40}$ and $A\beta_{42}$ fibrils (166,167). When my methodology under agitation was used, $A\beta_{40}$ formed amyloid fibrils monitored by ThT and LS at pH 7 and approximately 40 ℃. On the other hand, without agitation, no fibril formation was observed (**Fig. 4-7A**). These were confirmed by CD measurements and TEM images (**Fig. 4-7B**). However, even without agitation, the heat treatment and subsequent overnight incubation caused amyloid formation monitored by TEM (**Fig. 4-7B**). I obtained the similar results for a 29-residue peptide hormone glucagon, i.e. fibrous aggregates monitored by TEM were formed upon a long incubation after the ThT assay despite no reaction was observed by the ThT assay (**Fig. 4-7C, D**).

Islet amyloid polypeptide (IAPP), also known as amylin, is a 37-residue peptide hormone and the amyloid deposition of IAPP to the pancreatic β-cells may cause type II diabetes (168). Upon heating at 1 ℃/min, IAPP showed amyloid formation both in the presence and absence of stirring at pH 7, confirmed by ThT assays, CD spectroscopy, and TEM observation (**Fig. 4-8A, B**), suggesting that supersaturation barrier is not very high.

Insulin, one of the peptide hormones secreted by the pancreatic islets as well as IAPP, is composed of a 21-residue A chain and a 30-residue B chain, which are linked by two disulfide bonds. It is known that insulin forms amyloid fibrils upon heating and the degree of agitation affects the fibril morphology of insulin (169). I found that, under agitation, ThT increased at approximately 80 ℃ (**Fig. 4-8C**). Without stirring, no increase in ThT was observed upon heating. Upon cooling, LS increased significantly indicating the formation of amorphous aggregates (**Fig. 4-8C**). These results were confirmed by CD and TEM (**Fig. 4-8D**). It is possible that insulin entered an alternative pathway leading to amorphous aggregation upon heating and cooling under quiescence.

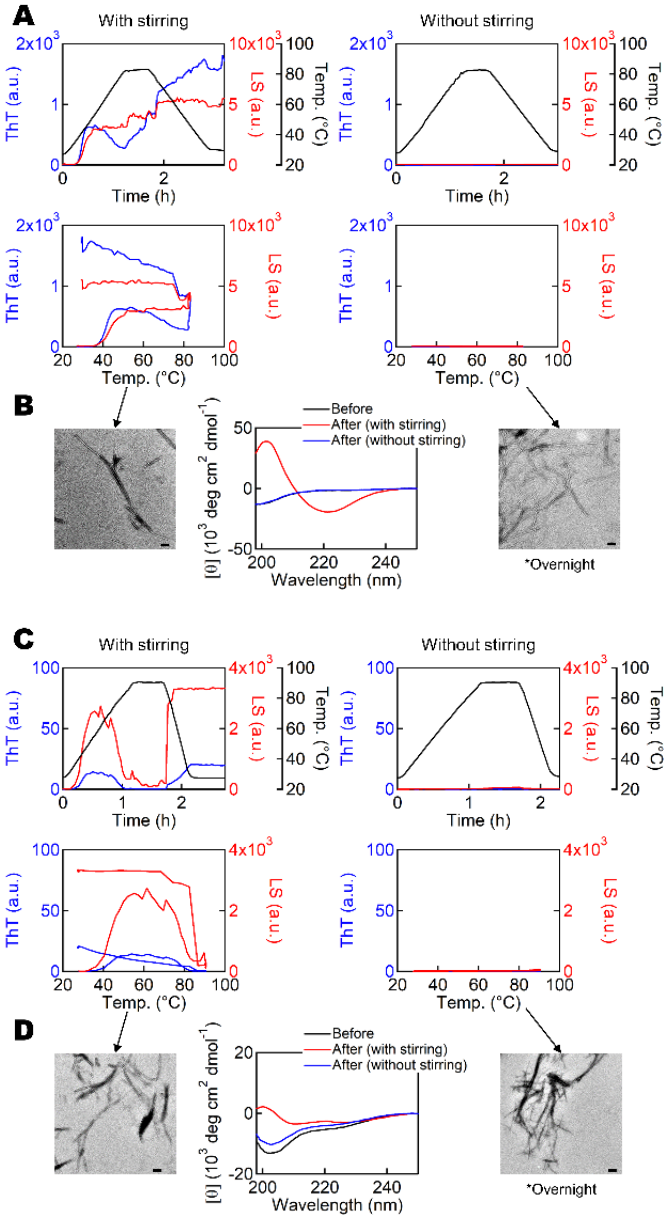



**Figure 4-7. Heating- and agitation-dependent amyloid formation of the amyloidogenic peptides. A, C,** ThT assays of 0.1 mg/mL Aβ$_{40}$ (A) and 0.2 mg/mL glucagon (C) at pH 7.0 with 100 mM NaCl, upon heating in the presence (each left panel) or absence (each right panel) of stirring. The intensities of ThT fluorescence and LS are indicated by blue and red, respectively. In upper panels, the time courses of temperature change are shown by the black lines. **B, D,** CD spectra and TEM images of the Aβ$_{40}$ (B) and glucagon (D) samples after ThT assays. The CD measurements were performed at 25 ℃ and the line representations for the spectra are described in the panels. Scale bars of the TEM images; 200 nm.

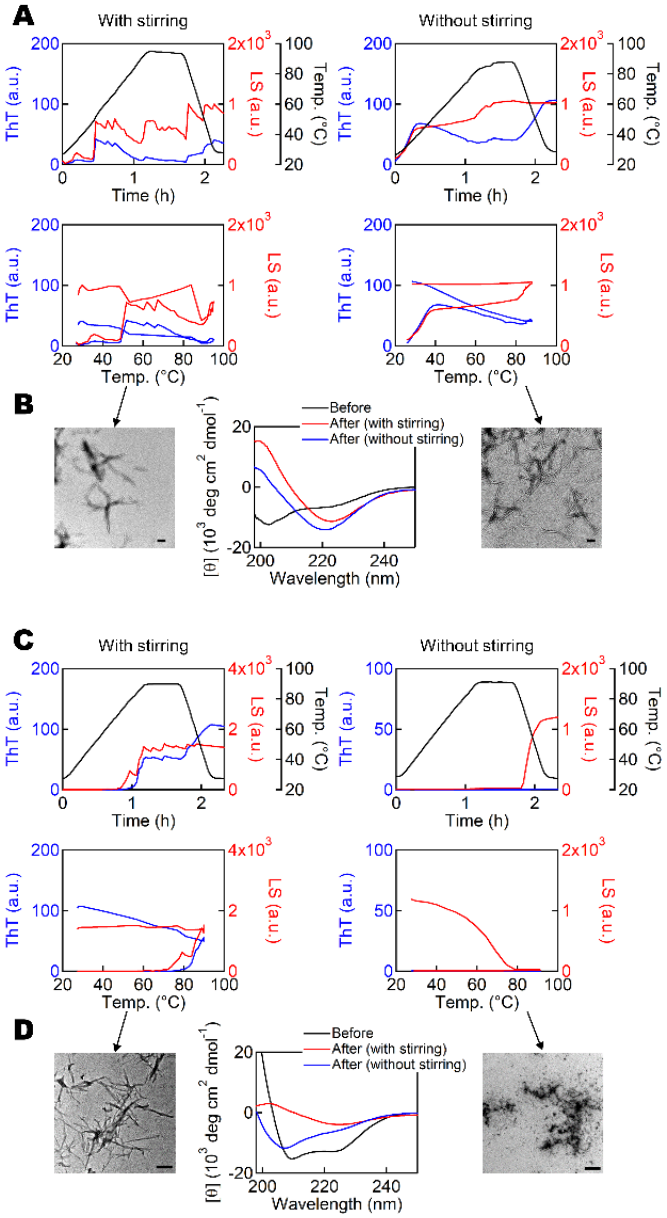



**Figure 4-8. Agitation-independent aggregation of the amyloidogenic peptides. A, C,** ThT assays of 0.1 mg/mL IAPP (A) and 0.2 mg/mL insulin (C) at pH 7.0 with 100 mM NaCl, upon heating in the presence (each left panel) or absence (each right panel) of stirring. The intensities of ThT fluorescence and LS are indicated by blue and red, respectively. In upper panels, the time courses of temperature change are shown by the black lines. **B, D,** CD spectra and TEM images of the IAPP (B) and insulin (D) samples after ThT assays. The CD measurements were performed at 25 ℃ and the line representations for the spectra are described in the panels. Scale bars of the TEM images; 200 nm.

*Intrinsically-disordered relatively large proteins*

Finally, I examined the heating-induced amyloid formation with several IDPs. IDPs stay out of the Anfinsen's dogma because of the lack of the ordered stable native structures. One of the most amyloidogenic IDPs is αSyn. Amyloid formation of αSyn is tightly associated with three types of synucleinopathies; Parkinson's disease, dementia with Lewy bodies, and multiple system atrophy (170). According to the ThT assays under stirring at 1.0 M NaCl and pH 7, heating-induced amyloid formation of αSyn occurred significantly starting at approximately 60 ℃, whereas it did not without stirring (**Fig. 4-9A**). Although some changes in the LS intensities occurred during heating without stirring, CD spectra and TEM images exhibited amyloid formation only under stirring (**Fig. 4-9B**).

Mr. Samejima carried out detailed experiments examining the dependence of αSyn amyloid formation on various sodium sulfate concentrations and temperatures. The results showed that amyloid formation was promoted at high temperatures and relatively high concentrations of sodium sulfate without a symptom of amorphous aggregation (**Fig. 4-9C, D**). The results showed that even αSyn, one of the IDPs, follows a pattern of amyloid formation by heating under agitation.

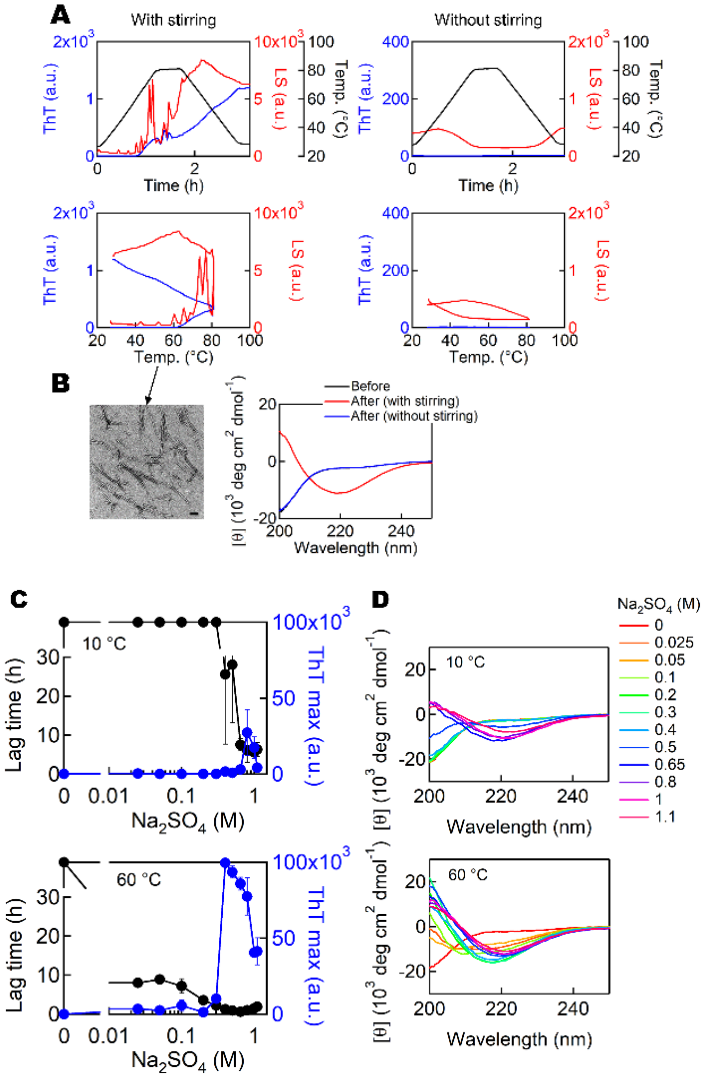



**Figure 4-9. Heating- and agitation-dependent amyloid formation of αSyn. A,** ThT assays of 0.2 mg/mL αSyn at pH 7.0 with 1.0 M NaCl, upon heating in the presence (left panels) or absence (right panels) of stirring. The intensities of ThT fluorescence and LS are indicated by blue and red, respectively. In upper panels, the time courses of temperature change are shown by the black lines. **B,** CD spectra and TEM image of the αSyn samples after ThT assays. The CD measurements were performed at 25 °C and the line representations for the spectra are described in the panels. Scale bar of the TEM image; 200 nm. **C, D,** Dependence of 0.1 mg/mL αSyn amyloid formation on various sodium sulfate concentrations (0–1.1 M) at 10 (upper) or 60 (lower) °C monitored by ThT assays (C) and CD measurements (D). In panels C, reaction lag times and ThT maximal intensities are indicated by black and blue lines, respectively. The original data were provided by Mr. Samejima (Osaka University) for these panels C and D.

Microtubule-associated protein tau made of 441 amino acid residues is one of the most extensively investigated IDPs because tau filamentous aggregates (i.e., paired helical filaments) are the main component of neurofibrillary tangles in the brain of Alzheimer's disease patients. Neurofibrillary tangles are symptom of Alzheimer's disease as well as senile plaques of Aβ, suggesting that tau and Aβ work synergistically causing the disease (171,172). On the other hand, TAR DNA-binding protein 43 (TDP-43), a 414-residue nuclear IDP playing a central role in RNA metabolism, forms aggregates in patients with amyotrophic lateral sclerosis (ALS) and frontotemporal dementia (FTD). Therefore, TDP-43 has also been studied actively in terms of the mechanism of aggregation (173).

With tau and TDP-43, I examined the effects of heating in the presence or absence of stirring. For both proteins, ThT assays suggested the heating-induced amyloid formation independent of stirring, although no apparent conformational change was observed by the CD measurements (**Fig. 4-10**). Although both exhibited relatively strong ThT fluorescence signals, when examined by TEM, only tau showed a clear fibrous morphology (**Fig. 4-10B, D**). These results were completely different from those of αSyn or the amyloidogenic globular proteins, indicating that amorphous aggregates dominated although they might contain amyloid core regions like OVA (Chapter 2).

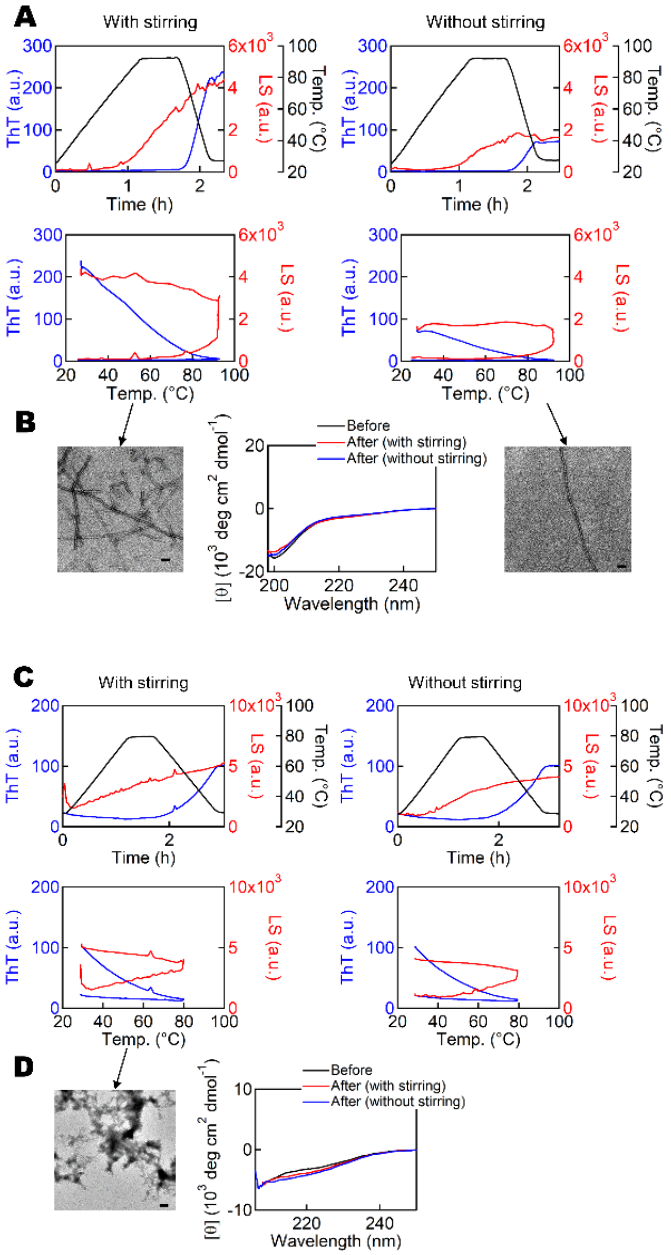



**Figure 4-10. Heating-dependent amyloid formation of IDPs. A, C,** ThT assays of 0.4 mg/mL tau (A) and 0.2 mg/mL TDP-43 (C) at pH 7.0 with 0.15 and 1.0 M NaCl, respectively, upon heating in the presence (each left panel) or absence (each right panel) of stirring. The intensities of ThT fluorescence and LS are indicated by blue and red, respectively. In upper panels, the time courses of temperature change are shown by the black lines. **B, D,** CD spectra and TEM images of the tau (B) and TDP-43 (D) samples after ThT assays. The CD measurements were performed at 25 ℃ and the line representations for the spectra are described in the panels. Scale bars of the TEM images; 200 nm.

## 4.4. Discussion

*Requirement of the breakdown of supersaturation for amyloid formation*

I previously revealed that, without the breakdown of supersaturation, β2m stayed in the unfolding/folding equilibrium and that, upon the breakdown of supersaturation, a solubility-dependent misfolding pathway opens, establishing the coupled thermodynamic equilibrium of the unfolding/folding and amyloid polymerization/depolymerization. In other words, reversible unfolding/refolding previously assumed to be a thermodynamic process on the basis of Anfinsen's dogma holds within the kinetic barriers of supersaturation (pseudo-thermodynamic equilibrium) and the true thermodynamic equilibrium often dominated by solubility of unfolded state is achieved upon breakdown of supersaturation. The phase transition from the pseudo-thermodynamic equilibrium to the true thermodynamic equilibrium drives overall populations to amyloid state by the law of mass action, causing the decrease in population of the native state (Chapter 3).

The results showed that supersaturation, which is known to be a required condition to form crystals of solutes, is also required for amyloid formation because amyloid fibrils are crystal-like aggregates of denatured proteins. It is important to recognize that formation of crystal-like amyloid fibrils is controlled by supersaturation. The supersaturation of some denatured proteins is so stable that dramatic phase transition producing amyloid fibrils is possible only under intensive agitation at high temperatures, where the driving forces of precipitation are strengthened. Although the validity of Anfinsen's dogma is often questioned under high protein concentrations where intermolecular interactions are allowed, the persistence of supersaturation and thus difficulty of amyloid formation under quiescent conditions prevented the question to be considered seriously. Now that the atomic structures were clarified for various amyloid fibrils, showing that they are indeed ordered crystal-like structures achieved by hydrophobic and hydrogen bond interactions, it is important to establish a comprehensive mechanism accommodating both protein folding/unfolding and amyloid polymerization/depolymerization.

In this chapter, I extended the results of the previous chapter showing that the same mechanism holds for several well-folded globular proteins such as $V_L$, $C_L$, RNaseA and HEWL. In the absence of stirring, i.e. under supersaturated conditions, these proteins

did not form any aggregates during heat treatments and showed reversible unfolding and refolding, consistent with Anfinsen's dogma. On the other hand, they exhibited amyloid formation when heated under stirring.

These results were similar to those of β2m. Therefore, I introduce the same three-state mechanism as I used for β2m; both folding and misfolding purely depend on the Gibbs free energy change (**Fig. 4-11**). Before the breakdown of supersaturation, a two-state mechanism between the native and unfolded states determines the overall equilibrium (**Fig. 4-11A**). Upon the breakdown of supersaturation, a three-state mechanism between the native, unfolded, and amyloid states determines the overall equilibrium. The transition from the two-state mechanism to the three-state mechanism drives overall equilibrium to the direction of amyloid fibrils apparently destabilizing the native state by the law of mass action (**Fig. 4-11B**). I indeed succeeded in the impregnable amyloid formation of wild-type TTR and wild-type RNaseA, thus directly supporting the validity of my idea.

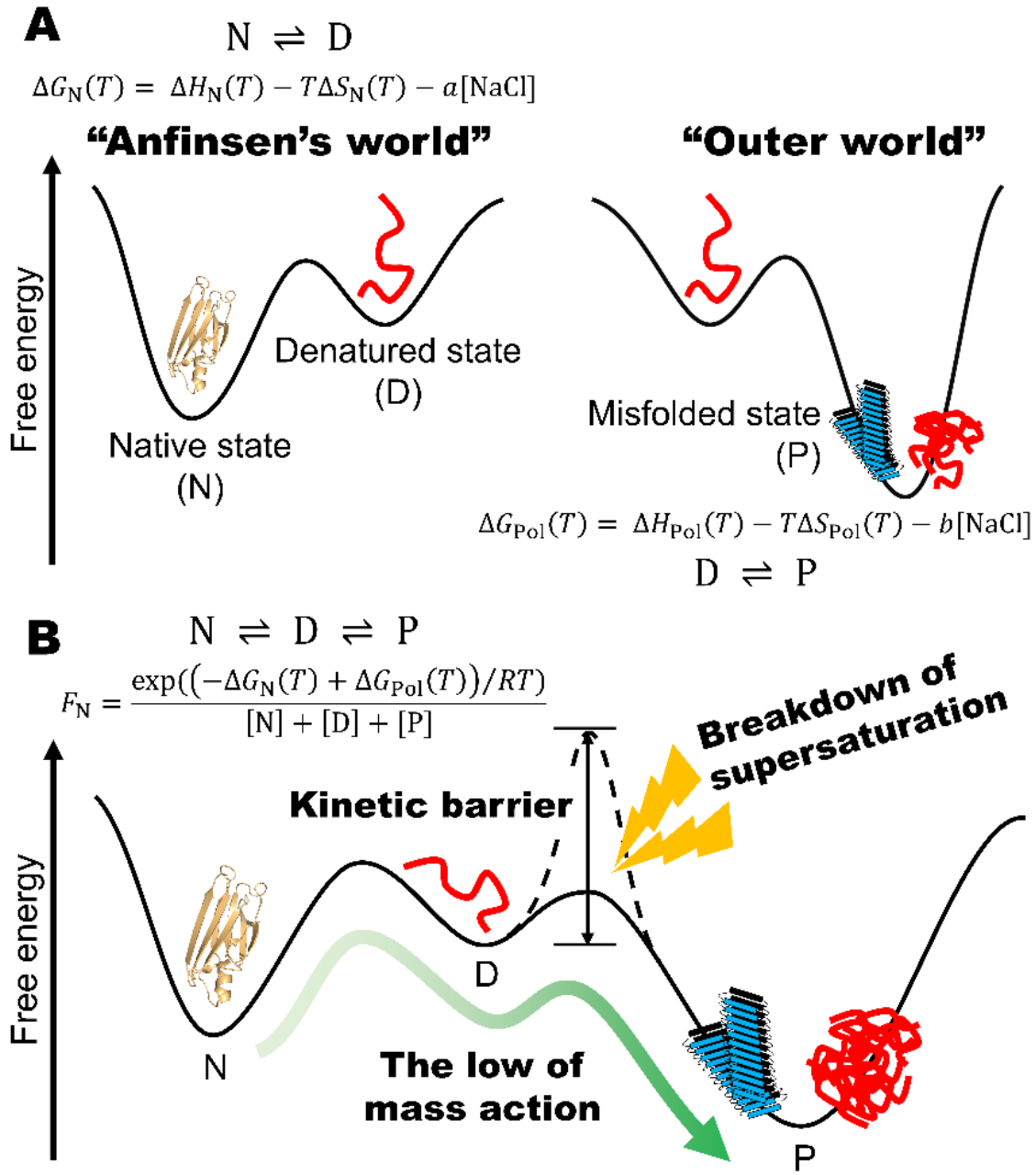



**Figure 4-11. Schematic representations of comprehensive mechanisms of protein folding and misfolding. A,** Two-state mechanisms of protein folding/unfolding (left) and misfolding (right). **B,** A three-state mechanism of protein folding linked with misfolding by supersaturation. All equations inserted in the panels are described in Chapter 3.

*Weak supersaturation barrier for highly amyloidogenic short peptides*

Although I demonstrated the persistence of supersaturation for various globular proteins, short peptides without ordered structures behaved much differently. IAPP and insulin formed amyloid fibrils upon heating even without stirring. $A\beta_{40}$ and glucagon formed amyloid fibrils during sample storage even under quiescence at room temperature. These results seemed to be due to the low free energy-barrier of supersaturation. Even though these short peptides may exist in the Anfinsen's intramolecular folding world, their sequences are occupied by too much proportion of hydrophobic regions relative to the length (**Fig. 4-12**) to keep supersaturation persistent. This may result in the low barrier of supersaturation and amyloid formation even without agitation.

Generally, hydrophobic interactions contribute to enthalpy change of misfolding as well as folding and stabilize the ordered conformational states including both native and amyloid structures. In the case of short peptides, they are too short to construct intramolecular folded structure, thus they highly tend to form intermolecular misfolded aggregates even in the absence of any agitations. Moreover, these phenomena are consistent with those of pOVA (Chapter 2).

*Unique aggregation characteristics of relatively large IDPs*

Aggregates of αSyn, tau, and TDP-43 are associated with the patients of related amyloidosis. However, it is still far from clear if the aggregates in patients are amorphous aggregates or amyloid fibrils. In this chapter, I showed that αSyn indeed formed amyloid fibrils in the same manner as the small globular proteins. Tau and TDP-43 also formed ThT-positive aggregates upon heating, although the reactions were independent of agitation. Moreover, their conformational changes monitored by CD were not significant.

I assume that a proportion of hydrophobic residues in their sequences affects misfolding propensities. αSyn has 140 amino acid residues and about 14% of them are hydrophobic, so that αSyn is a highly soluble IDP (**Fig. 4-12**). For a relatively large protein without disulfide bond, like αSyn, the intrinsic high solubility seems important for preventing amorphous aggregation and for acheiving cooperative transition from monomeric disordered states to amyloid fibrils.

In the case of tau and TDP-43, they have over 400 amino acid residues and their hydrophobic portions are around 10% or below (**Fig. 4-12**). This low proportion of hydrophobic residues will keep them unstructured IDP. However, because of the long primary structures, heating-dependent hydrophobic interactions tended to form local amorphous condensates except a small proportion of amyloid core regions with possible β-spine structures. Therefore, the overall aggregates may show disordered conformations in CD spectra and TEM images may be similar to those so called "fuzzy coat". I already presented the amorphous-like aggregates with β-spines observed in the case of heat-treated hen egg ovalbumin, which has nearly 400 amino acid residues (Chapter 2). Moreover, protein local condensation followed by amyloid-like aggregation has been really reported for fused in sarcoma and my considerations may be consistent with the context of liquid-liquid phase separation (31).

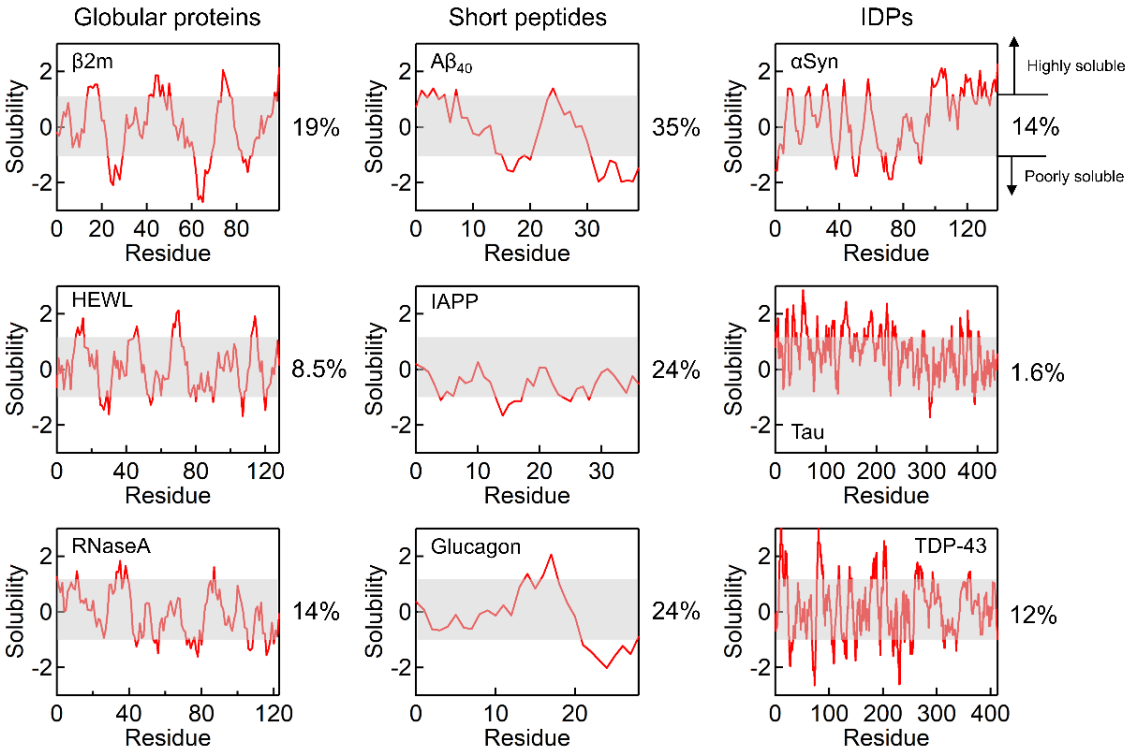



**Figure 4-12. Lengths and hydrophobic portions of the representative proteins used in this thesis.** Intrinsic solubility was predicted by CamSol (102). Hydrophobic portion of each protein is indicated beside the panels estimated by following;

$$\text{Occupancy}(\%) = \frac{\text{Poorly soluble residues}}{\text{Full length}} \times 100$$

*Locating various proteins on a general aggregation phase diagram*

Various types of proteins with distinct responses against heating and agitation can be located on a general phase diagram dependent on the driving force of precipitation and protein solubility (**Fig. 4-13**). This type of diagram is often used for illustrating crystallization and amorphous precipitation of native proteins depending on the concentrations of protein and precipitant (174). Driving force of precipitation changes by various parameters such as salt concentration or temperature. In the case of temperature, hydrophobic interactions increase and then decrease upon increasing the temperature, so that amyloid formation as well as protein folding show cold-denaturation and heat-denaturation phenomena (Chapter 3)(118). Here, for a simplicity, only the low temperature side of heating effects is shown where hydrophobic interactions and thus the driving force of precipitation increases with an increase in temperature.

The general phase diagram dependent on temperature consists of a soluble region (Region I), metastable region (Region II), labile region (Region III), and glassy region (Region IV). Below solubility (Region I), monomers are thermodynamically stable. In metastable region (Region II), supersaturation is assumed to be stable without seeding. In labile region (Region III), spontaneous nucleation can occur after a certain lag time. In glassy region (Region IV), amorphous aggregation occurs without a lag time possibly by rapid formation of too many nuclei. It has been assumed that agitation causes a downward shift of the metastability curve, which is indicated by an arrow.

Type 1 proteins showing strict dependence on agitation represent a transition from under saturation (Region I) to metastable region (Region II). I call this transition as "Strictly supersaturation-dependent transition" or "S transition" (**Fig. 4-13**, green arrow). Agitation shift the region to a labile region making spontaneous nucleation possible. Seeding also breaks supersaturation. Type 1 proteins include those with a native conformation (β2m, $V_L$, $C_L$, HEWL, and RNaseA) and small IDP (αSyn). TTR can be also included into Type 1. Although the linkage of protein unfolding and amyloid polymerization shift the apparent unfolding transition of the native state, amyloid formation is strictly dependent on agitation or seeding.

Type 2 proteins represent the transition from under saturation (Region I) to labile region (Region III), where spontaneous amyloid formation occurs even without agitation,

although agitation can accelerate the amyloid formation. I call this transition as "Autonomous amyloid-forming transition" or "A transition" (**Fig. 4-13**, yellow arrow). Type 2 proteins include insulin, glucagon, IAPP, and $A\beta_{40}$. In other words, high amyloidogenicity of these relatively short amyloid peptide can be explained by the location (i.e. labile region) in the phase diagram.

Type 3 proteins, which often result in amorphous aggregation without a lag phase, can be located to a transition from under saturation (Region I) to glassy region (Region IV) and include TDP-43, tau, and OVA. I call this transition as "Boiled egg-like transition" or "B transition" (**Fig. 4-13**, purple arrow). These are relatively large proteins and it is possible that overall amorphous characteristics include amyloid cores (β-spines) producing a fuzzy coat morphology.

Although various proteins are categorized into three types depending on results performed under particular experimental conditions, it is likely that their types changes depending on experimental conditions. It is also obvious that the exact phase diagram varies significantly depending of proteins. Generally speaking, with larger proteins, amyloid regions (Regions II and III) are narrower and instead glassy region (Region IV) expand. As for TTR, the difficulty of amyloid formation in vitro except our conditions at low pH produced a very narrow amyloid region although full length TTR forms rigid amyloid fibrils in patients.

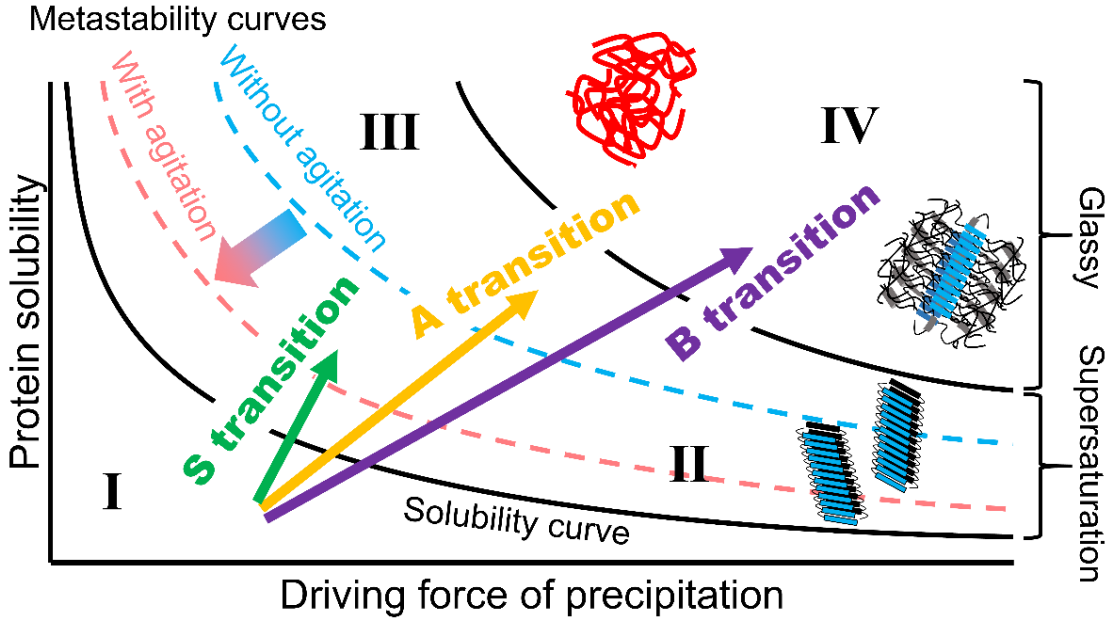



**Figure 4-13. General conformational phase diagram and three types of transition.**

## 4.5. Conclusion

In this chapter, I examined the applicability of heating under agitation methodology which I developed in Chapter 3. I demonstrated that the combined heating under agitation methodology effectively triggered protein misfolding, especially amyloid formation of the stably well-structured globular proteins. As I previously suggested, breakdown of supersaturation played a key role in the reactions and misfolding pathway itself might destabilize the stable native conformations by the law of mass action. Of note, I achieved the impregnable amyloid formation of wild-type TTR spontaneously, which had never been done before despite the dozens of efforts. Christian Anfinsen advocated the famous thermodynamic hypothesis, "Anfinsen's dogma", however he did not describe the "outer" misfolding world. My results suggest that his intramolecular folding world is surrounded by the barriers of supersaturation and breakdown of them can connect the "inner" world to the "outer" intermolecular misfolding world (**Fig. 4-11**). Although my methodology is non-physiological, it will be powerful for further addressing the mysterious mechanisms of protein misfolding.

# Chapter 5.

## Summary and conclusions

Although Anfinsen's dogma explains intramolecular protein folding/unfolding phenomena in terms of thermodynamics, the mechanisms of intermolecular protein misfolding still remains unclear. Amyloid formation is one of the misfolding aggregation of denatured proteins and deeply associated with various fatal diseases. Pathophysiological motivation has driven thousands of studies, whereas the critical factor, which governs the fate whether proper folding or risky amyloid formation occurs, is unknown. In this thesis, I worked on the comprehensive understanding of protein folding and misfolding by the investigation of the amyloid formation of various proteins. I focused on the effects of heating under agitation, and then suggested that breakdown of supersaturation combines the intramolecular folding world with the intermolecular misfolding world on the basis of similarity between amyloid formation and crystallization of solutes.

In Chapter 2, I studied the heat-induced aggregation of intact OVA using an amyloid-specific ThT assay with a fluorometer or direct imaging with an LED lamp and several physicochemical approaches. The results confirmed that intact OVA formed aggregates with a small part of amyloid cores and dominantly amorphous aggregates. I isolated the amyloidogenic core peptide by proteolysis with trypsin. The isolated 23-residue peptide, pOVA, with marked amyloidogenicity, corresponded to one of the key regions (s3A) involved in serpin latency transition and domain-swap polymerization leading to serpinopathies. Predictions indicated that the high amyloidogenicity of the s3A region is common to various serpins. This suggests that the high amyloidogenicity of s3A is retained in OVA and constitutes β-spine amyloid cores upon heat aggregation.

In Chapter 3, to further understand the mechanism underlying amyloid formation, I investigated amyloid formation of β2m at neutral pH. Although amyloid fibrils of β2m are observed in vivo, formation of β2m amyloids in vitro has been difficult to discern at neutral pH because of the amyloid-resistant native structure. Using ThT assays, CD spectroscopy, and TEM analyses, I found that β2m efficiently formed amyloid fibrils even at neutral pH upon heating under agitation at high-salt conditions. I constructed temperature- and NaCl concentration-dependent conformational phase diagrams in the presence or absence of agitation, revealing how amyloid formation under neutral pH conditions is related to thermal unfolding and breakdown of supersaturation. Of note,

after supersaturation breakdown and following the law of mass action, the β2m monomer equilibrium shifted to the unfolded state, destabilizing the native state and thereby enabling amyloid formation even under physiological conditions with a low amount of unfolded precursor. The amyloid fibrils depolymerized at both lower and higher temperatures, resembling cold- or heat-induced denaturation of globular proteins. My results suggest an important role for heating in the onset of related amyloidoses.

In Chapter 4, to confirm and expand my consideration, I applied my methodology of "heating under agitation" to various proteins including both typical amyloidogenic proteins and textbook proteins. The relatively small and well-folded globular proteins such as $V_L$, HEWL, and TTR showed strict dependence on agitation for amyloid formation like β2m did. On the other hand, the highly-amyloidogenic short peptides such as $A\beta_{40}$ and IAPP exhibited agitation-independent amyloid formation like pOVA did. This is because of the weak energy-barrier of supersaturation. In the case of the relatively large IDPs such as tau and TDP-43, dominantly amorphous aggregates with a small proportion of amyloid core were observed like OVA formed. The lengths and hydrophobicity of their primary structures seem to play key roles to control the unique behavior. These results can be explained by a general phase diagram dependent on the driving force of precipitation and protein solubility.

Taken together, breakdown of supersaturation leading reduction of energy-barrier combines folding/unfolding equilibrium with additional misfolding pathway, and then the low of mass action drives the overall equilibrium to the direction of misfolding state even under physiological conditions with a low amount of unfolded precursor. Therefore, recognizing the importance of supersaturation is essential for comprehensive understanding of protein folding and misfolding phenomena.

# References


1. Sela, M., Anfinsen, C. B., and Harrington, W. F. (1957) The correlation of ribonuclease activity with specific aspects of tertiary structure. *Biochim Biophys Acta* **26**, 502-512
2. Sela, M., White, F. H., Jr., and Anfinsen, C. B. (1957) Reductive cleavage of disulfide bridges in ribonuclease. *Science* **125**, 691-692
3. Haber, E., and Anfinsen, C. B. (1961) Regeneration of enzyme activity by air oxidation of reduced subtilisin-modified ribonuclease. *J Biol Chem* **236**, 422-424
4. Anfinsen, C. B. (1973) Principles that govern the folding of protein chains. *Science* **181**, 223-230
5. Shirdel, S. A., and Khalifeh, K. (2019) Thermodynamics of protein folding: methodology, data analysis and interpretation of data. *Eur Biophys J* **48**, 305-316
6. Dill, K. A. (1990) Dominant forces in protein folding. *Biochemistry* **29**, 7133-7155
7. Tanford, C. (1997) How protein chemists learned about the hydrophobic factor. *Protein Sci* **6**, 1358-1366
8. Dobson, C. M. (2003) Protein folding and misfolding. *Nature* **426**, 884-890
9. Kim, Y. E., Hipp, M. S., Bracher, A., Hayer-Hartl, M., and Hartl, F. U. (2013) Molecular chaperone functions in protein folding and proteostasis. *Annu Rev Biochem* **82**, 323-355
10. Moreau, K. L., and King, J. A. (2012) Protein misfolding and aggregation in cataract disease and prospects for prevention. *Trends Mol Med* **18**, 273-282
11. Fink, A. L. (1998) Protein aggregation: folding aggregates, inclusion bodies and amyloid. *Fold Des* **3**, R9-23
12. Wang, W. (2005) Protein aggregation and its inhibition in biopharmaceutics. *Int J Pharm* **289**, 1-30
13. Go, N. (1984) The consistency principle in protein structure and pathways of folding. *Adv Biophys* **18**, 149-164
14. Bryngelson, J. D., and Wolynes, P. G. (1987) Spin glasses and the statistical mechanics of protein folding. *Proc Natl Acad Sci U S A* **84**, 7524-7528
15. Leopold, P. E., Montal, M., and Onuchic, J. N. (1992) Protein folding funnels: a kinetic approach to the sequence-structure relationship. *Proc Natl Acad Sci U S A* **89**, 8721-8725
16. Dill, K. A., and MacCallum, J. L. (2012) The protein-folding problem, 50 years on. *Science* **338**, 1042-1046
17. Onuchic, J. N., Luthey-Schulten, Z., and Wolynes, P. G. (1997) Theory of protein folding: the energy landscape perspective. *Annu Rev Phys Chem* **48**, 545-600
18. Riek, R., and Eisenberg, D. S. (2016) The activities of amyloids from a structural

perspective. *Nature* **539**, 227-235

19. Iadanza, M. G., Jackson, M. P., Hewitt, E. W., Ranson, N. A., and Radford, S. E. (2018) A new era for understanding amyloid structures and disease. *Nat Rev Mol Cell Biol* **19**, 755-773
20. Eanes, E. D., and Glenner, G. G. (1968) X-ray diffraction studies on amyloid filaments. *J Histochem Cytochem* **16**, 673-677
21. Sunde, M., Serpell, L. C., Bartlam, M., Fraser, P. E., Pepys, M. B., and Blake, C. C. (1997) Common core structure of amyloid fibrils by synchrotron X-ray diffraction. *J Mol Biol* **273**, 729-739
22. Nelson, R., Sawaya, M. R., Balbirnie, M., Madsen, A. O., Riekel, C., Grothe, R., and Eisenberg, D. (2005) Structure of the cross-beta spine of amyloid-like fibrils. *Nature* **435**, 773-778
23. Colvin, M. T., Silvers, R., Ni, Q. Z., Can, T. V., Sergeyev, I., Rosay, M., Donovan, K. J., Michael, B., Wall, J., Linse, S., and Griffin, R. G. (2016) Atomic Resolution Structure of Monomorphic Abeta42 Amyloid Fibrils. *J Am Chem Soc* **138**, 9663-9674
24. Guerrero-Ferreira, R., Taylor, N. M., Mona, D., Ringler, P., Lauer, M. E., Riek, R., Britschgi, M., and Stahlberg, H. (2018) Cryo-EM structure of alpha-synuclein fibrils. *Elife* **7**
25. Benditt, E. P., Eriksen, N., and Berglund, C. (1970) Congo red dichroism with dispersed amyloid fibrils, an extrinsic cotton effect. *Proc Natl Acad Sci U S A* **66**, 1044-1051
26. Naiki, H., Higuchi, K., Hosokawa, M., and Takeda, T. (1989) Fluorometric determination of amyloid fibrils in vitro using the fluorescent dye, thioflavin T1. *Anal Biochem* **177**, 244-249
27. Khurana, R., Coleman, C., Ionescu-Zanetti, C., Carter, S. A., Krishna, V., Grover, R. K., Roy, R., and Singh, S. (2005) Mechanism of thioflavin T binding to amyloid fibrils. *J Struct Biol* **151**, 229-238
28. Sipe, J. D., Benson, M. D., Buxbaum, J. N., Ikeda, S. I., Merlini, G., Saraiva, M. J., and Westermark, P. (2016) Amyloid fibril proteins and amyloidosis: chemical identification and clinical classification International Society of Amyloidosis 2016 Nomenclature Guidelines. *Amyloid* **23**, 209-213
29. Chiti, F., and Dobson, C. M. (2017) Protein Misfolding, Amyloid Formation, and Human Disease: A Summary of Progress Over the Last Decade. *Annu Rev Biochem* **86**, 27-68
30. Rapezzi, C., Quarta, C. C., Riva, L., Longhi, S., Gallelli, I., Lorenzini, M., Ciliberti, P., Biagini, E., Salvi, F., and Branzi, A. (2010) Transthyretin-related amyloidoses and the heart: a clinical overview. *Nat Rev Cardiol* **7**, 398-408
31. Patel, A., Lee, H. O., Jawerth, L., Maharana, S., Jahnel, M., Hein, M. Y., Stoynov, S.,

Mahamid, J., Saha, S., Franzmann, T. M., Pozniakovski, A., Poser, I., Maghelli, N., Royer, L. A., Weigert, M., Myers, E. W., Grill, S., Drechsel, D., Hyman, A. A., and Alberti, S. (2015) A Liquid-to-Solid Phase Transition of the ALS Protein FUS Accelerated by Disease Mutation. *Cell* **162**, 1066-1077

32. Van Gerven, N., Van der Verren, S. E., Reiter, D. M., and Remaut, H. (2018) The Role of Functional Amyloids in Bacterial Virulence. *J Mol Biol* **430**, 3657-3684
33. Slotta, U., Hess, S., Spiess, K., Stromer, T., Serpell, L., and Scheibel, T. (2007) Spider silk and amyloid fibrils: a structural comparison. *Macromol Biosci* **7**, 183-188
34. Maji, S. K., Perrin, M. H., Sawaya, M. R., Jessberger, S., Vadodaria, K., Rissman, R. A., Singru, P. S., Nilsson, K. P., Simon, R., Schubert, D., Eisenberg, D., Rivier, J., Sawchenko, P., Vale, W., and Riek, R. (2009) Functional amyloids as natural storage of peptide hormones in pituitary secretory granules. *Science* **325**, 328-332
35. Mishra, P., Ayyannan, S. R., and Panda, G. (2015) Perspectives on Inhibiting beta-Amyloid Aggregation through Structure-Based Drug Design. *ChemMedChem* **10**, 1467-1474
36. Bulawa, C. E., Connelly, S., Devit, M., Wang, L., Weigel, C., Fleming, J. A., Packman, J., Powers, E. T., Wiseman, R. L., Foss, T. R., Wilson, I. A., Kelly, J. W., and Labaudiniere, R. (2012) Tafamidis, a potent and selective transthyretin kinetic stabilizer that inhibits the amyloid cascade. *Proc Natl Acad Sci U S A* **109**, 9629-9634
37. Li, C., Qin, R., Liu, R., Miao, S., and Yang, P. (2018) Functional amyloid materials at surfaces/interfaces. *Biomater Sci* **6**, 462-472
38. Bolisetty, S., Arcari, M., Adamcik, J., and Mezzenga, R. (2015) Hybrid Amyloid Membranes for Continuous Flow Catalysis. *Langmuir* **31**, 13867-13873
39. Li, D., Jones, E. M., Sawaya, M. R., Furukawa, H., Luo, F., Ivanova, M., Sievers, S. A., Wang, W., Yaghi, O. M., Liu, C., and Eisenberg, D. S. (2014) Structure-based design of functional amyloid materials. *J Am Chem Soc* **136**, 18044-18051
40. Yoshimura, Y., Lin, Y., Yagi, H., Lee, Y. H., Kitayama, H., Sakurai, K., So, M., Ogi, H., Naiki, H., and Goto, Y. (2012) Distinguishing crystal-like amyloid fibrils and glass-like amorphous aggregates from their kinetics of formation. *Proc Natl Acad Sci U S A* **109**, 14446-14451
41. Kitayama, H., Yoshimura, Y., So, M., Sakurai, K., Yagi, H., and Goto, Y. (2013) A common mechanism underlying amyloid fibrillation and protein crystallization revealed by the effects of ultrasonication. *Biochim Biophys Acta* **1834**, 2640-2646
42. Arosio, P., Knowles, T. P., and Linse, S. (2015) On the lag phase in amyloid fibril formation. *Phys Chem Chem Phys* **17**, 7606-7618
43. Jarrett, J. T., and Lansbury, P. T., Jr. (1993) Seeding "one-dimensional crystallization" of

amyloid: a pathogenic mechanism in Alzheimer's disease and scrapie? *Cell* **73**, 1055-1058

44. Westermark, G. T., Fandrich, M., Lundmark, K., and Westermark, P. (2018) Noncerebral Amyloidoses: Aspects on Seeding, Cross-Seeding, and Transmission. *Cold Spring Harb Perspect Med* **8**
45. Chatani, E., Yagi, H., Naiki, H., and Goto, Y. (2012) Polymorphism of beta2-microglobulin amyloid fibrils manifested by ultrasonication-enhanced fibril formation in trifluoroethanol. *J Biol Chem* **287**, 22827-22837
46. Annamalai, K., Guhrs, K. H., Koehler, R., Schmidt, M., Michel, H., Loos, C., Gaffney, P. M., Sigurdson, C. J., Hegenbart, U., Schonland, S., and Fandrich, M. (2016) Polymorphism of Amyloid Fibrils In Vivo. *Angew Chem Int Ed Engl* **55**, 4822-4825
47. Durbin, S. D., and Feher, G. (1996) Protein crystallization. *Annu Rev Phys Chem* **47**, 171-204
48. Asherie, N. (2004) Protein crystallization and phase diagrams. *Methods* **34**, 266-272
49. Ciryam, P., Tartaglia, G. G., Morimoto, R. I., Dobson, C. M., and Vendruscolo, M. (2013) Widespread aggregation and neurodegenerative diseases are associated with supersaturated proteins. *Cell Rep* **5**, 781-790
50. Ciryam, P., Kundra, R., Morimoto, R. I., Dobson, C. M., and Vendruscolo, M. (2015) Supersaturation is a major driving force for protein aggregation in neurodegenerative diseases. *Trends Pharmacol Sci* **36**, 72-77
51. LeVine, H., 3rd. (1993) Thioflavine T interaction with synthetic Alzheimer's disease beta-amyloid peptides: detection of amyloid aggregation in solution. *Protein Sci* **2**, 404-410
52. LeVine, H., 3rd. (1999) Quantification of beta-sheet amyloid fibril structures with thioflavin T. *Methods Enzymol* **309**, 274-284
53. Schlein, M. (2017) Insulin Formulation Characterization-the Thioflavin T Assays. *AAPS J* **19**, 397-408
54. Nitani, A., Muta, H., Adachi, M., So, M., Sasahara, K., Sakurai, K., Chatani, E., Naoe, K., Ogi, H., Hall, D., and Goto, Y. (2017) Heparin-dependent aggregation of hen egg white lysozyme reveals two distinct mechanisms of amyloid fibrillation. *J Biol Chem* **292**, 21219-21230
55. Greenfield, N. J. (2006) Using circular dichroism spectra to estimate protein secondary structure. *Nat Protoc* **1**, 2876-2890
56. Rangachari, V., Reed, D. K., Moore, B. D., and Rosenberry, T. L. (2006) Secondary structure and interfacial aggregation of amyloid-beta(1-40) on sodium dodecyl sulfate micelles. *Biochemistry* **45**, 8639-8648
57. Ban, T., Hamada, D., Hasegawa, K., Naiki, H., and Goto, Y. (2003) Direct observation of amyloid fibril growth monitored by thioflavin T fluorescence. *J Biol Chem* **278**, 16462-

16465

58. Ban, T., Hoshino, M., Takahashi, S., Hamada, D., Hasegawa, K., Naiki, H., and Goto, Y. (2004) Direct observation of Abeta amyloid fibril growth and inhibition. *J Mol Biol* **344**, 757-767
59. Teoh, C. L., Yagi, H., Griffin, M. D., Goto, Y., and Howlett, G. J. (2011) Visualization of polymorphism in apolipoprotein C-II amyloid fibrils. *J Biochem* **149**, 67-74
60. Zako, T., Sakono, M., Hashimoto, N., Ihara, M., and Maeda, M. (2009) Bovine insulin filaments induced by reducing disulfide bonds show a different morphology, secondary structure, and cell toxicity from intact insulin amyloid fibrils. *Biophys J* **96**, 3331-3340
61. Sipe, J. D., Benson, M. D., Buxbaum, J. N., Ikeda, S., Merlini, G., Saraiva, M. J., and Westermark, P. (2014) Nomenclature 2014: Amyloid fibril proteins and clinical classification of the amyloidosis. *Amyloid* **21**, 221-224
62. Chiti, F., and Dobson, C. M. (2006) Protein misfolding, functional amyloid, and human disease. *Annu Rev Biochem* **75**, 333-366
63. Ohhashi, Y., Kihara, M., Naiki, H., and Goto, Y. (2005) Ultrasonication-induced amyloid fibril formation of beta2-microglobulin. *J Biol Chem* **280**, 32843-32848
64. Nakajima, K., Ogi, H., Adachi, K., Noi, K., Hirao, M., Yagi, H., and Goto, Y. (2016) Nucleus factory on cavitation bubble for amyloid beta fibril. *Sci Rep* **6**, 22015
65. So, M., Hall, D., and Goto, Y. (2016) Revisiting supersaturation as a factor determining amyloid fibrillation. *Curr Opin Struct Biol* **36**, 32-39
66. Adachi, M., So, M., Sakurai, K., Kardos, J., and Goto, Y. (2015) Supersaturation-limited and Unlimited Phase Transitions Compete to Produce the Pathway Complexity in Amyloid Fibrillation. *J Biol Chem* **290**, 18134-18145
67. Painter, P. C., and Koenig, J. L. (1976) Raman spectroscopic study of the proteins of egg white. *Biopolymers* **15**, 2155-2166
68. Nisbet, A. D., Saundry, R. H., Moir, A. J., Fothergill, L. A., and Fothergill, J. E. (1981) The complete amino-acid sequence of hen ovalbumin. *Eur J Biochem* **115**, 335-345
69. Huntington, J. A., Fan, B., Karlsson, K. E., Deinum, J., Lawrence, D. A., and Gettins, P. G. (1997) Serpin conformational change in ovalbumin. Enhanced reactive center loop insertion through hinge region mutations. *Biochemistry* **36**, 5432-5440
70. Gettins, P. G. (2002) Serpin structure, mechanism, and function. *Chem Rev* **102**, 4751-4804
71. Whisstock, J. C., and Bottomley, S. P. (2006) Molecular gymnastics: serpin structure, folding and misfolding. *Curr Opin Struct Biol* **16**, 761-768
72. Huntington, J. A. (2011) Serpin structure, function and dysfunction. *J Thromb Haemost* **9 Suppl 1**, 26-34

73. Yamasaki, M., Li, W., Johnson, D. J., and Huntington, J. A. (2008) Crystal structure of a stable dimer reveals the molecular basis of serpin polymerization. *Nature* **455**, 1255-1258
74. Yamasaki, M., Sendall, T. J., Pearce, M. C., Whisstock, J. C., and Huntington, J. A. (2011) Molecular basis of alpha1-antitrypsin deficiency revealed by the structure of a domain-swapped trimer. *EMBO Rep* **12**, 1011-1017
75. Carrell, R. W., and Gooptu, B. (1998) Conformational changes and disease--serpins, prions and Alzheimer's. *Curr Opin Struct Biol* **8**, 799-809
76. Kaiserman, D., Whisstock, J. C., and Bird, P. I. (2006) Mechanisms of serpin dysfunction in disease. *Expert Rev Mol Med* **8**, 1-19
77. Gettins, P. G., and Olson, S. T. (2016) Inhibitory serpins. New insights into their folding, polymerization, regulation and clearance. *Biochem J* **473**, 2273-2293
78. Azakami, H., Mukai, A., and Kato, A. (2005) Role of amyloid type cross beta-structure in the formation of soluble aggregate and gel in heat-induced ovalbumin. *J Agric Food Chem* **53**, 1254-1257
79. Pearce, F. G., Mackintosh, S. H., and Gerrard, J. A. (2007) Formation of amyloid-like fibrils by ovalbumin and related proteins under conditions relevant to food processing. *J Agric Food Chem* **55**, 318-322
80. Naeem, A., Khan, T. A., Muzaffar, M., Ahmad, S., and Saleemuddin, M. (2011) A partially folded state of ovalbumin at low pH tends to aggregate. *Cell Biochem Biophys* **59**, 29-38
81. Lara, C., Gourdin-Bertin, S., Adamcik, J., Bolisetty, S., and Mezzenga, R. (2012) Self-assembly of ovalbumin into amyloid and non-amyloid fibrils. *Biomacromolecules* **13**, 4213-4221
82. Yagi, H., Mizuno, A., So, M., Hirano, M., Adachi, M., Akazawa-Ogawa, Y., Hagihara, Y., Ikenoue, T., Lee, Y. H., Kawata, Y., and Goto, Y. (2015) Ultrasonication-dependent formation and degradation of alpha-synuclein amyloid fibrils. *Biochim Biophys Acta* **1854**, 209-217
83. Hudson, S. A., Ecroyd, H., Kee, T. W., and Carver, J. A. (2009) The thioflavin T fluorescence assay for amyloid fibril detection can be biased by the presence of exogenous compounds. *FEBS J* **276**, 5960-5972
84. Yamamoto, S., Hasegawa, K., Yamaguchi, I., Tsutsumi, S., Kardos, J., Goto, Y., Gejyo, F., and Naiki, H. (2004) Low concentrations of sodium dodecyl sulfate induce the extension of beta 2-microglobulin-related amyloid fibrils at a neutral pH. *Biochemistry* **43**, 11075-11082
85. So, M., Ishii, A., Hata, Y., Yagi, H., Naiki, H., and Goto, Y. (2015) Supersaturation-Limited and Unlimited Phase Spaces Compete to Produce Maximal Amyloid Fibrillation near the Critical Micelle Concentration of Sodium Dodecyl Sulfate. *Langmuir* **31**, 9973-

9982

86. So, M., Yagi, H., Sakurai, K., Ogi, H., Naiki, H., and Goto, Y. (2011) Ultrasonication-dependent acceleration of amyloid fibril formation. *J Mol Biol* **412**, 568-577
87. Cazzolli, G., Wang, F., a Beccara, S., Gershenson, A., Faccioli, P., and Wintrode, P. L. (2014) Serpin latency transition at atomic resolution. *Proc Natl Acad Sci U S A* **111**, 15414-15419
88. Jackson, M., and Mantsch, H. H. (1991) Beware of proteins in DMSO. *Biochim Biophys Acta* **1078**, 231-235
89. Hirota-Nakaoka, N., Hasegawa, K., Naiki, H., and Goto, Y. (2003) Dissolution of beta2-microglobulin amyloid fibrils by dimethylsulfoxide. *J Biochem* **134**, 159-164
90. Goto, Y., Adachi, M., Muta, H., and So, M. (2018) Salt-induced formations of partially folded intermediates and amyloid fibrils suggests a common underlying mechanism. *Biophys Rev* **10**, 493-502
91. Cremers, C. M., Knoefler, D., Gates, S., Martin, N., Dahl, J. U., Lempart, J., Xie, L., Chapman, M. R., Galvan, V., Southworth, D. R., and Jakob, U. (2016) Polyphosphate: A Conserved Modifier of Amyloidogenic Processes. *Mol Cell* **63**, 768-780
92. Munishkina, L. A., Henriques, J., Uversky, V. N., and Fink, A. L. (2004) Role of protein-water interactions and electrostatics in alpha-synuclein fibril formation. *Biochemistry* **43**, 3289-3300
93. Shirai, N., Tani, F., Higasa, T., and Yasumoto, K. (1997) Linear polymerization caused by the defective folding of a non-inhibitory serpin ovalbumin. *J Biochem* **121**, 787-797
94. Tanaka, N., Morimoto, Y., Noguchi, Y., Tada, T., Waku, T., Kunugi, S., Morii, T., Lee, Y. F., Konno, T., and Takahashi, N. (2011) The mechanism of fibril formation of a non-inhibitory serpin ovalbumin revealed by the identification of amyloidogenic core regions. *J Biol Chem* **286**, 5884-5894
95. Kawachi, Y., Kameyama, R., Handa, A., Takahashi, N., and Tanaka, N. (2013) Role of the N-terminal amphiphilic region of ovalbumin during heat-induced aggregation and gelation. *J Agric Food Chem* **61**, 8668-8675
96. Nelson, R., and Eisenberg, D. (2006) Structural models of amyloid-like fibrils. *Adv Protein Chem* **73**, 235-282
97. Sawaya, M. R., Sambashivan, S., Nelson, R., Ivanova, M. I., Sievers, S. A., Apostol, M. I., Thompson, M. J., Balbirnie, M., Wiltzius, J. J., McFarlane, H. T., Madsen, A. O., Riekel, C., and Eisenberg, D. (2007) Atomic structures of amyloid cross-beta spines reveal varied steric zippers. *Nature* **447**, 453-457
98. Wind, T., Jensen, J. K., Dupont, D. M., Kulig, P., and Andreasen, P. A. (2003) Mutational analysis of plasminogen activator inhibitor-1. *Eur J Biochem* **270**, 1680-1688

99. Yamasaki, M., Arii, Y., Mikami, B., and Hirose, M. (2002) Loop-inserted and thermostabilized structure of P1-P1' cleaved ovalbumin mutant R339T. *J Mol Biol* **315**, 113-120

100. Conchillo-Sole, O., de Groot, N. S., Aviles, F. X., Vendrell, J., Daura, X., and Ventura, S. (2007) AGGRESCAN: a server for the prediction and evaluation of "hot spots" of aggregation in polypeptides. *BMC Bioinformatics* **8**, 65

101. Rousseau, F., Schymkowitz, J., and Serrano, L. (2006) Protein aggregation and amyloidosis: confusion of the kinds? *Curr Opin Struct Biol* **16**, 118-126

102. Sormanni, P., Aprile, F. A., and Vendruscolo, M. (2015) The CamSol method of rational design of protein mutants with enhanced solubility. *J Mol Biol* **427**, 478-490

103. Davis, R. L., Shrimpton, A. E., Holohan, P. D., Bradshaw, C., Feiglin, D., Collins, G. H., Sonderegger, P., Kinter, J., Becker, L. M., Lacbawan, F., Krasnewich, D., Muenke, M., Lawrence, D. A., Yerby, M. S., Shaw, C. M., Gooptu, B., Elliott, P. R., Finch, J. T., Carrell, R. W., and Lomas, D. A. (1999) Familial dementia caused by polymerization of mutant neuroserpin. *Nature* **401**, 376-379

104. Lomas, D. A., and Carrell, R. W. (2002) Serpinopathies and the conformational dementias. *Nat Rev Genet* **3**, 759-768

105. Powers, G. A., Pham, C. L., Pearce, M. C., Howlett, G. J., and Bottomley, S. P. (2007) Serpin acceleration of amyloid fibril formation: a role for accessory proteins. *J Mol Biol* **366**, 666-676

106. Piejko, M., Dec, R., Babenko, V., Hoang, A., Szewczyk, M., Mak, P., and Dzwolak, W. (2015) Highly amyloidogenic two-chain peptide fragments are released upon partial digestion of insulin with pepsin. *J Biol Chem* **290**, 5947-5958

107. Mangione, P. P., Porcari, R., Gillmore, J. D., Pucci, P., Monti, M., Porcari, M., Giorgetti, S., Marchese, L., Raimondi, S., Serpell, L. C., Chen, W., Relini, A., Marcoux, J., Clatworthy, I. R., Taylor, G. W., Tennent, G. A., Robinson, C. V., Hawkins, P. N., Stoppini, M., Wood, S. P., Pepys, M. B., and Bellotti, V. (2014) Proteolytic cleavage of Ser52Pro variant transthyretin triggers its amyloid fibrillogenesis. *Proc Natl Acad Sci U S A* **111**, 1539-1544

108. Marcoux, J., Mangione, P. P., Porcari, R., Degiacomi, M. T., Verona, G., Taylor, G. W., Giorgetti, S., Raimondi, S., Sanglier-Cianferani, S., Benesch, J. L., Cecconi, C., Naqvi, M. M., Gillmore, J. D., Hawkins, P. N., Stoppini, M., Robinson, C. V., Pepys, M. B., and Bellotti, V. (2015) A novel mechano-enzymatic cleavage mechanism underlies transthyretin amyloidogenesis. *EMBO Mol Med* **7**, 1337-1349

109. Imoto, T., Yamada, H., and Ueda, T. (1986) Unfolding rates of globular proteins determined by kinetics of proteolysis. *J Mol Biol* **190**, 647-649

110. Yamada, H., Ueda, T., and Imoto, T. (1993) Thermodynamic and kinetic stabilities of

hen-egg lysozyme and its chemically modified derivatives: analysis of the transition state of the protein unfolding. *J Biochem* **114**, 398-403

111. Hoang, L., Bedard, S., Krishna, M. M., Lin, Y., and Englander, S. W. (2002) Cytochrome c folding pathway: kinetic native-state hydrogen exchange. *Proc Natl Acad Sci U S A* **99**, 12173-12178
112. Ferraro, D. M., Lazo, N., and Robertson, A. D. (2004) EX1 hydrogen exchange and protein folding. *Biochemistry* **43**, 587-594
113. Raman, B., Chatani, E., Kihara, M., Ban, T., Sakai, M., Hasegawa, K., Naiki, H., Rao Ch, M., and Goto, Y. (2005) Critical balance of electrostatic and hydrophobic interactions is required for beta 2-microglobulin amyloid fibril growth and stability. *Biochemistry* **44**, 1288-1299
114. Zhang, C. M., Yamaguchi, K., So, M., Sasahara, K., Ito, T., Yamamoto, S., Narita, I., Kardos, J., Naiki, H., and Goto, Y. (2019) Possible mechanisms of polyphosphate-induced amyloid fibril formation of beta2-microglobulin. *Proc Natl Acad Sci U S A* **116**, 12833-12838
115. Sasahara, K., Yamaguchi, K., So, M., and Goto, Y. (2019) Polyphosphates diminish solubility of a globular protein and thereby promote amyloid aggregation. *J Biol Chem* **294**, 15318-15329
116. Lesne, S., Koh, M. T., Kotilinek, L., Kayed, R., Glabe, C. G., Yang, A., Gallagher, M., and Ashe, K. H. (2006) A specific amyloid-beta protein assembly in the brain impairs memory. *Nature* **440**, 352-357
117. Sengupta, U., Nilson, A. N., and Kayed, R. (2016) The Role of Amyloid-beta Oligomers in Toxicity, Propagation, and Immunotherapy. *EBioMedicine* **6**, 42-49
118. Adachi, M., Noji, M., So, M., Sasahara, K., Kardos, J., Naiki, H., and Goto, Y. (2018) Aggregation-phase diagrams of beta2-microglobulin reveal temperature and salt effects on competitive formation of amyloids versus amorphous aggregates. *J Biol Chem* **293**, 14775-14785
119. Yamamoto, S., and Gejyo, F. (2005) Historical background and clinical treatment of dialysis-related amyloidosis. *Biochim Biophys Acta* **1753**, 4-10
120. Naiki, H., Okoshi, T., Ozawa, D., Yamaguchi, I., and Hasegawa, K. (2016) Molecular pathogenesis of human amyloidosis: Lessons from beta2 -microglobulin-related amyloidosis. *Pathol Int* **66**, 193-201
121. Iadanza, M. G., Silvers, R., Boardman, J., Smith, H. I., Karamanos, T. K., Debelouchina, G. T., Su, Y., Griffin, R. G., Ranson, N. A., and Radford, S. E. (2018) The structure of a beta2-microglobulin fibril suggests a molecular basis for its amyloid polymorphism. *Nat Commun* **9**, 4517

122. Kihara, M., Chatani, E., Sakai, M., Hasegawa, K., Naiki, H., and Goto, Y. (2005) Seeding-dependent maturation of beta2-microglobulin amyloid fibrils at neutral pH. *J Biol Chem* **280**, 12012-12018

123. Myers, S. L., Jones, S., Jahn, T. R., Morten, I. J., Tennent, G. A., Hewitt, E. W., and Radford, S. E. (2006) A systematic study of the effect of physiological factors on beta2-microglobulin amyloid formation at neutral pH. *Biochemistry* **45**, 2311-2321

124. Valleix, S., Gillmore, J. D., Bridoux, F., Mangione, P. P., Dogan, A., Nedelec, B., Boimard, M., Touchard, G., Goujon, J. M., Lacombe, C., Lozeron, P., Adams, D., Lacroix, C., Maisonobe, T., Plante-Bordeneuve, V., Vrana, J. A., Theis, J. D., Giorgetti, S., Porcari, R., Ricagno, S., Bolognesi, M., Stoppini, M., Delpech, M., Pepys, M. B., Hawkins, P. N., and Bellotti, V. (2012) Hereditary systemic amyloidosis due to Asp76Asn variant beta2-microglobulin. *N Engl J Med* **366**, 2276-2283

125. Relini, A., De Stefano, S., Torrassa, S., Cavalleri, O., Rolandi, R., Gliozzi, A., Giorgetti, S., Raimondi, S., Marchese, L., Verga, L., Rossi, A., Stoppini, M., and Bellotti, V. (2008) Heparin strongly enhances the formation of beta2-microglobulin amyloid fibrils in the presence of type I collagen. *J Biol Chem* **283**, 4912-4920

126. Pedersen, J. S., Dikov, D., Flink, J. L., Hjuler, H. A., Christiansen, G., and Otzen, D. E. (2006) The changing face of glucagon fibrillation: structural polymorphism and conformational imprinting. *J Mol Biol* **355**, 501-523

127. Jeppesen, M. D., Hein, K., Nissen, P., Westh, P., and Otzen, D. E. (2010) A thermodynamic analysis of fibrillar polymorphism. *Biophys Chem* **149**, 40-46

128. Surmacz-Chwedoruk, W., Malka, I., Bozycki, L., Nieznanska, H., and Dzwolak, W. (2014) On the heat stability of amyloid-based biological activity: insights from thermal degradation of insulin fibrils. *PLoS One* **9**, e86320

129. Sasahara, K., Yagi, H., Naiki, H., and Goto, Y. (2007) Heat-induced conversion of beta(2)-microglobulin and hen egg-white lysozyme into amyloid fibrils. *J Mol Biol* **372**, 981-991

130. Ikenoue, T., Lee, Y. H., Kardos, J., Yagi, H., Ikegami, T., Naiki, H., and Goto, Y. (2014) Heat of supersaturation-limited amyloid burst directly monitored by isothermal titration calorimetry. *Proc Natl Acad Sci U S A* **111**, 6654-6659

131. Kardos, J., Yamamoto, K., Hasegawa, K., Naiki, H., and Goto, Y. (2004) Direct measurement of the thermodynamic parameters of amyloid formation by isothermal titration calorimetry. *J Biol Chem* **279**, 55308-55314

132. Griko, Y. V., Privalov, P. L., Venyaminov, S. Y., and Kutyshenko, V. P. (1988) Thermodynamic study of the apomyoglobin structure. *J Mol Biol* **202**, 127-138

133. Makhatadze, G. I., and Privalov, P. L. (1995) Energetics of protein structure. *Adv Protein Chem* **47**, 307-425

134. Wang, Y., Bunce, S. J., Radford, S. E., Wilson, A. J., Auer, S., and Hall, C. K. (2019) Thermodynamic phase diagram of amyloid-beta (16-22) peptide. *Proc Natl Acad Sci U S A* **116**, 2091-2096

135. Kozhukh, G. V., Hagihara, Y., Kawakami, T., Hasegawa, K., Naiki, H., and Goto, Y. (2002) Investigation of a peptide responsible for amyloid fibril formation of beta 2-microglobulin by achromobacter protease I. *J Biol Chem* **277**, 1310-1315

136. Ohhashi, Y., Hagihara, Y., Kozhukh, G., Hoshino, M., Hasegawa, K., Yamaguchi, I., Naiki, H., and Goto, Y. (2002) The intrachain disulfide bond of beta(2)-microglobulin is not essential for the immunoglobulin fold at neutral pH, but is essential for amyloid fibril formation at acidic pH. *J Biochem* **131**, 45-52

137. Sasahara, K., Yagi, H., Naiki, H., and Goto, Y. (2009) Thermal response with exothermic effects of beta2-microglobulin amyloid fibrils and fibrillation. *J Mol Biol* **389**, 584-594

138. Kardos, J., Yamamoto, K., Hasegawa, K., Naiki, H., and Goto, Y. (2004) Direct measurement of the thermodynamic parameters of amyloid formation by isothermal titration calorimetry. *J. Biol. Chem.* **279**, 55308-55314

139. Wetzel, R. (2006) Kinetics and thermodynamics of amyloid fibril assembly. *Acc Chem Res* **39**, 671-679

140. Tanford, C. (1970) Protein denaturation. C. Theoretical models for the mechanism of denaturation. *Adv Protein Chem* **24**, 1-95

141. Ikenoue, T., Lee, Y. H., Kardos, J., Saiki, M., Yagi, H., Kawata, Y., and Goto, Y. (2014) Cold denaturation of alpha-synuclein amyloid fibrils. *Angew Chem Int Ed Engl* **53**, 7799-7804

142. Relini, A., Canale, C., De Stefano, S., Rolandi, R., Giorgetti, S., Stoppini, M., Rossi, A., Fogolari, F., Corazza, A., Esposito, G., Gliozzi, A., and Bellotti, V. (2006) Collagen plays an active role in the aggregation of beta2-microglobulin under physiopathological conditions of dialysis-related amyloidosis. *J Biol Chem* **281**, 16521-16529

143. Stoppini, M., and Bellotti, V. (2015) Systemic amyloidosis: lessons from beta2-microglobulin. *J Biol Chem* **290**, 9951-9958

144. Kuhlman, B., and Bradley, P. (2019) Advances in protein structure prediction and design. *Nat Rev Mol Cell Biol* **20**, 681-697

145. Uversky, V. N. (2003) Protein folding revisited. A polypeptide chain at the folding-misfolding-nonfolding cross-roads: which way to go? *Cell Mol Life Sci* **60**, 1852-1871

146. Fink, A. L. (2005) Natively unfolded proteins. *Curr Opin Struct Biol* **15**, 35-41

147. Yagi, H., Kusaka, E., Hongo, K., Mizobata, T., and Kawata, Y. (2005) Amyloid fibril formation of alpha-synuclein is accelerated by preformed amyloid seeds of other proteins: implications for the mechanism of transmissible conformational diseases. *J Biol Chem* **280**,

38609-38616

148. Dasari, S., Theis, J. D., Vrana, J. A., Meureta, O. M., Quint, P. S., Muppa, P., Zenka, R. M., Tschumper, R. C., Jelinek, D. F., Davila, J. I., Sarangi, V., Kurtin, P. J., and Dogan, A. (2015) Proteomic detection of immunoglobulin light chain variable region peptides from amyloidosis patient biopsies. *J Proteome Res* **14**, 1957-1967
149. Klimtchuk, E. S., Gursky, O., Patel, R. S., Laporte, K. L., Connors, L. H., Skinner, M., and Seldin, D. C. (2010) The critical role of the constant region in thermal stability and aggregation of amyloidogenic immunoglobulin light chain. *Biochemistry* **49**, 9848-9857
150. Blancas-Mejia, L. M., Horn, T. J., Marin-Argany, M., Auton, M., Tischer, A., and Ramirez-Alvarado, M. (2015) Thermodynamic and fibril formation studies of full length immunoglobulin light chain AL-09 and its germline protein using scan rate dependent thermal unfolding. *Biophys Chem* **207**, 13-20
151. Weber, B., Hora, M., Kazman, P., Gobl, C., Camilloni, C., Reif, B., and Buchner, J. (2018) The Antibody Light-Chain Linker Regulates Domain Orientation and Amyloidogenicity. *J Mol Biol* **430**, 4925-4940
152. Nokwe, C. N., Hora, M., Zacharias, M., Yagi, H., John, C., Reif, B., Goto, Y., and Buchner, J. (2015) The Antibody Light-Chain Linker Is Important for Domain Stability and Amyloid Formation. *J Mol Biol* **427**, 3572-3586
153. Booth, D. R., Sunde, M., Bellotti, V., Robinson, C. V., Hutchinson, W. L., Fraser, P. E., Hawkins, P. N., Dobson, C. M., Radford, S. E., Blake, C. C., and Pepys, M. B. (1997) Instability, unfolding and aggregation of human lysozyme variants underlying amyloid fibrillogenesis. *Nature* **385**, 787-793
154. Dumoulin, M., Kumita, J. R., and Dobson, C. M. (2006) Normal and aberrant biological self-assembly: Insights from studies of human lysozyme and its amyloidogenic variants. *Acc Chem Res* **39**, 603-610
155. Frare, E., Polverino De Laureto, P., Zurdo, J., Dobson, C. M., and Fontana, A. (2004) A highly amyloidogenic region of hen lysozyme. *J Mol Biol* **340**, 1153-1165
156. Arnaudov, L. N., and de Vries, R. (2005) Thermally induced fibrillar aggregation of hen egg white lysozyme. *Biophys J* **88**, 515-526
157. Sekijima, Y. (2014) Recent progress in the understanding and treatment of transthyretin amyloidosis. *J Clin Pharm Ther* **39**, 225-233
158. Hurshman, A. R., White, J. T., Powers, E. T., and Kelly, J. W. (2004) Transthyretin aggregation under partially denaturing conditions is a downhill polymerization. *Biochemistry* **43**, 7365-7381
159. Ingenbleek, Y. (2019) Plasma Transthyretin as A Biomarker of Sarcopenia in Elderly Subjects. *Nutrients* **11**

160. Liu, Y., Gotte, G., Libonati, M., and Eisenberg, D. (2001) A domain-swapped RNase A dimer with implications for amyloid formation. *Nat Struct Biol* **8**, 211-214
161. Sambashivan, S., Liu, Y., Sawaya, M. R., Gingery, M., and Eisenberg, D. (2005) Amyloid-like fibrils of ribonuclease A with three-dimensional domain-swapped and native-like structure. *Nature* **437**, 266-269
162. Goers, J., Permyakov, S. E., Permyakov, E. A., Uversky, V. N., and Fink, A. L. (2002) Conformational prerequisites for alpha-lactalbumin fibrillation. *Biochemistry* **41**, 12546-12551
163. Swatek, K. N., and Komander, D. (2016) Ubiquitin modifications. *Cell Res* **26**, 399-422
164. Wintrode, P. L., Makhatadze, G. I., and Privalov, P. L. (1994) Thermodynamics of ubiquitin unfolding. *Proteins* **18**, 246-253
165. Morimoto, D., Walinda, E., Fukada, H., Sou, Y. S., Kageyama, S., Hoshino, M., Fujii, T., Tsuchiya, H., Saeki, Y., Arita, K., Ariyoshi, M., Tochio, H., Iwai, K., Namba, K., Komatsu, M., Tanaka, K., and Shirakawa, M. (2015) The unexpected role of polyubiquitin chains in the formation of fibrillar aggregates. *Nat Commun* **6**, 6116
166. Masters, C. L., Simms, G., Weinman, N. A., Multhaup, G., McDonald, B. L., and Beyreuther, K. (1985) Amyloid plaque core protein in Alzheimer disease and Down syndrome. *Proc Natl Acad Sci U S A* **82**, 4245-4249
167. Hamley, I. W. (2012) The amyloid beta peptide: a chemist's perspective. Role in Alzheimer's and fibrillization. *Chem Rev* **112**, 5147-5192
168. Akter, R., Cao, P., Noor, H., Ridgway, Z., Tu, L. H., Wang, H., Wong, A. G., Zhang, X., Abedini, A., Schmidt, A. M., and Raleigh, D. P. (2016) Islet Amyloid Polypeptide: Structure, Function, and Pathophysiology. *J Diabetes Res* **2016**, 2798269
169. Loksztejn, A., and Dzwolak, W. (2010) Vortex-induced formation of insulin amyloid superstructures probed by time-lapse atomic force microscopy and circular dichroism spectroscopy. *J Mol Biol* **395**, 643-655
170. Wong, Y. C., and Krainc, D. (2017) alpha-synuclein toxicity in neurodegeneration: mechanism and therapeutic strategies. *Nat Med* **23**, 1-13
171. Giacobini, E., and Gold, G. (2013) Alzheimer disease therapy--moving from amyloid-beta to tau. *Nat Rev Neurol* **9**, 677-686
172. Nizynski, B., Dzwolak, W., and Nieznanski, K. (2017) Amyloidogenesis of Tau protein. *Protein Sci* **26**, 2126-2150
173. van Es, M. A., Hardiman, O., Chio, A., Al-Chalabi, A., Pasterkamp, R. J., Veldink, J. H., and van den Berg, L. H. (2017) Amyotrophic lateral sclerosis. *Lancet* **390**, 2084-2098
174. Bergfors, T. (2003) Seeds to crystals. *J Struct Biol* **142**, 66-76

# List of publications

## *Main papers*

Noji, M., So, M., Yamaguchi, K., Hojo, H., Onda, M., Akazawa-Ogawa, Y., Hagihara, Y., and Goto, Y. (2018) Heat-Induced Aggregation of Hen Ovalbumin Suggests a Key Factor Responsible for Serpin Polymerization. *Biochemistry* **57**, 5415-5426

Noji, M., Sasahara, K., Yamaguchi, K., So, M., Sakurai, K., Kardos, J., Naiki, H., and Goto, Y. (2019) Heating during agitation of $\beta_2$-microglobulin reveals that supersaturation breakdown is required for amyloid fibril formation at neutral pH. *J. Biol. Chem.* **294**, 15826-15835

Noji, M., Samejima, T., Yuzu, K., Sasahara, K., Yamaguchi, K., So, M., Akazawa-Ogawa, Y., Hagihara, Y., Chatani, E., Buchner, J., Bellotti, V., Otzen, D., and Goto, Y. Combining the Anfinsen's intramolecular folding world with the supersaturation-limited intermolecular misfolding world. *in preparation*

## *Related papers*

Adachi, M., Noji, M., So, M., Sasahara, K., Kardos, J., Naiki, H., and Goto, Y. (2018) Aggregation-phase diagrams of $\beta_2$-microglobulin reveal temperature and salt effects on competitive formation of amyloids versus amorphous aggregates. *J. Biol. Chem.* **293**, 14775-14785

Taricska, N., Horváth, D., Menyhárd, D., Ákontz-Kiss, H., Noji, M., So, M., Goto, Y., Fujiwara, T., and Perczel, A. (2019) The route from the folded to the amyloid state: exploring the potential energy surface of a drug-like miniprotein. *Chemistry* 10.1002/chem.201903826 (in press)